A STUDY OF THE DISTRIBUTED RC LOW-PASS AND NOTCH FILTERS AS FEEDBACK NETWORKS IN ACTIVE CIRCUIT DESIGN

by

W. R. EMERSON JOHNSTON, B.Sc.(HONS.),
(Queen's University of Belfast)

A Thesis

Submitted to the School of Graduate Studies

in Partial Fulfilment of the Requirements

for the Degree

Master of Engineering

McMaster University

March 1972

MASTER OF ENGINEERING (1972)
(Electrical Engineering)

McMASTER UNIVERSITY
Hamilton, Ontario

TITLE: "A Study of the Distributed RC Low-pass and Notch Filters as Feedback Networks in Active Circuit Design"

AUTHOR: W. R. Emerson Johnston, B.Sc. (Hons.) (Queen's University of Belfast)

SUPERVISOR: Professor C. K. Campbell

NUMBER OF PAGES: x, 99.

SCOPE AND CONTENTS:

The application of thin film distributed RC networks in active filter and oscillator design has been both theoretically and experimentally (using Mylar - Teledeltos models) investigated. The frequency selectivity of the distributed notch filter has been exploited in the development of a high-Q active band-pass filter. The influence of amplifier characteristics and the notch parameter on the active filter response has been studied.

ACKNOWLEDGEMENTS

The author is indebted to his research supervisor, Dr. C. K. Campbell for his encouragement and guidance throughout the course of this work. Thanks are due to Dr. S. S. Haykim for his helpful suggestions concerning the stability of active distributed circuits. The author wishes to acknowledge his benefit from discussions with his colleague, Mr. J. Wragg.

This project was financed through a grant-in-aid from the National Research Council of Canada to Dr. C. K. Campbell. The author is also indebted to McMaster University for financial support in the form of a McMaster Assistantship.

The author wishes to express his appreciation to the authorities of the British Post Office for permission to persue this research program.

The author wishes to thank Rita Gibson for typing this thesis.

ABSTRACT

The application of uniformly distributed RC networks as feedback elements in the design of active circuits has been investigated. Distributed RC structures were fabricated using Mylar Film, Teledeltos resistance paper and metallic foil, and used to experimentally verify the predicted responses of particular active and passive configurations.

By exploiting the frequency selective feedback provided by a distributed notch filter it was possible to construct an active band-pass filter operating at 1 MHz which achieved a Q of 50 without the use of inductance. For the design it was important that the notch parameter was deliberately chosen to be less than optimum (i.e., $\alpha < 17.78$) so that the feedback circuit did not apply positive feedback in the region of the notch frequency.

Application of positive feedback ($\alpha > 17.78$) and sufficient amplifier gain would convert the active filter into a feedback oscillator. As predicted, the band-pass filter response was strongly influenced by the amplifier gain and phase characteristic, while amplifier impedance exerted only minor effects.

TABLE OF CONTENTS

LIST OF FIGURES

CHAPTER I

INTRODUCTION

1.0 History and Development

In a sense, all systems are distributed and require the use of partial differential equations for their exact mathematical description, their dynamic response being a function of spatial location as well as time. When an excitation is applied to a distributed system the response is not instantaneous but takes a finite time to propagate. These time delays are particularly marked when the physical dimensions of the network are large in comparison to the wavelengths associated with the signals propagating through the system.

There are many cases where these propagation delays are negligible and these lumped systems may be analysed using ordinary differential equations, because spatial variations need no longer be considered. This approach is valid providing the system dimensions are small in comparison to the wavelengths of the propagating signals.

The analysis and synthesis of distributed circuits is not a trivial problem and this probably accounts for the fact that until the late 1950's, with the exception of transmission-line theory, there had been little interest in the subject.

However, by the early 1960's the availability of general purpose digital computers at least partially solved the analysis problem, and people began to realize that several benefits could accrue from the use of distributed parameter networks.

The Thick and Thin Film technologies that had been developed for the manufacture of lumped resistors and capacitors could be easily adapted to economically produce distributed circuits capable of very high packing densities. Often the use of distributed parameter circuits could result in greater system reliability, by reducing the number of components and component interconnections, required to achieve a specified function.

These factors, coupled with the possibility of achieving novel networks unattainable with lumped components, explain the interest that developed in the early 1960's. Though intensive theoretical studies were completed, only a few circuit designs evolved that were of practical value.

1.1 Scope of this Thesis

This thesis is concerned with a study of distributed parameter networks as applied to bandpass filter and oscillator circuits. Thin film distributed circuits operating over the frequency 100 KHz to 32 MHz were constructed using Teledeltos paper, Mylar film and brass foil. A 1 MHz band-pass filter and two 1 MHz oscillators were built and tested.

Chapter II of this thesis is devoted to a survey of distributed parameter network analysis and synthesis techniques, while Chapter III presents an analysis of the uniformly distributed resistance and capacitance (URC) network, as particularly applied to a simple low-pass filter and to a high-Q notch (rejection) network.

Chapter IV reviews the mathematics of linear feedback theory including conditions for sustained oscillation and stability criteria. Following this review, an extremely simple phase-shift oscillator is described in which a distributed parameter network is used to replace

the three section lumped RC feedback network of conventional designs. A second design is proposed which exploits the phase characteristic of the distributed notch filter to achieve an oscillator with very good frequency stability. The modifications to this design that would be necessary to obtain a stable active band-pass amplifier are discussed.

The experimental details of the construction and evaluation of the low-pass and notch filters are included in Chapter V.

Chapter VI is devoted to the evaluation of the feedback circuits, with particular emphasis on problems of stability and amplifier limitations as applied to operational distributed circuits.

CHAPTER II

REVIEW OF ANALYSIS AND SYNTHESIS TECHNIQUES

2.0 Introduction

A brief survey of distributed parameter linear circuit analysis and synthesis techniques is included in this chapter to give perspective to the research which will be described in this thesis.

2.1 Analysis

The general case of a three layer thin film distributed resistance and capacitance network is shown in Figure 1, and consists of a dielectric film sandwiched between a resistive layer and a conducting sheet. The resistance per square R(X1,X2) and the capacitance per unit area C(X1,X2) are determined by the thickness of the resistive and dielectric layers respectively. Though structures consisting of more than three layers have been proposed[1,2], the complexity of the mathematics involved in the analysis of these multilayered structures precludes them from the scope of this thesis. Referring to Figure 1, the geometry of the resistive layer and the location of the conducting strips A and B are arbitrary. The analysis of this structure is a boundary value problem which is in general anything but a trivial exercise.

This thesis will be restricted to distributed networks which support only 1-dimensional current flow. Expediency is the main justification for this approach which permits the application of uniform transmission line theory to the problem. In general, the terminal

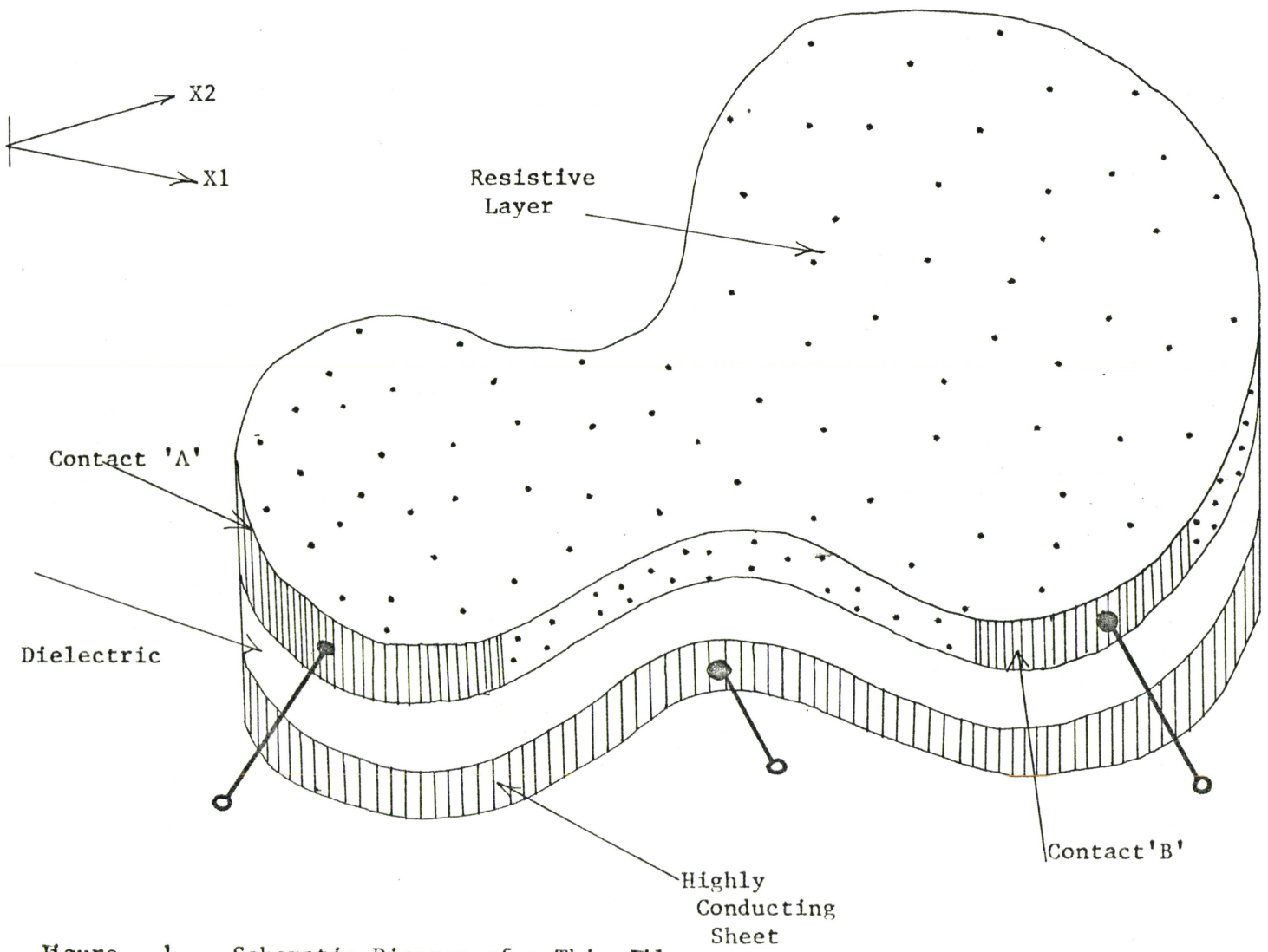

Figure 1 Schematic Diagram of a Thin Film
RC Distributed Network of Arbitrary Geometry (not drawn to scale)

characteristics of a tapered transmission line must be expressed in the form of a series solution, but interest will be focused on uniformly distributed RC networks (URC) for which closed form solutions exist. Closed form solutions also exist for certain geometrically defined tapers[3]. As these systems are considerably more difficult to analyse and introduce only a minor degree of flexibility in design, they will only be given cursory consideration.

2.2 Synthesis

Unlike lumped parameter networks, distributed systems are usually characterised by irrational functions of the complex frequency s and as a consequence are considerably more difficult to synthesise. Several approaches have been developed to overcome this problem.

The simplest of these methods are empirical. The design which will satisfy the specifications being selected on the basis of response curves obtained by analysis[4], or upon approximations such as the use of dominant poles[3]. These techniques have only limited application.

Heizer[5] has investigated the use of specially defined distributed parameter networks whose immittances are rational functions of s, so that conventional lumped parameter synthesis techniques can be used. Unfortunately, the elaborate mathematics of this technique does not lend itself to practical engineering.

Several conformal transformations have been suggested such that the distributed parameter networks when described in the transformed frequency domain W are characterised by rational functions of W, so that the distributed parameter synthesis problem is reduced to an exercise in

lumped parameter synthesis. Having completed the design in the W domain the inverse transformation is applied to yield the distributed parameter realisation Figure 2.

A major problem associated with these methods is the difficulty in defining an engineering specification in a form appropriate for the transformed frequency W domain.

Wyndrum[6] has developed a cascade synthesis procedure using uniformly distributed RC sections as building blocks based on the transformation W = tanh (RCs). Where R is the total distributed resistance, C the total distributed capacitance and s the complex frequency. This converts the distributed circuit synthesis into an LC lumped parameter problem.

O'Shea[7] has proposed a synthesis technique based on the transformation W = cosh (RCs) which enables the distributed synthesis to be treated as a lumped RL problem. Though these methods may be attractive to network theorists their mathematical sophistication and limited application renders them less than attractive to the practising engineer. O'Shea's synthesis has the additional disadvantage in that its implementation often produces elaborate design involving the complex interconnections of many URC elements. This aggravates the problem of reliability instead of alleviating it.

These transform techniques fail to develop the full potential of distributed parameter network synthesis, because only URC elements are used and for a given design the RC product of each section must be constrained to a certain common value. These constraints do not stem from physical considerations such as limitations in fabrication techniques,

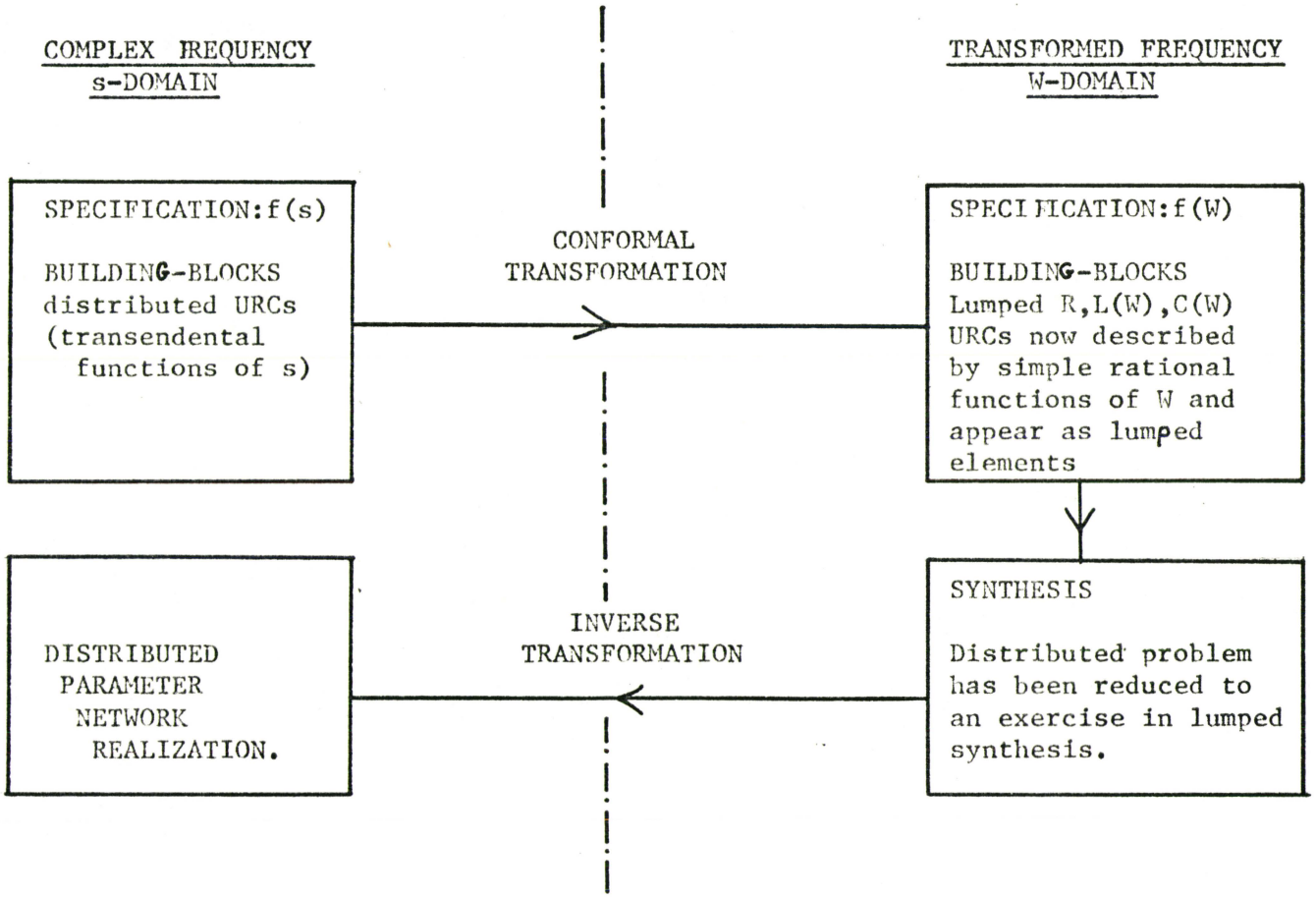

Figure 2 Synthesis Using Conformal Transformation

but are artificially imposed by the mathematics of the transformation. This inadequacy was recognised by Chinn[8] who developed these synthesis techniques to incorporate exponentially tapered sections. Possibly a more promising approach would be the use of numerical optimization techniques to improve the initial design derived, using transform synthesis methods[21].

Rather than develop a comprehensive synthesis theory, which would be a mammoth task, it was decided to focus attention on two simple distributed circuits and their application as feedback elements in active filter and oscillator design.

It was decided to develop a high-Q band-pass filter based on a design proposed by Kaufman[10] in 1960, which used a distributed notch filter as a feedback element across a high gain wide-band amplifier. An oscillator was constructed by modifying the band-pass amplifier circuit. A literature search has failed to reveal any reports of the successful implementation of these designs todate.

As a preliminary exercise a phase shift oscillator was constructed using a URC element as a feedback network[11]. This was not original work but it was felt that useful experience could be gained from the exercise.

CHAPTER III

URC LOW-PASS AND URC NOTCH FILTERS

3.0 Introduction

This Chapter is devoted to an analysis of the URC low-pass and URC notch filters. A clear appreciation of the operation of these circuits is a prerequisite to an understanding of their application as feedback networks in the design of active circuits.

The uniformly distributed RC structure is treated as a two port network and transmission line theory is applied to yield the open circuit impedance matrix description of the terminal characteristics of the device. The use of this circuit element as a low-pass filter will then be discussed, and the URC notch filter will be analysed using standard two port network theory.

3.1 URC Element

The construction of a URC element is shown schematically in Figure 3. It consists of a dielectric layer sandwiched between a resistive layer and a highly conducting film, each layer has uniform thickness and uniform material consistency. The structure is assumed to be rectangular in shape with contacts extending completely across the ends as indicated in the diagram. Assuming that the fringing effects are negligible, the lines of electric flux in the resistive layer will be parallel to each other and perpendicular to the X-axis as shown. These simplifications enable the network to be treated as a 1-dimensional transmission line problem, and avoid the necessity of tackling the much more complex problem

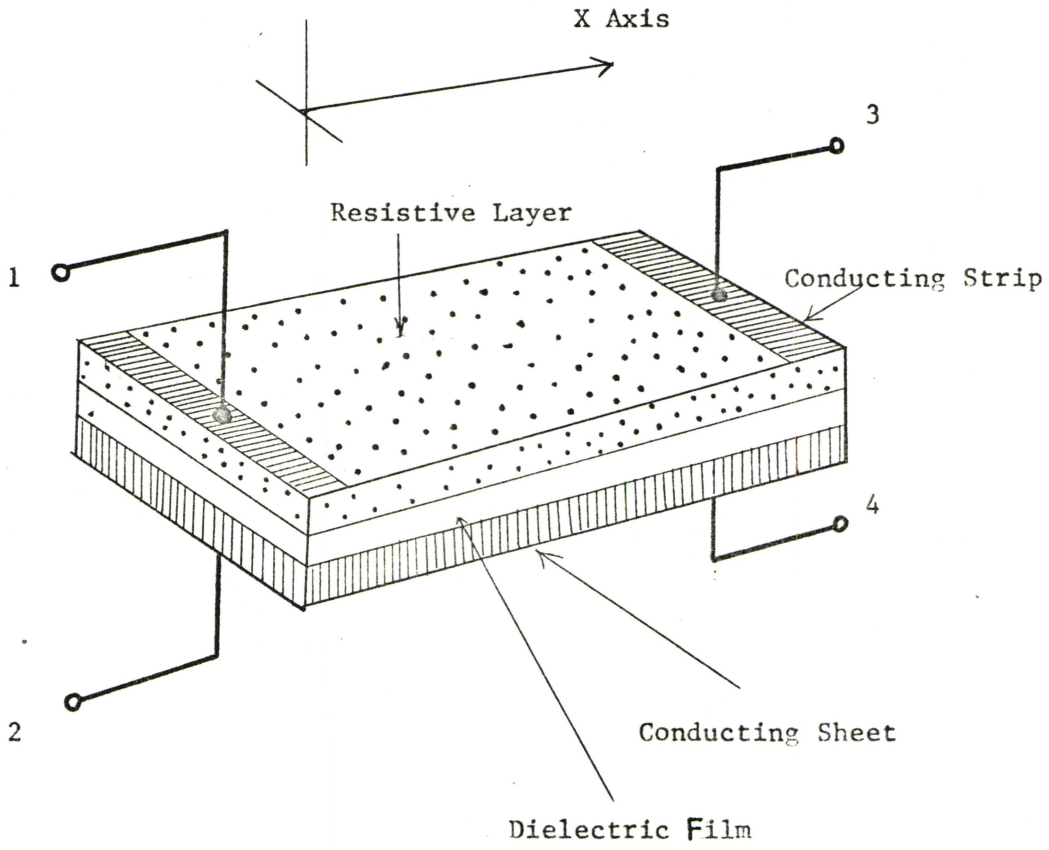

Schematic Representation of the Construction of URC.
(not drawn to scale)

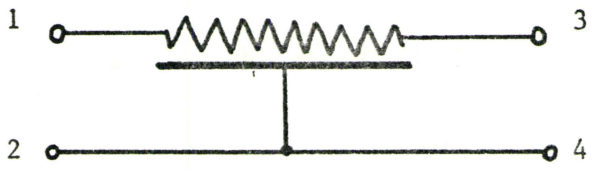

Circuit Symbol for a URC Element.

Figure 3

of 2-dimensional flow.

A lumped equivalent circuit for an incremental section of thin film structure is shown in Figure 4. The dielectric material is assumed to have negligible losses and leakage conductance[18]. The resistance of the conducting film is neglected because it is several orders of magnitude smaller than the resistance of the resistive layer.

The series inductance of the thin film network will also be neglected. This is best justified by the fact that the resulting theory is in close agreement with the experimental results which were obtained.

The lumped circuit model representing an incremental section length ΔX becomes increasingly more accurate as ΔX tends to zero. In the limit the time domain description of the infinitesimally small section is given by equations (3.1) and (3.2), where r_o and c_o are the distributed capacitance and resistance per unit length.

$$\frac{\partial v}{\partial x}(x, t) = -r_o i(x, t) \tag{3.1}$$

$$\frac{\partial i}{\partial x}(x, t) = -c_o \frac{\partial v}{\partial x}(x, t) \tag{3.2}$$

The complex frequency domain description (Laplace) of the element is given by equations (3.3) and (3.4).

$$\frac{dV}{dx}(x, s) = -r_o I(x, s) \tag{3.3}$$

$$\frac{dI}{dx}(x, s) = -sc_o V(x, s) \tag{3.4}$$

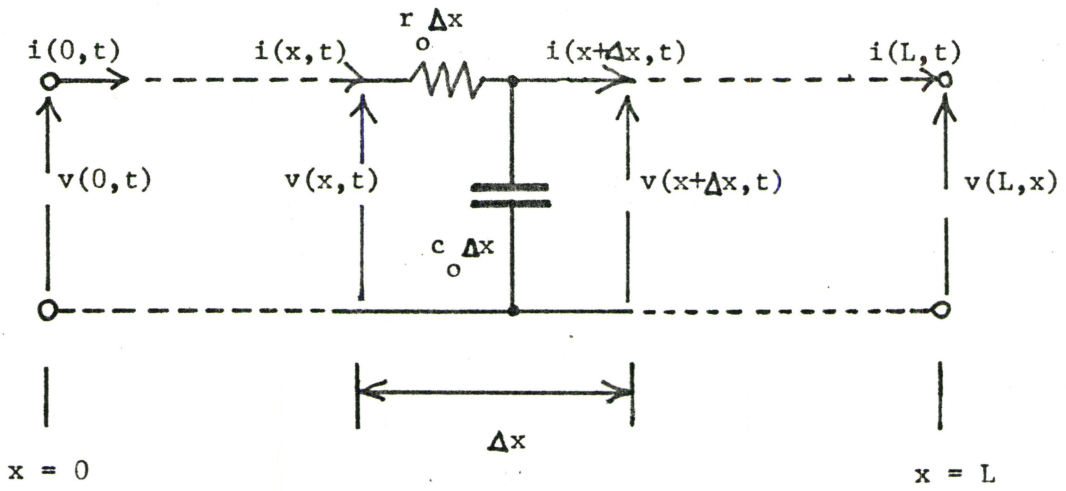

Figure 4 Equivalent circuit for an Incremental Section of the URC network.

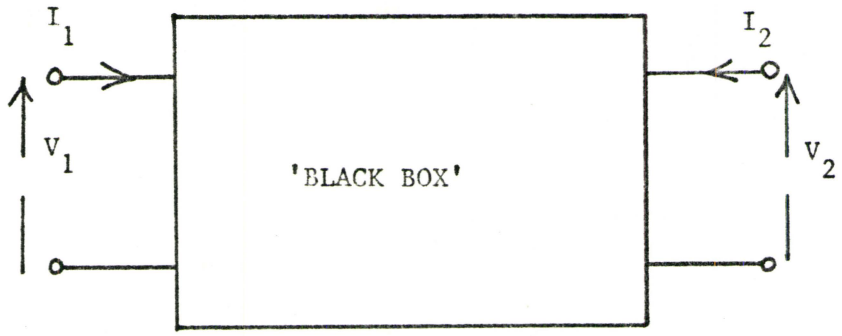

Figure 5 Two - port 'Black box' representation.

Equations (3.1) and (3.2) are then combined to obtain a parabolic second order differential equation, also known as the Heat or the Diffusion Equation.

$$\frac{\partial^2 v}{\partial x}(x, t) = r_o c_o \frac{\partial v}{\partial t}(x, t) \tag{3.5}$$

$$\frac{\partial^2 i}{\partial x^2}(x, t) = r_o c_o \frac{\partial i}{\partial t}(x, t) \tag{3.6}$$

The Laplace-transformed equations are then

$$\frac{d^2 I}{dx^2}(x, s) = r_o c_o s\, I(x, s) \tag{3.7}$$

$$\frac{d^2 V}{dx^2}(x, s) = r_o c_o s\, V(x, s) \tag{3.8}$$

The initial conditions are assumed to be zero when obtaining the Laplace-transformed equations. Partial derivatives do not appear in the transformed equations. In the complex frequency domain the response is an explicit function of position alone; temporal variations have been 'frozen'[13].

The solution of equation (3.8) is of the form[14]

$$V(x, s) = A.\cosh(\gamma x) + B.\sinh(\gamma x) \tag{3.9}$$

where the propagation function γ is defined by equation (3.10).

$$\gamma^2 = r_o c_o s \tag{3.10}$$

The characteristic impedance of the line Z_o given by equation (3.11)

$$Z_o = \sqrt{\frac{r_o}{sc_o}} \tag{3.11}$$

Combining equations (3.3), (3.9) and (3.11) yields a solution for the current distribution along the transmission line equation,

$$I(x, s) = 1/Z_o[A.\sinh(\gamma x) - B.\cosh(\gamma x)] \tag{3.12}$$

Because equation (3.9) is the solution of a second order differential equation it contains two arbitrary constants A and B, which must be chosen to satisfy the boundary conditions of the problem. Figure 5 shows the transmission line represented as a two-port 'black-box'. The boundary conditions are specified by the terminal currents and voltages. Thus, equations (3.13) through (3.16) are obtained, where L is the total length of the structure.

$$V_1 = V(o, s) \tag{3.13}$$

$$V_2 = V(L, s) \tag{3.14}$$

$$I_1 = I(0, s) \tag{3.15}$$

$$I_2 = -I(L, s) \tag{3.16}$$

Note the minus sign used in equation (3.16), by convention I_2 is assumed to be positive when it flows into the upper terminal of the output port. The arbitrary constants may be eliminated from the equations by combining (3.9), (3.12) and (3.13) through (3.16). The terminal characteristics of

the network can then be described by the short circuit admittance parameters defined by

$$\begin{bmatrix} I_1 \\ I_2 \end{bmatrix} = \begin{bmatrix} y_{ij} \end{bmatrix} \begin{bmatrix} V_1 \\ V_2 \end{bmatrix} \tag{3.17}$$

Where

$$[y_{ij}] = \frac{1}{Z_o} \begin{bmatrix} \coth(\gamma L) & -\operatorname{csch}(\gamma L) \\ -\operatorname{csch}(\gamma L) & \coth(\gamma L) \end{bmatrix} \tag{3.18}$$

The chain matrix parameters and the open circuit impedance parameters may be derived from the admittance parameters by using standard formulae[3]. The open circuit impedance matrix defined by

$$\begin{bmatrix} V_1 \\ V_2 \end{bmatrix} = \begin{bmatrix} z_{ij} \end{bmatrix} \begin{bmatrix} I_1 \\ I_2 \end{bmatrix} \tag{3.19}$$

is given by equation

$$[z_{ij}] = Z_o \begin{bmatrix} \coth(\gamma L) & \operatorname{csch}(\gamma L) \\ \operatorname{csch}(\gamma L) & \coth(\gamma L) \end{bmatrix} \tag{3.20}$$

and the chain matrix defined by

$$\begin{bmatrix} V_1 \\ I_1 \end{bmatrix} = \begin{bmatrix} A & B \\ C & D \end{bmatrix} \begin{bmatrix} V_2 \\ -I_2 \end{bmatrix} \tag{3.21}$$

where

$$\begin{bmatrix} A & B \\ C & D \end{bmatrix} = \begin{bmatrix} \cosh(\gamma L) & Z_o \sinh(\gamma L) \\ \frac{1}{Z_o}\sinh(\gamma L) & \cosh(\gamma L) \end{bmatrix} \tag{3.22}$$

Note that in equations (3.18), (3.20) and (3.22) the matrix coefficients are hyperbolic trignometric functions whose argument is the square root of the complex frequency s. These functions are characterised by an infinite number of poles and/or zeros. The pole-zero locations may be defined by considering the infinite product expansions of these hyperbolic functions.

$$\frac{\sinh(x)}{x} = \prod_{n=1}^{\infty} [1 + (\frac{x}{n\pi})^2] \tag{3.23}$$

$$\cosh(x) = \prod_{n=1}^{\infty} [1 + (\frac{2x}{(2n-1)\pi})^2] \tag{3.24}$$

3.2 URC Low-Pass Filter

The open circuit voltage transfer characteristic $T(s) = V_2/V_1$ can be derived from matrix equation (3.17) by considering the special case when $I_2 = 0$ to obtain equation (3.25),

$$V_1 y_{21} + V_2 y_{22} = 0 \tag{3.25}$$

Therefore,

$$T(s) = -\frac{y_{21}}{y_{22}} \tag{3.26}$$

and combining equations (3.18) and (3.26) yields

$$T(s)_{\text{URC Low-pass}} = \frac{1}{\cosh(\gamma L)} \tag{3.27}$$

If the following substitution is made for convenience

$$\omega_o = \frac{1}{r_o c_o L^2} \tag{3.28}$$

Then the frequency response is given by

$$T(j\omega) = \frac{1}{\cosh\sqrt{j\frac{\omega}{\omega_o}}} \tag{3.29}$$

The phase and amplitude responses of this function are shown in Figures 6 and 7 where the URC low-pass characteristics are compared with a simple lumped RC filter. In these figures the cut-off frequencies of the filters are normalized so that they exhibit the same -3dB point.

Note that at high frequencies the URC network has an exponential cut-off and a phase shift that increases without bound with measuring frequency. These features can be easily deduced from a study of the transfer function[12]. The polar plot of the URC low-pass response is shown in Figure 8.

3.3 The URC Resistive Notch Filter (Mathematical Description)

The URC low-pass characteristic can be converted to a frequency selective null network by the suitable interconnection of one additional component. It can be seen from Figure 9 that a transmission null will be

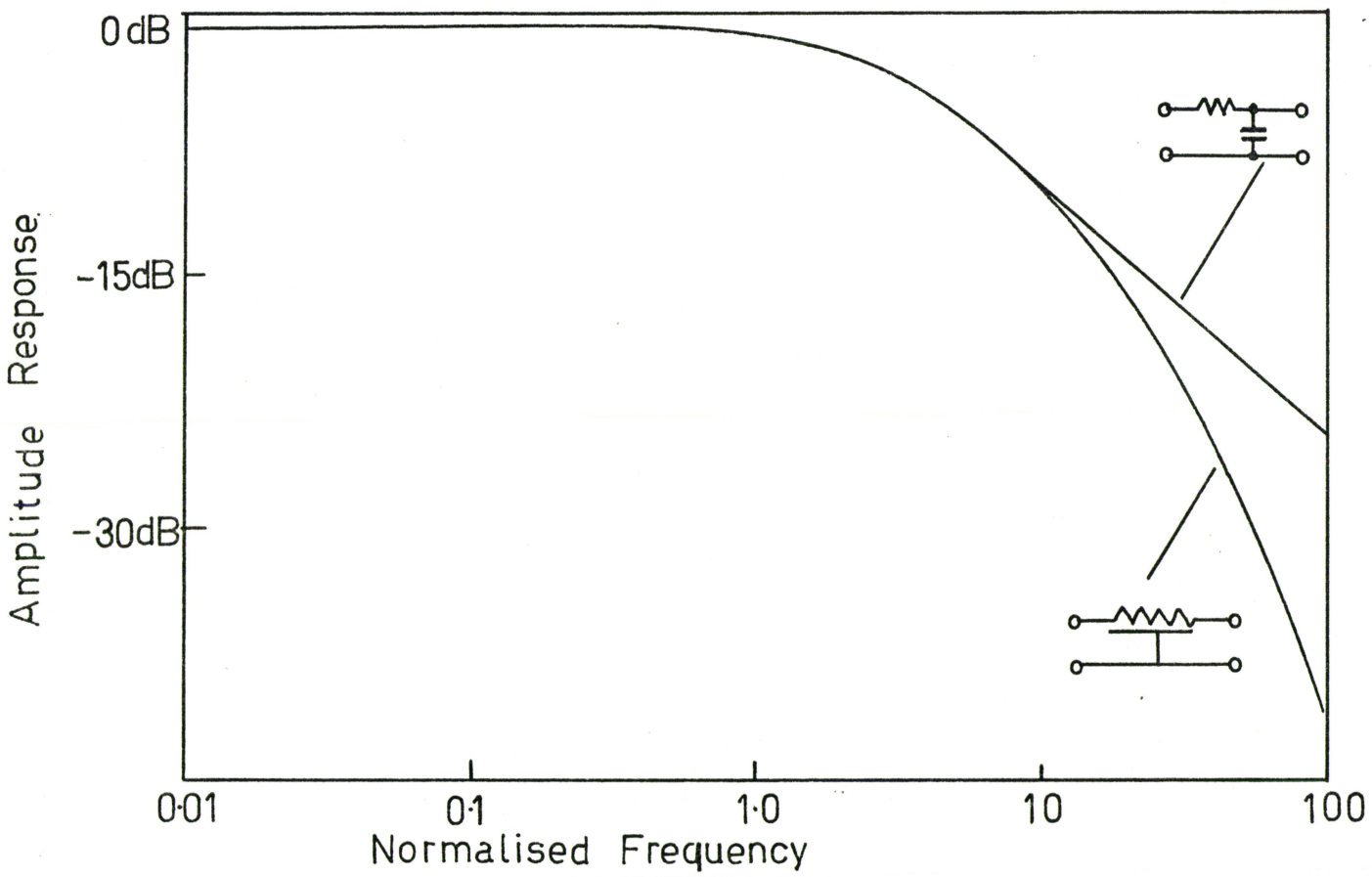

Figure 6 Theoretical Amplitude Response for Single-Pole and URC Low Pass Filters.

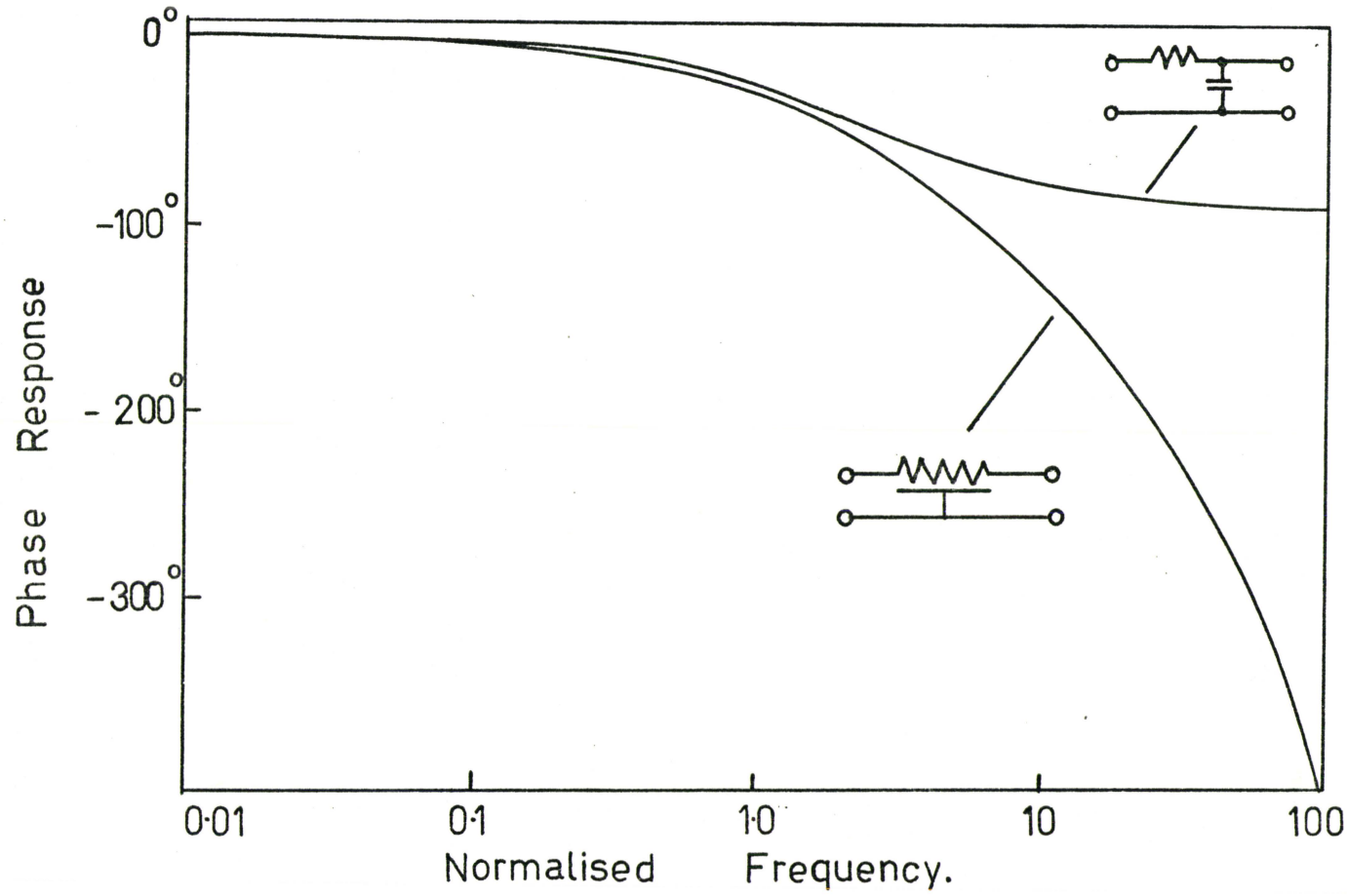

Figure 7 Theoretical Phase Response for Single-Pole and URC Low-Pass Filters.

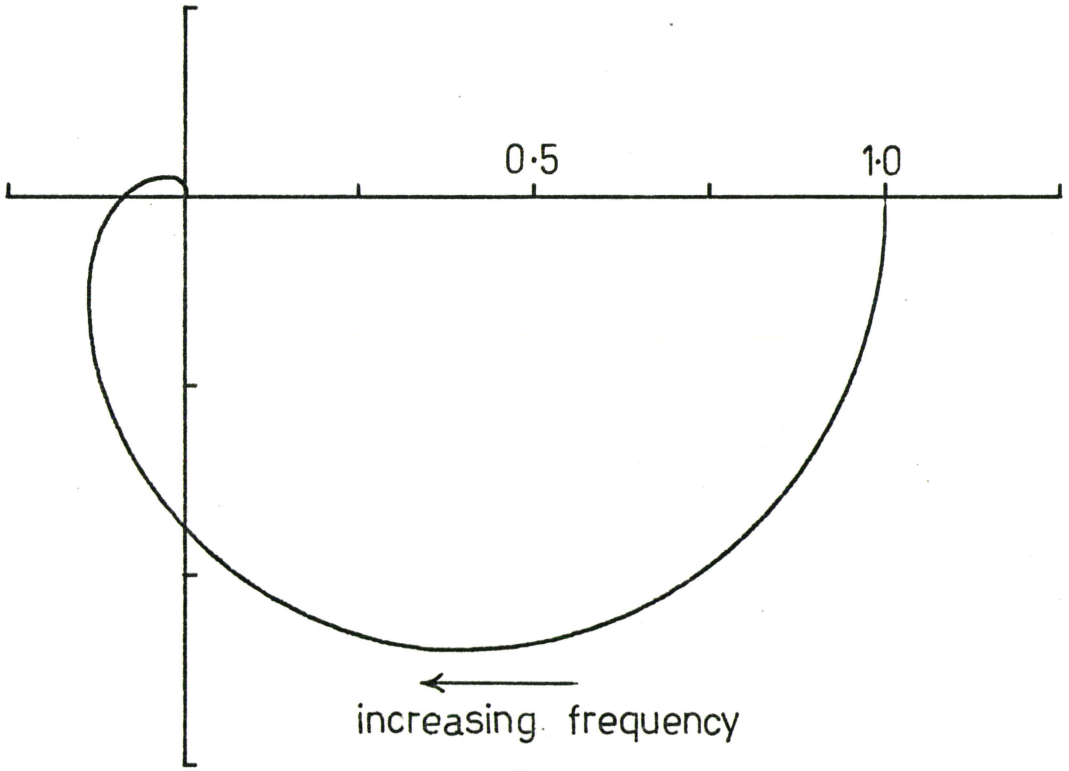

Figure 8 Theoretical Response for URC Low Pass Filter using Polar Co ordinates

produced by either connecting an impedance $Z_s = -Z_b$ in series with the URC, or by shunting the URC element with an admittance $Y_p = -Y_2$.

Distributed networks have been studied by Fuller and Castro[15], and by Stein[16]. Stein has shown that an infinite number of designs exist which use one lumped element to achieve a notch characteristic. However, practical considerations limit interest to the two designs shown in Figure 9.

The limitations of the thin film technology usually rule out those solutions involving inductance or negative resistance. Other notches can be produced using only resistive or capacitive lumped elements. These designs produce notches which occur at higher frequencies but they do not exhibit any advantages over the two basic designs in Figure 9.

The decision to use the resistive notch circuit in preference to the capacitive equivalent was influenced by several factors. Generally it is good engineering to use resistors where possible and avoid the use of capacitors, which are more costly to manufacture, may be less reliable and are more difficult to manufacture to a close tolerance. A secondary advantage of this design is that simply by varying the distributed capacitance of the URC, the notch frequency could be tuned through a band of frequencies and still maintain the optimum notch condition. Using Mytar-Teledeltos models the capacitance can be changed by varying the pressure holding the structure together.

For a mathematical treatment of the analysis of the resistive notch filter it is convenient to use the z-parameters because the URC element and the notch resistor are in series-series connection. The z-matrix of the composite network is obtained by summing the z matrices of

Π Equivalent of URC

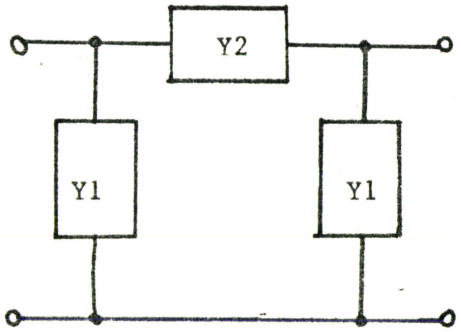

Where $Y1 = (y_{11} + y_{12})$

$Y2 = -y_{12} = -y_{21}$

Associated Null Network.

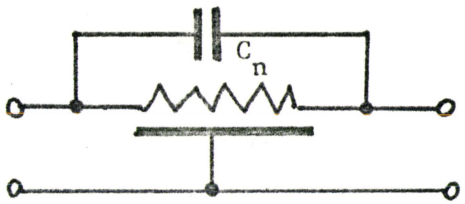

Where $(c_o L)/Cn = 17.78$

$\omega_n = 11.19\omega_o$

T Equivalent of URC

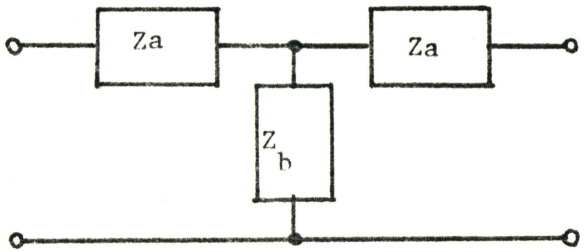

Where $Za = (z_{11} - z_{21})$

$Zb = z_{12} = z_{21}$

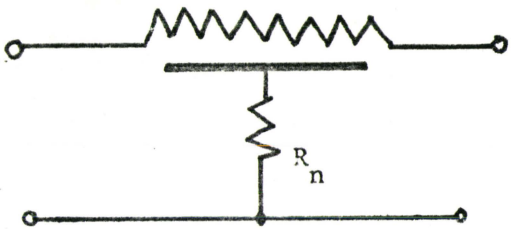

Where $(r_o L)/ Rn = 17.78$

$\omega_n = 11.19\omega_o$

Figure 9 URC Parameters r_o, c_o, L

the URC and the notch resistor, to yield

$$[z_{ij}] = \begin{bmatrix} (Z_o \coth(\gamma L) + R_n) & (Z_o \operatorname{csch}(\gamma L) + R_n) \\ (Z_o \operatorname{csch}(\gamma L) + R_n) & (Z_o \coth(\gamma L) + R_n) \end{bmatrix} \quad (3.30)$$

The open loop transfer function is obtained from the z parameters as follows: Substituting $I_2 = 0$ into matrix equation (3.19) yields

$$V_1 = z_{11} I_1 \quad (3.31)$$

$$V_2 = z_{21} I_1 \quad (3.32)$$

Hence the transfer function T(s) may be defined

$$T(s) = V_2/V_1 = z_{21}/z_{11} \quad (3.33)$$

Combining equations (3.30) and (3.33) to obtain

$$T(s) = \frac{Z_o + R_n \sinh(\gamma L)}{Z_o \cosh(\gamma L) + R_n \sinh(\gamma L)} \quad (3.34)$$

In order to specify the condition for optimum notch (optimum in the sense of zero transmission) it is necessary to solve equation (3.34) for R_n such that $T(s) = (0, j0)$. The solution of this trancendental equation is an exercise in algebra and numerical methods which is tedious and contributes little to the physical understanding of the network, so only the results will be quoted[12]. As stated earlier, the solution is not unique; however, the solution which is of practical importance is defined

Figure 10 Flow Chart for the Program to Calculate the Response of the URC Notch Filter.

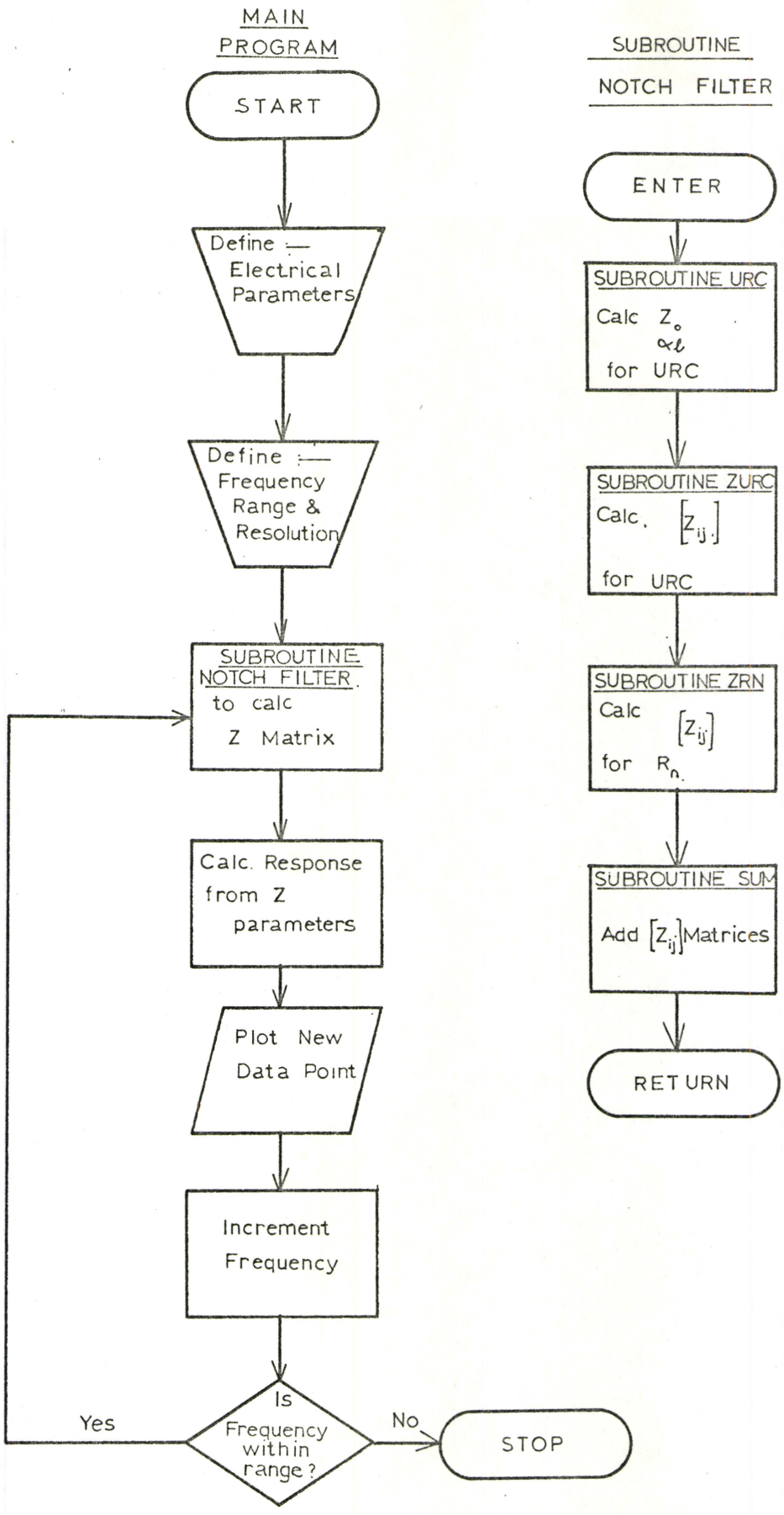
MAIN PROGRAM
START
Define :— Electrical Parameters
Define :— Frequency Range & Resolution
SUBROUTINE NOTCH FILTER. to calc Z Matrix
Calc. Response from Z parameters
Plot New Data Point
Increment Frequency
Is Frequency within range ?
Yes
No
STOP
SUBROUTINE NOTCH FILTER
ENTER
SUBROUTINE URC
Calc Z_o $\alpha\ell$ for URC
SUBROUTINE ZURC
Calc. $[Z_{ij}]$ for URC
SUBROUTINE ZRN
Calc $[Z_{ij}]$ for R_n.
SUBROUTINE SUM
Add $[Z_{ij}]$ Matrices
RETURN

by equations (3.35) and (3.36).

$$\text{Notch parameter } \alpha = r_o L/R_n \tag{3.35}$$

(For optimum notch depth $\alpha_n = 17.78$)

$$\text{Angular frequency of notch } \omega_n = 11.19\omega_o \tag{3.36}$$

The voltage transfer function for the notch filter was evaluated for different values of notch resistance. Had this been the only circuit of interest, the response could have been evaluated directly from equation (3.34) using a digital computer. As many distributed circuits would have to be analysed, a more flexible computation system was required such that a change in circuit configuration could be easily accommodated and not necessitate drastic modifications to the analysis program. The solution was to develop a strategy based on the use of a comprehensive set of subroutines and two port network theory. The subroutines define the two port parameters for each circuit element, and perform all the operations of matrix algebra. With such a scheme a change in the configuration of the circuit would result in only minor changes in the program which calls the subroutines. A flow chart for the calculation of the transfer function of the notch filter is shown in Figure 10.

The phase and amplitude characteristics of the filter are shown in Figures 12 and 13. The phase rises steeply in the range of frequencies straddling the notch when the notch parameter α is less than optimum (i.e., $\alpha < 17.786$), and the phase falls steeply when the notch parameter is equal or greater than the optimum value. This feature is of more than just academic interest. The stability of a circuit using a notch network

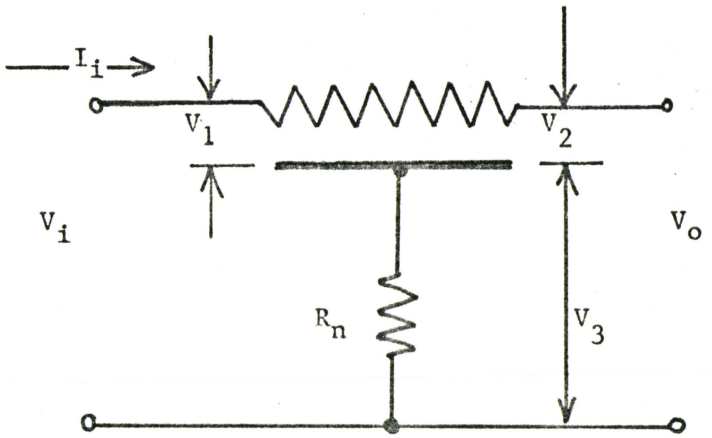

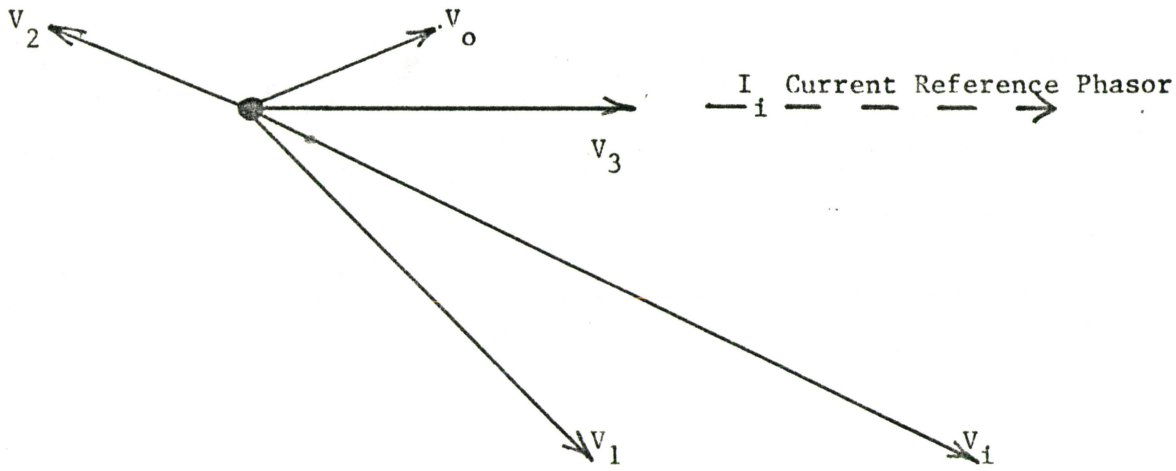

Figure (11) Voltage and Current Phasor Relationships for the URC Notch Filter.

as a feedback element is controlled by the phase and amplitude characteristics of the null network. This will be discussed in greater detail in Chapter IV. The polar plot of the notch filter response is shown in Figure 14.

3.4 URC Notch Filter (Physical Explanation)

A physical appreciation of the operation of the distributed notch network can be gained by studying the phasor relationships of the voltages across the input and output of the URC and the voltage developed across the notch resistor (Figure 11).

A signal applied at the input of the URC will propagate along the structure to the output where it will be reflected back towards the input. Because the structure is very lossy the reflected wave has negligible amplitude when it reaches the input. Consequently, the impedance when 'looking' in the input of the URC is essentially Z_o the characteristic impedance of the line.

Because the URC and the notch resistor are connected in series the current makes an appropriate reference phasor. V_3 is the voltage developed across the notch resistor and is in phase with the input current I_i and has a magnitude $V_3 = I_i R_n$. V_1, the voltage developed across the input of the URC, is defined by $V_1 = Z_o I_i$. The input impedance, Z_o, is capacitive and resistive and so the voltage lags the current by 45°. The total voltage applied to the input V_i is the vector sum of the voltage across the input of the URC and across the notch resistor. Thus, $V_i = V_1 + V_3$.

The output of the URC structure V_2 lags V_1, and is attenuated by the losses. The notch filter output is defined by the vector sum of the

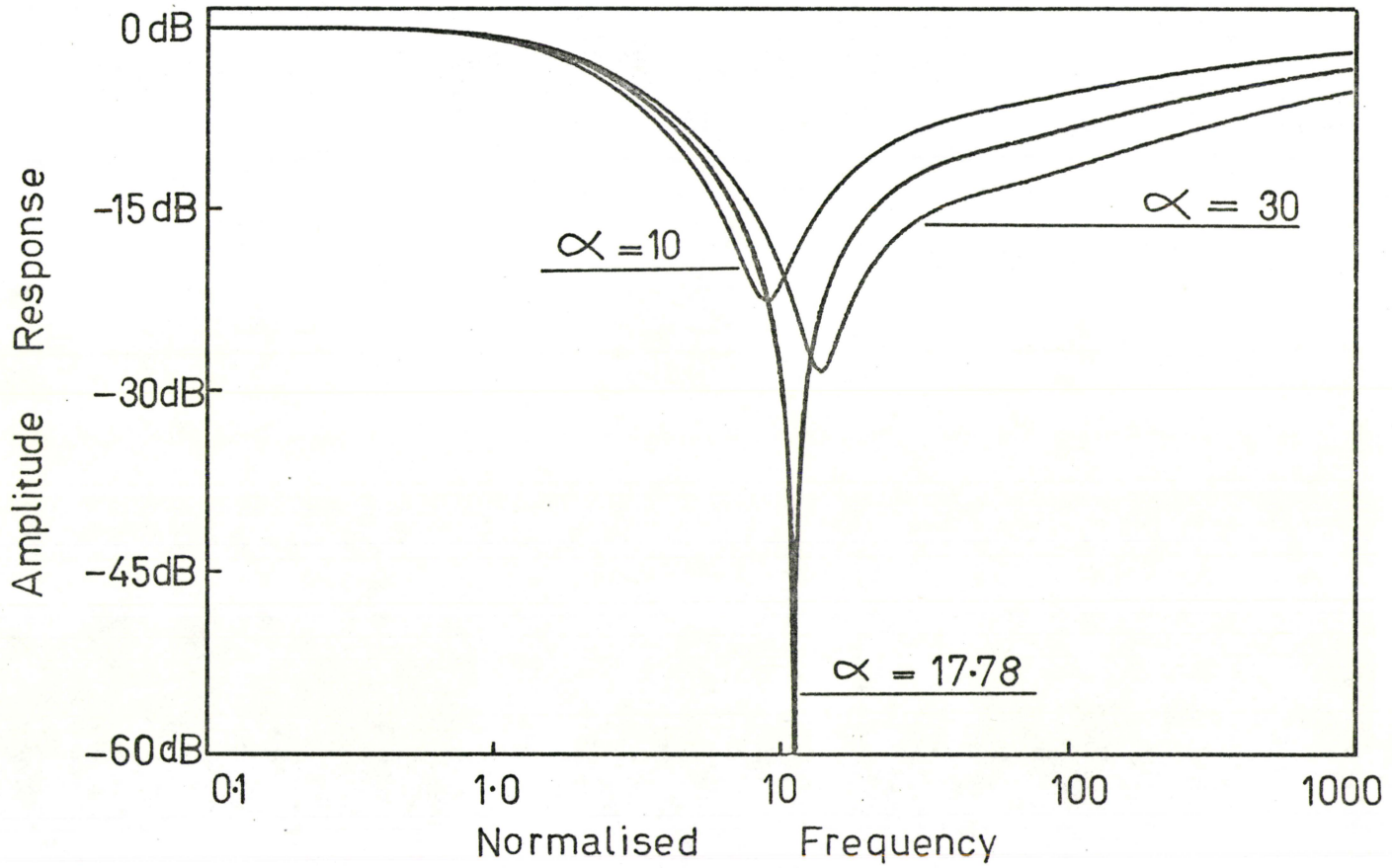

Figure 12 Theoretical Amplitude Response for URC Notch Filter for different values of notch parameter α.

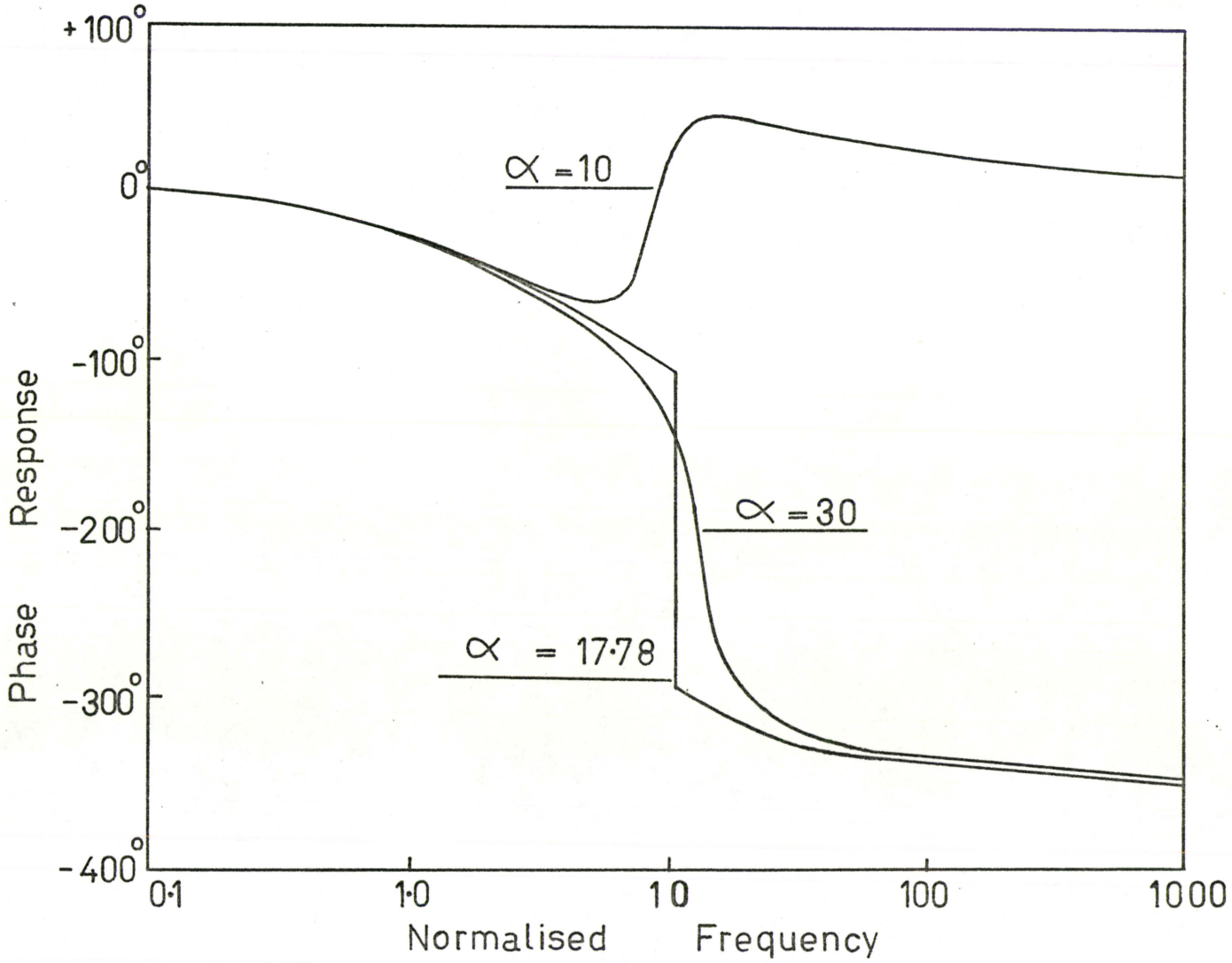

Figure 13 Theoretical Phase Response for URC Notch Filter for different values of notch parameter ∝

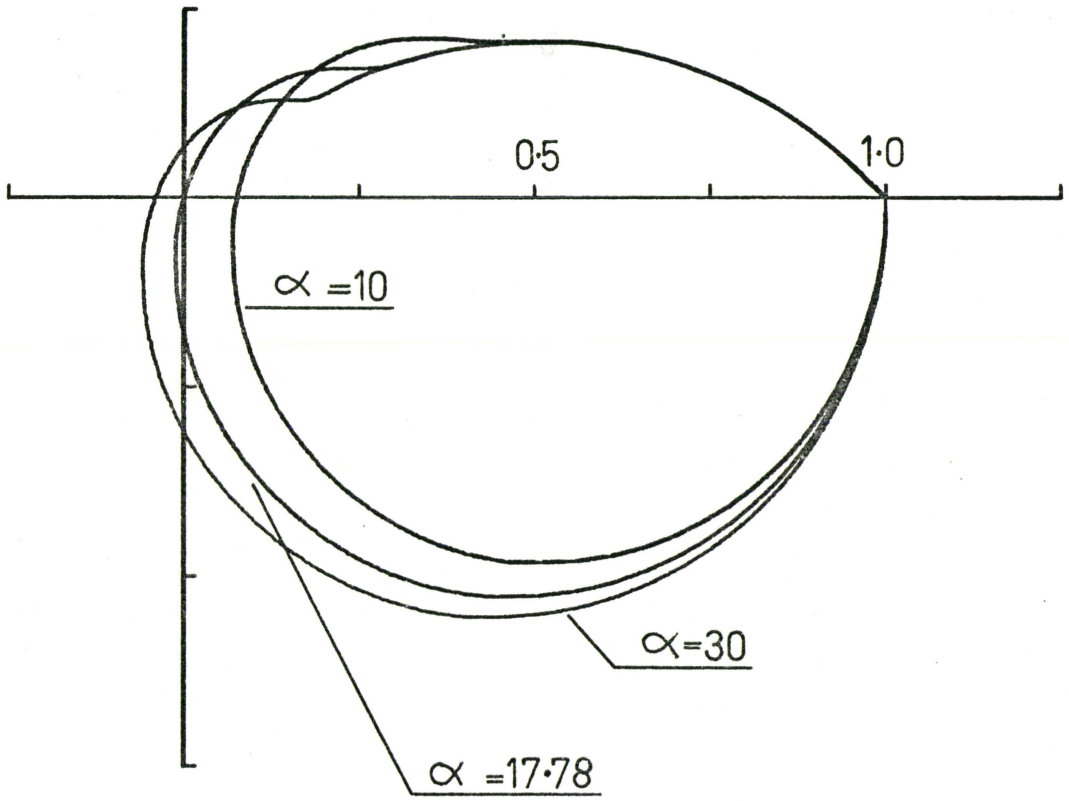

Figure 14 Theoretical Response for URC Notch Filter using Polar Co ordinates

voltage across the output of the URC and voltage across the notch resistor. Thus, $V_o = V_2 + V_3$, and it can be seen that for a transmission null V_2 must be equal to V_3 in magnitude but in phase opposition. For a fuller treatment of this approach see Campbell[17] who develops this physical interpretation to deduce the conditions for optimum notch.

CHAPTER IV

DISTRIBUTED NETWORKS AS FEEDBACK ELEMENTS

4.0 Introduction

A survey of the techniques that are available for the analysis of feedback systems is given and their ability to deal with distributed parameter system discussed. The designs of two types of feedback oscillator and an active band-pass filter are presented. Bode plots are used to analyse the operation of these circuits[25,26,27,28].

4.1 Analysis of Feedback Systems

A feedback system is one in which some fraction of the output signal is combined with the input signal to modify the system response. The block schematic diagram representing a single loop feedback system is presented in Figure 15 where H(s) is the transfer function of the feedback network, and G(s) the amplifier transfer function. The closed loop response of this system is described by equation (4.0).

Closed Loop Response

$$\frac{V_o}{V_i}(s) = \frac{G(s)}{1 + GH(s)} \qquad (4.0)$$

Several assumptions are implicit in equation (4.0). These are:

(1) Linear system,

(2) Unidirectional signal flow through amplifier and feedback path,

(3) There are no loading efforts when the networks are

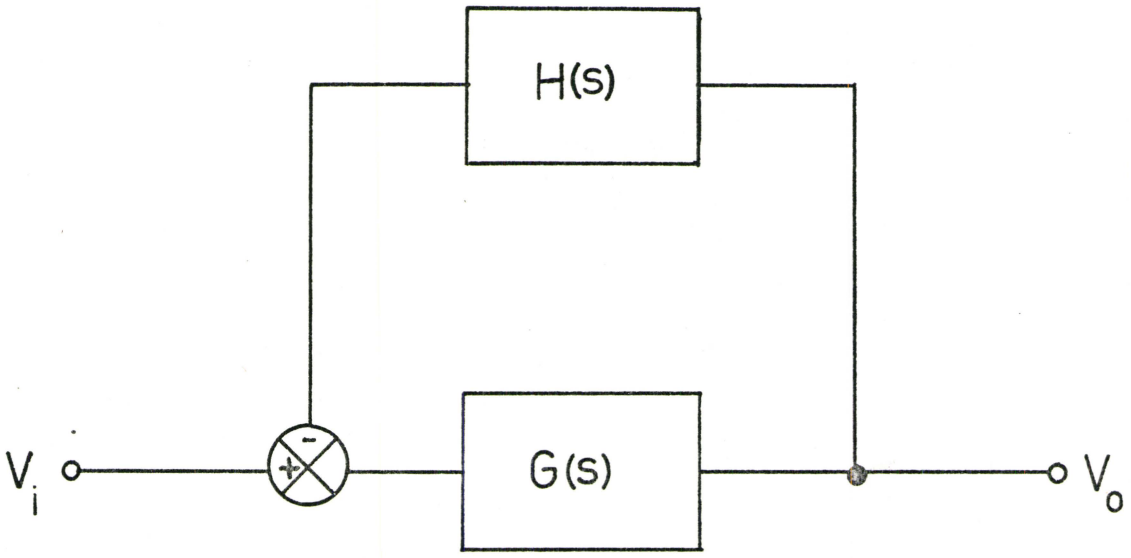

General Single Loop Feedback System

Figure 15

connected together.

An unstable system is characterised by transients which grow exponentially with time and are associated with poles located in the right half of the complex frequency plane s (R.H.P.). The poles of the closed loop system are defined by the zeros of the denominator of equation (4.0), i.e., the zeros of the characteristic equation and the poles of G(s), the amplifier response.

Characteristic Equation

$$1 + GH(s) = 0 \qquad (4.1)$$

Since the amplifier itself is usually stable the closed loop response will only be stable if the characteristic equation does not possess zeros in the R.H.P.

All the analysis techniques which will be discussed involve an investigation of the location of the roots of the characteristic equation.

The Classical Approach and Root Locus methods involve finding the exact location of these roots, while Routh Hurwitz, Bode, and Nyquist methods involve defining the region within which the roots are located.

The Classical Approach involves factorizing the characteristic equation to locate the zeros, and is so mathematically tedious that it is unattractive even for the analysis of simple lumped parameter systems. The method is nothing but an algebraic endurance test and does not afford the user with any appreciation of the physical operation of the system. In most practical situations the coefficients of the characteristic equation are not directly available so this method is difficult to apply.

The Root Locus method presents the user with the additional physical insight necessary to devise system modifications, should these be required. But the infinity of poles associated with hyperbolic functions makes it difficult to apply these methods to distributed parameter systems. Several researchers have developed Root Locus techniques for distributed systems but this approach will not be prosecuted as more convenient alternatives exist[3].

The Routh Hurwitz criterion is an algebraic procedure to test system stability. It is performed by examining the coefficients of the characteristic equation without actually having to find the roots of the equation; otherwise, this system suffers from most of the short comings associated with the Classical Approach.

The Nyquist method is a graphical procedure for stability analysis, based on a plot of the open loop steady state sinusoidal system response in the complex plane 'T'. A derivation of the Nyquist stability criteria is based on the Complex Variable theory and can be stated thus:

> "A feedback system is STABLE, only if its open loop transfer locus does not pass through the (-1, 0) point and the number of anticlockwise encirclements of this point equals the number of poles of the open loop response which are located in R.H.P."

The networks which will be discussed have stable open loop responses so that the Nyquist criteria may be restated:

> "A feedback system will be stable if the open loop response is stable and if the transfer locus does not encircle or pass through the point (-1, 0) in the complex plane 'T'.

The plot of the open loop transfer locus in the complex 'T' plane is called the Nyquist Diagram. The Nyquist method offers several advantages over the Classical Approach, Routh Hurwitz and Root Locus methods in that it does not require a knowledge of the coefficients of the characteristic equation. The Nyquist plot can be obtained experimentally and the open loop response of a distributed system can be measured just as easily as a lumped system. The Nyquist method also yields information about the relative stability (or instability) of a system.

One inadequacy of the Nyquist method should be considered. To obtain the Nyquist diagram interest has been narrowed from the entire complex frequency s plane to the $s = j\omega$ axis. Consequently this method automatically discards important information about the transient response of the closed loop system, and is in sharp contrast with the Root Locus method which by searching the entire s plane simultaneously yields information about both, the steady state and transient responses.

Bode plots are an alternative means of presenting the phase and amplitude information of the Nyquist diagram. This method is adopted because the network analyser used to measure the open loop transfer function uses Bode format to display the system response. Should compensation be necessary it is generally easier to interpret Bode diagrams, than work directly with the Nyquist plots. If the open loop response is stable the closed loop system will be unstable if at any frequency the net phase shift of the open loop response is zero (or integral multiples of 360°) and the net loop gain is greater than 0 dB.

4.2 Feedback Oscillators

The application of feedback to an amplifier may induce oscillation. The Barkhausen criteria for oscillation require that the total loop phase shift be zero (or an integral multiple of 2Π radians) and the voltage gain of the loop be unity, 0 dB.

4.2.1 Phase Shift Oscillators:

A phase shift network which will introduce -Π radians of phase shift (or -(2n - 1)Π radians) can be used to convert a wide band amplifier into an oscillator. For oscillations to be sustained, the amplifier gain should exactly compensate for the losses of the feedback network (see Figure 16).

The frequencies at which the $\overline{URC}$ low-pass filter introduces a phase shift of -Π radians or -(2n - 1)Π radians, are defined by the expression[20]

$$\frac{\omega_{/\Pi}}{\omega_o} = 2n^2\Pi^2 \qquad (4.2)$$

where n = 1,2,3,4, etc.

Note that there an infinite number of oscillation modes designated by the integer index n. However, the oscillation of practical interest is defined by n = 1. For oscillations to be sustained the amplifier gain should be sufficient to compensate for the losses of the feedback network. From Figures 6 and 7, it can be seen that the $\overline{URC}$ phase shift network introduces an attenuation of 22 dB at the frequency associated with the phase shift of -Π radians. Conventionally a 3 section lumped RC network is used to obtain the -Π radians of phase shift. This network introduces

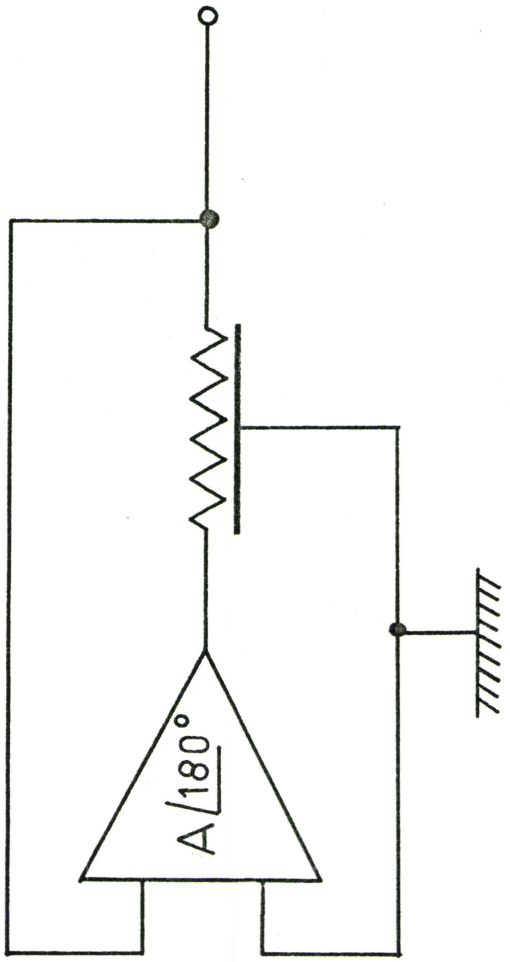

URC Phase Shift Oscillator

Figure 16

29 dB attenuation to achieve this phase shift. By reducing the number of components required, the $\overline{URC}$ feedback network not only results in cheaper and more reliable designs, but the amplifier gain requirements have been reduced from 29 dB to 22 dB. Even further improvement could accrue from the use of exponentially tapered structures which could provide Π radians of phase shift with even less attenuation[18]. In this simplified analysis terminal phase shifts and loading effects have been neglected.

4.2.2 Frequency Stability:

Frequency stability is an important design consideration in many oscillator applications. Frequency deviations are attributable to fluctuations in the system phase and amplitude characteristics or to changes in the load to which the oscillator is coupled. For good frequency stability the slope of the open loop transfer function should be as steep as possible in the region of the oscillation frequency. The steeper the phase and amplitude characteristic, the smaller will be the frequency deviation necessary to compensate for these undesirable fluctuations.

In considering this problem, Happ and Castro[4] compared the responses of the $\overline{URC}$ network with the conventional 3-section RC filter, and showed that in the region of frequencies associated with 180° phase shift, the $\overline{URC}$ network exhibited a much steeper phase and amplitude characteristic. Thus better frequency stability should accrue from the use of the $\overline{URC}$ phase-shift network.

4.2.3 Spectral Purity:

There are two different aspects to this problem. If the loop gain were sufficiently high the $\overline{URC}$ phase oscillator could support a multitude of oscillation modes, each mode being associated with an extra 360° phase shift in the $\overline{URC}$. These modes are not generated by system non-linearities. The frequencies of these extra modes are not harmonically related. They depend on the $\overline{URC}$ phase characteristic.

Fortunately the problem of multi-mode oscillation is unlikely to arise in practice as an excessive amount of gain is necessary to support even the lowest of these higher order modes. The gain of 22 dB necessary to sustain the fundamental oscillation is to be contrasted with a gain of 76 dB that would be necessary to support the next mode.

Multi-mode behaviour cannot exist if a 3-section RC phase shift network is used, as the maximum phase of this network is limited to 270°.

If the amplifier is perfectly linear and if the loop gain is greater than unity the amplitude of the oscillation will grow exponentially with time. In practice the amplitude does not increase indefinitely, but will be bounded by system non-linearities and amplifier saturation effects. It is these system non-linearities which generate harmonics and degrade the waveform purity.

To achieve good spectral purity the amplifier should be designed with stabilizing networks to automatically restrict the signal amplitude and avoid hard limiting. Further improvement should result from exploitation of the low-pass filter action of the phase shift network. The oscillator signal should be derived after it has passed through the phase shift network rather than directly from the amplifier output. Though the

improved high frequency rejection of the $\overline{\text{URC}}$ should result in lower harmonic content, a rigorous comparison of distributed and lumped component oscillators would be difficult, as it would be necessary to incorporate phase as well as amplitude effects into the analysis.

4.2.4 Amplitude Stability:

The oscillator output power level will be susceptible to any fluctuations in system parameters. Because they utilize similar design configurations, both the URC and lumped RC phase shift oscillators should be effected in a similar manner. The problem of minimising this instability requires careful selection of system components and careful amplifier design, and is beyond the scope of this thesis.

Loading is another factor influencing oscillator signal level. Because of the similarity in impedance levels of the discrete RC and distributed RC phase shift networks, both oscillator designs should show similar loading effects.

In situations where amplitude stability is important, the oscillator should be isolated from the load by a buffer amplifier.

4.2.5 Notch Oscillator:

As explained earlier, the frequency stability is controlled by the steepness of the open-loop transfer function. By exploiting the very steep phase response associated with the distributed notch filter it should be possible to obtain a very stable oscillator. This design was first proposed by Kaufman[10].

At both low frequencies and high frequencies, the notch filter introduces negligible attenuation and phase shift, and so large amounts

of negative feedback are applied to the amplifier. Near the notch frequency the amount of attenuation is greatly reduced and the phasing of this feedback will depend on the value of notch parameter. For positive feedback it is necessary for the notch filter to introduce 180° phase shift to the open loop response. To achieve this the value of notch parameter α should not be less than the optimum value. Oscillations will then be sustained if the gain of the amplifier is adequate to compensate for the transmission losses in the feedback network (see Figure 17).

4.3 Notch Band-Pass Filter

4.3.1 Introduction:

One form of band-pass filter could be obtained by using a notch oscillator which has had the gain of the amplifier reduced so that the loop gain is inadequate to sustain oscillation. However, this would be poor engineering as the use of positive feedback increases the system noise and the sensitivity of the circuit to parameter changes. In order to prevent positive feedback from being applied to the amplifier the notch parameters should be constrained to be less than optimum, ie $\alpha < \alpha_n$ (so that the phase shift of the notch filter is restricted between approximately ±90°). This can be seen by studying Figure 14.

4.3.2 High-Q Band-Pass Filter (Ideal Analysis):

This analysis is based on the circuit shown in Figure 18. The amplifier characteristics are assumed to be ideal. Referring to the equivalent circuit in Figure 19 this implies

$$Z_{in} \rightarrow \infty$$

$$Z_{out} \rightarrow 0$$

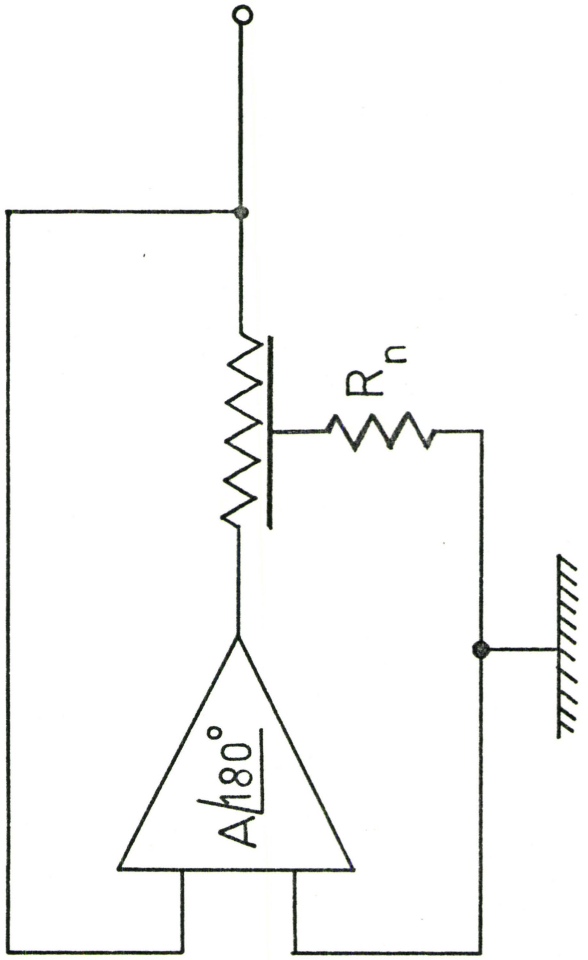

URC Notch Oscillator

Figure 17

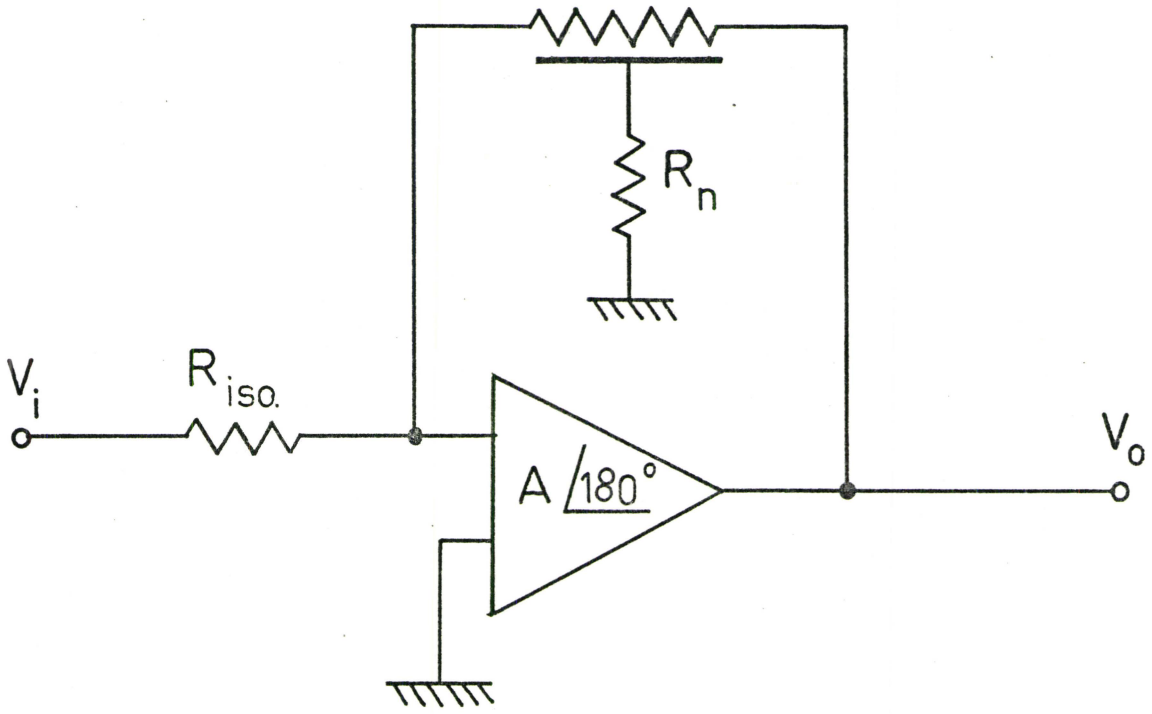

URC Notch Bandpass Filter

Figure 18

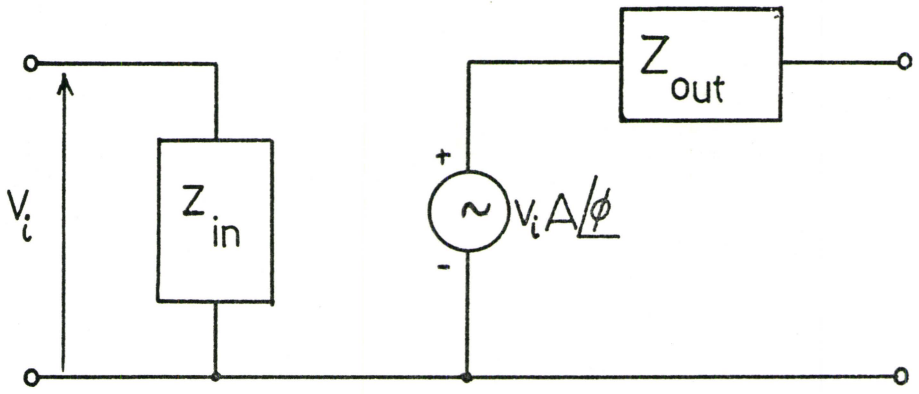

Amplifier Equivalent Circuit

Figure 19

Frequency Dependence of Y_{12} for URC Notch Filter (physical interpretation)

Definition

$$Y_{12} = \left.\frac{I_1}{V_2}\right|_{V_1 = 0}$$

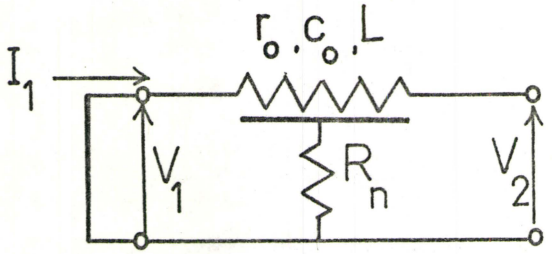

Low Frequency

$$Y_{12} \longrightarrow -\frac{1}{r_o L}$$

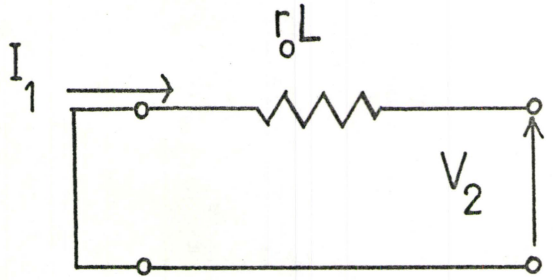

High Frequency

$$Y_{12} \longrightarrow -\infty$$

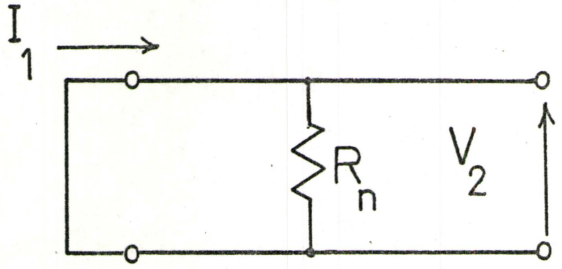

Notch Frequency

$Y_{12} \longrightarrow 0$ (Transmission Zero)

Figure 20

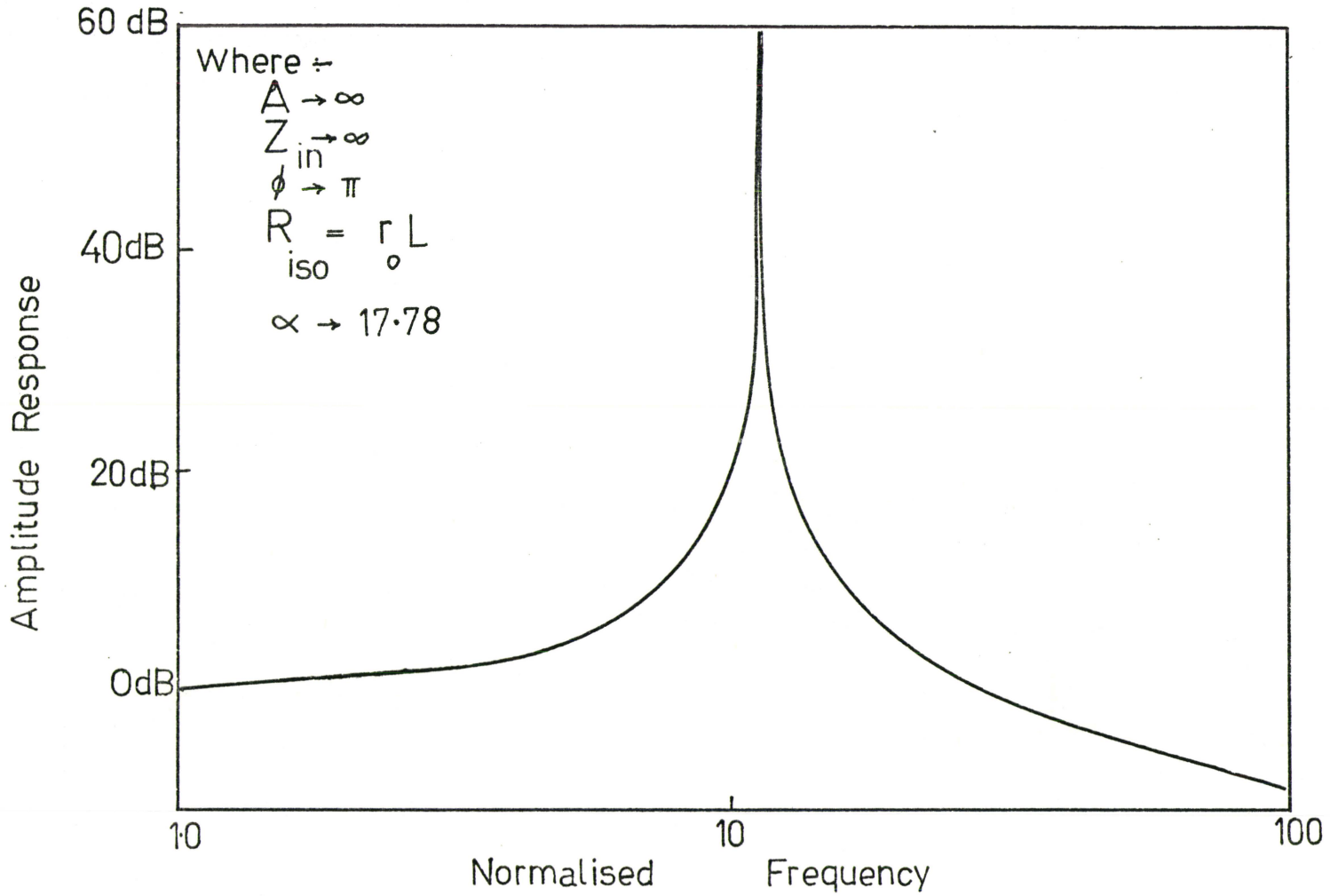

Figure 21

Theoretical Amplitude Response for Ideal Amplifier with URC Notch Feedback Network

$$A \rightarrow \infty$$

$$\phi \rightarrow \Pi$$

The voltage transfer functions for the network can then be described by

$$\frac{V_o}{V_i} = \frac{-A}{1 + y_{11} R_{1SO} - Ay_{12} R_{1SO}} \qquad (4.3)$$

where the y parameters refer to the feedback network. Since the amplifier gain is very large equation (4.3) can be approximated by the expression

$$\frac{V_o}{V_i} = \frac{1}{y_{12} R_{1SO}} \qquad (4.4)$$

To understand the operation of this circuit, the nature of y_{12} should be considered in Figure 20. The theoretical response defined by equation (4.4) has been evaluated and is shown in Figure 21.

4.3. Analysis of Band-Pass Filter Incorporating Non-Ideal Amplifier Characteristics:

In practise the assumptions implicit in the ideal analysis cannot be justified, because the gain and input impedance of the 'real' amplifier will be finite. A more elaborate analysis was required which would incorporate the influences of the non-ideal amplifier characteristic on the active filter response. The amplifier was modelled by the equivalent circuit shown in Figure 19 and the analysis was based on 2-port network theory. It essentially involved determining the y parameters for the notch filter and for the amplifier, and summing them to obtain the description of the closed loop response. The flow chart for this analysis program is shown in Figure 22.

Figure 22 Flow Chart for the Program to Calculate the Response of the Active Filter using Notch Filter Feedback.

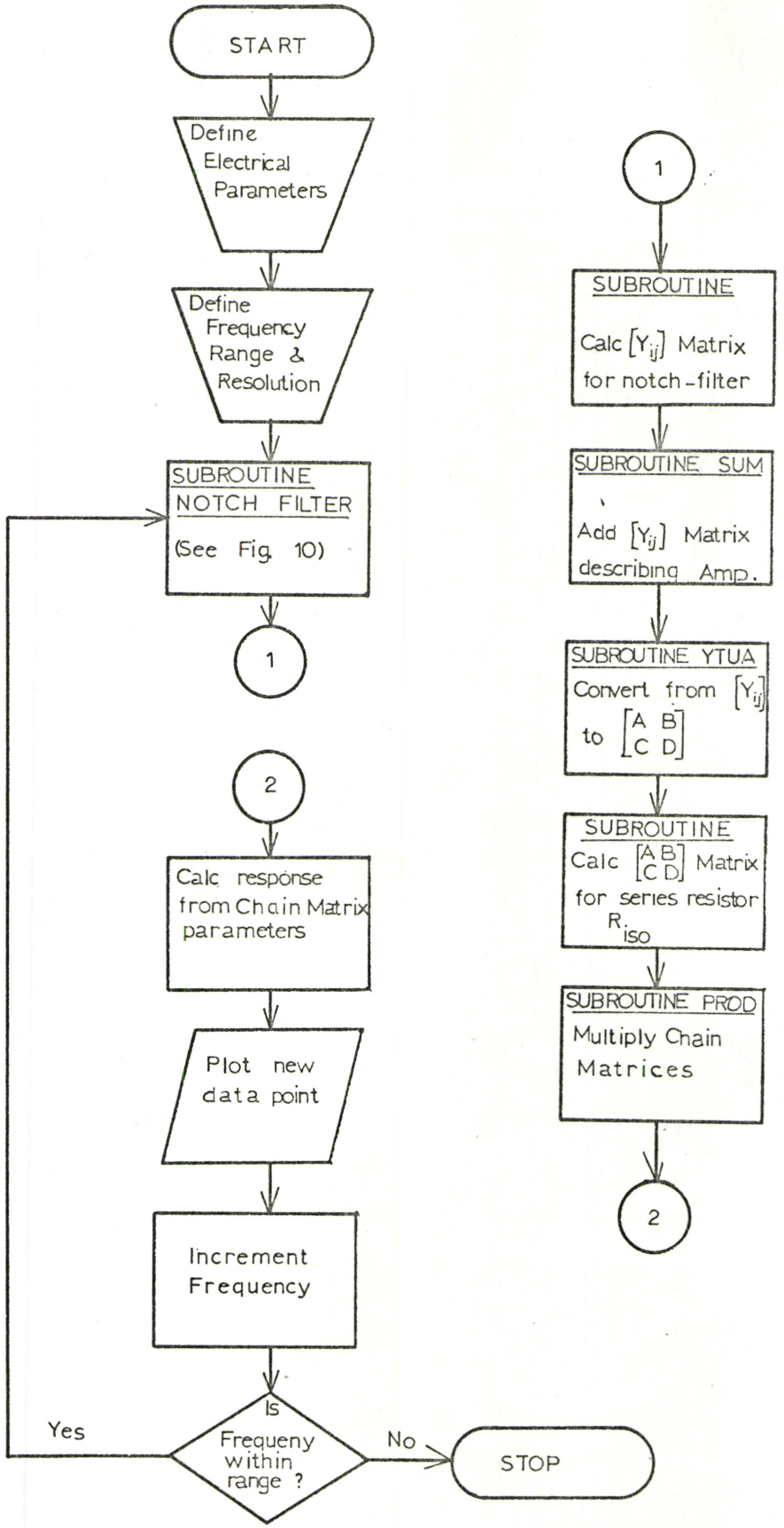
START
Define Electrical Parameters
Define Frequency Range & Resolution
SUBROUTINE NOTCH FILTER
(See Fig. 10)
1
2
Calc response from Chain Matrix parameters
Plot new data point
Increment Frequency
Is Frequeny within range ?
Yes
No
STOP
1
SUBROUTINE
Calc [Yij] Matrix for notch-filter
SUBROUTINE SUM
Add [Yij] Matrix describing Amp.
SUBROUTINE YTUA
Convert from [Yij] to [A B; C D]
SUBROUTINE
Calc [A B; C D] Matrix for series resistor Riso
SUBROUTINE PROD
Multiply Chain Matrices
2

CHAPTER V

URC LOW-PASS AND URC NOTCH FILTER CONSTRUCTION AND EVALUATION

5.0 Introduction

This Chapter is devoted to the practical details of construction and evaluation of the passive distributed filters.

5.1 Design and Construction

URC elements were constructed using Teledeltos paper for the resistive layer, Mylar film as the insulator material and brass foil for the conducting plane, and were held clamped between two sheets of 1/4 inch 'Perspex'. Using these materials the distributed parameter networks could be built quickly and cheaply and any design modifications (when they were required) usually involved nothing more drastic than the judicious application of a pair of scissors. These structures accurately model the behaviour of the evaporated thin film devices and because of the scaling involved (the Teledeltos-Mylar models are much larger than the equivalent thin film devices) are a much more convenient size to work with.

Vacuum coating techniques[23] were not employed for the fabrication of the URC elements because these methods are time consuming, require considerable expertise and are rather inflexible in that any changes in the structure geometry (except layer thickness) would require the manufacture of a new set of shadow masks -- a task in itself.

Several factors were considered in the design of these structures. It was important for these networks to operate at frequencies commensurate with the (0.3 - 32) MHz range of the automatic network analyser system used to experimentally evaluate their performance. The operating frequency is governed by the characteristic radiancy of the structure ω_o, defined by equation (3.28). If the width of the structure is W and the length L then the distributed resistance and capacitance per unit length are defined by equations (5.0) and (5.1), where P_s is the sheet resistivity of the Teledeltos (ohms/sq.), t is the thickness of dielectric and ε_r the relative permittivity.

$$r_o = \frac{P_s}{W} \tag{5.0}$$

$$c_o = \frac{\varepsilon_o \varepsilon_r WL}{t} \tag{5.1}$$

Substituting equations (5.0) and (5.1) into (3.28) yields an expression for ω_o as a function of the structure dimensions.

$$\omega_o = \frac{t}{\varepsilon_o \varepsilon_r P_s L^2} \tag{5.2}$$

The decision to use Mylar and Teledeltos paper (chosen because these materials were readily available) automatically defined the values of ε_r and P_s so that the characteristic radiancy was primarily controlled by L the length of the structure. The choice of t, the thickness of the dielectric, afforded some additional control. It should be noted that the characteristic radiancy ω_o is independent of the structure width W.

The choice of structure dimensions also governed the characteristic impedance Z_o. When these distributed circuits are used as feedback networks they load the amplifier, so the characteristic impedance should be made as high as possible. Unfortunately, high impedance levels make measurements more difficult by aggravating the loading effects of the signal sensing probes. The final design was a compromise between these conflicting requirements. Substituting equations (5.0) and (5.1) into (3.11) yields

$$Z_o = \frac{P_s t}{\varepsilon_o \varepsilon_r W^2} \tag{5.3}$$

Note that the characteristic impedance is primarily governed by the width of the stucture W, but the thickness of the dielectric film t, is another controlling factor. The characteristic impedance is not influenced by the length of the structure L.

The accuracy to which these structures can be built is limited. Inaccuracies due to marking and cutting errors and due to stray capacitances will be increased in designs with wide width-to-length ratios. As non-uniformity of distributed capacitance is largely attributed to the inability to apply uniform pressure to the structure, the layout of the $\overline{\text{URC}}$ was designed to be compact and occupy as small an area as possible. All these factors indicated that the structure should be square, i.e., the width and length should be the same.

It was necessary to use a resiliant pad between the Perspex and the Teledeltos to ensure that the Teledeltos was held firmly against the Mylar to obtain a uniformly distributed capacitance. Ordinary foam backed household place mats were ideal for this purpose. Eccobond solder (type

Figure 23 Photograph of URC constructed from Mylar film and Teledeltos paper.

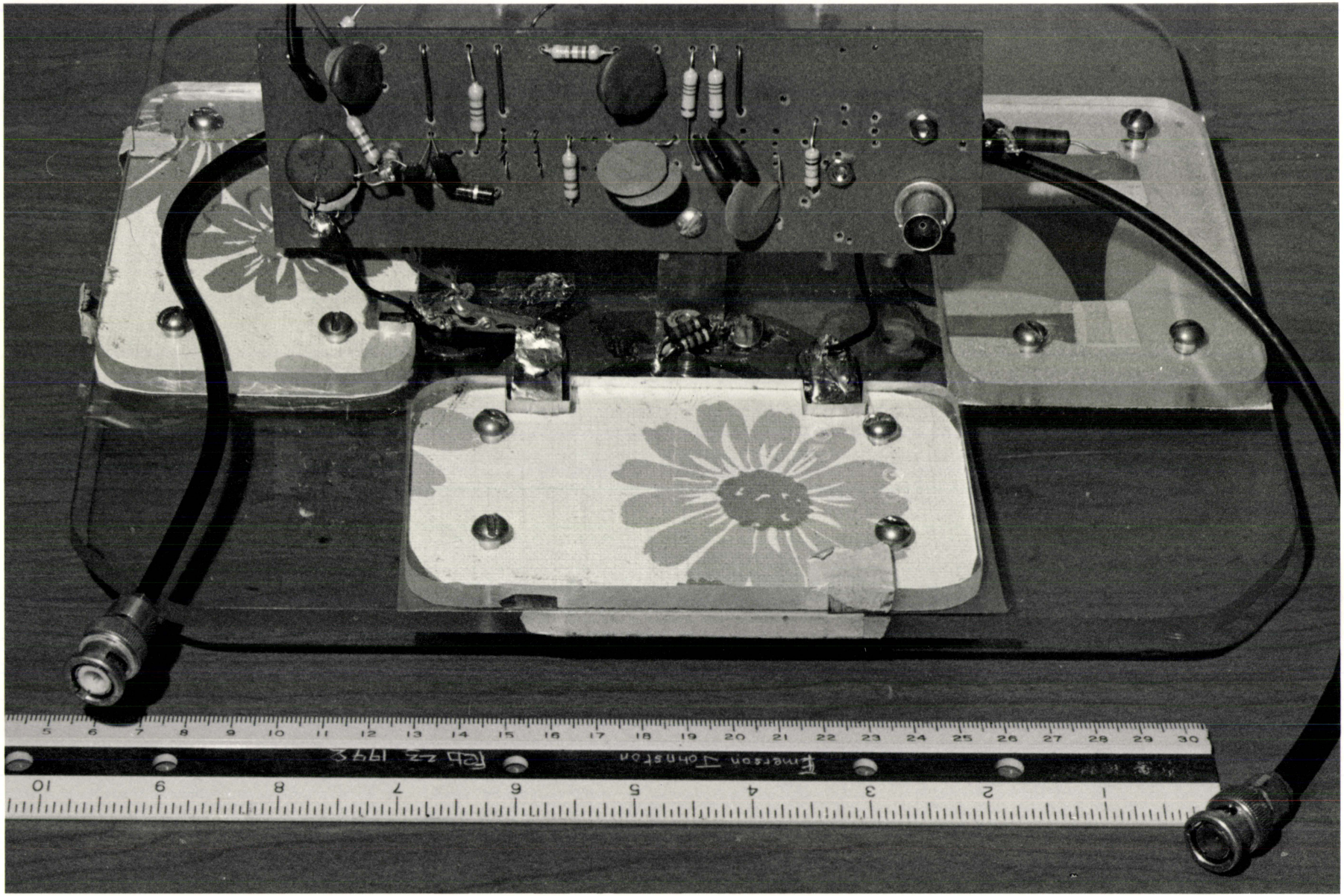
Emerson Johnston
Feb 22 1992

#56C) was used to obtain low contact resistance between the Teledeltos paper and the brass foil equipotential strips. Thick copper strips were used to obtain low impedance connections between the URC conducting plane and the BNC connectors. For the final design the length and width of the structure were chosen to be 4.6 cms and 3/1000" Mylar was used, yielding a theoretically predicted notch at 1.4 MHz. A photograph of the actual structure is shown in Figure 23.

Initially miniature carbon potentiometers were used to obtain the required value of notch resistance, but they were unsatisfactory as they were difficult to adjust to the precision necessary to achieve a deep notch. Another problem associated with the use of these components was how to maintain the optimum condition once it had been achieved. Attempts to seal the potentiometers in wax were unsuccessful because the value of resistance was perturbed. The problem was finally overcome by using two or three fixed carbon resistors in parallel combination to synthesis the required values of notch resistance.

5.2 Measurement of URC Parameters

5.2.1 Capacitance:

The dielectric properties of the Mylar and hence the distributed capacitance of the $\overline{\text{URC}}$ are frequency dependent. In order to compare the theoretically predicted notch frequency with the measured value, the distributed capacitance should therefore be measured at the notch frequency.

If the URC input terminals were connected to a capacitance bridge the values obtained would be a measure of the effective capacitance, C_{eff} associated with the reactive component of the input impedance, namely,

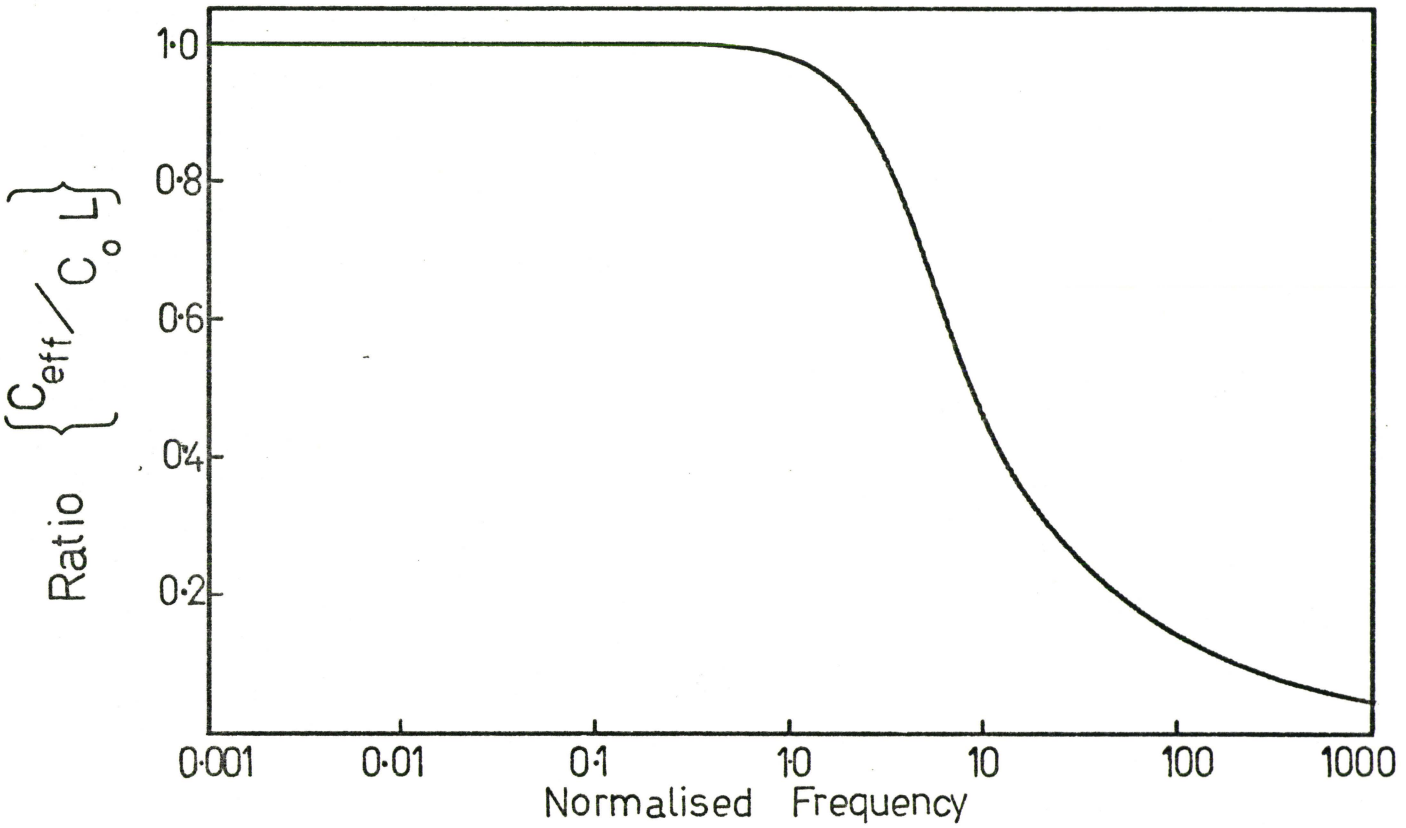

Figure 24 Ratio of URC Effective Input Capacitance C_{eff} to Total Distributed Capacitance $C_o L$ Evaluated Theoretically as a Function of Frequency

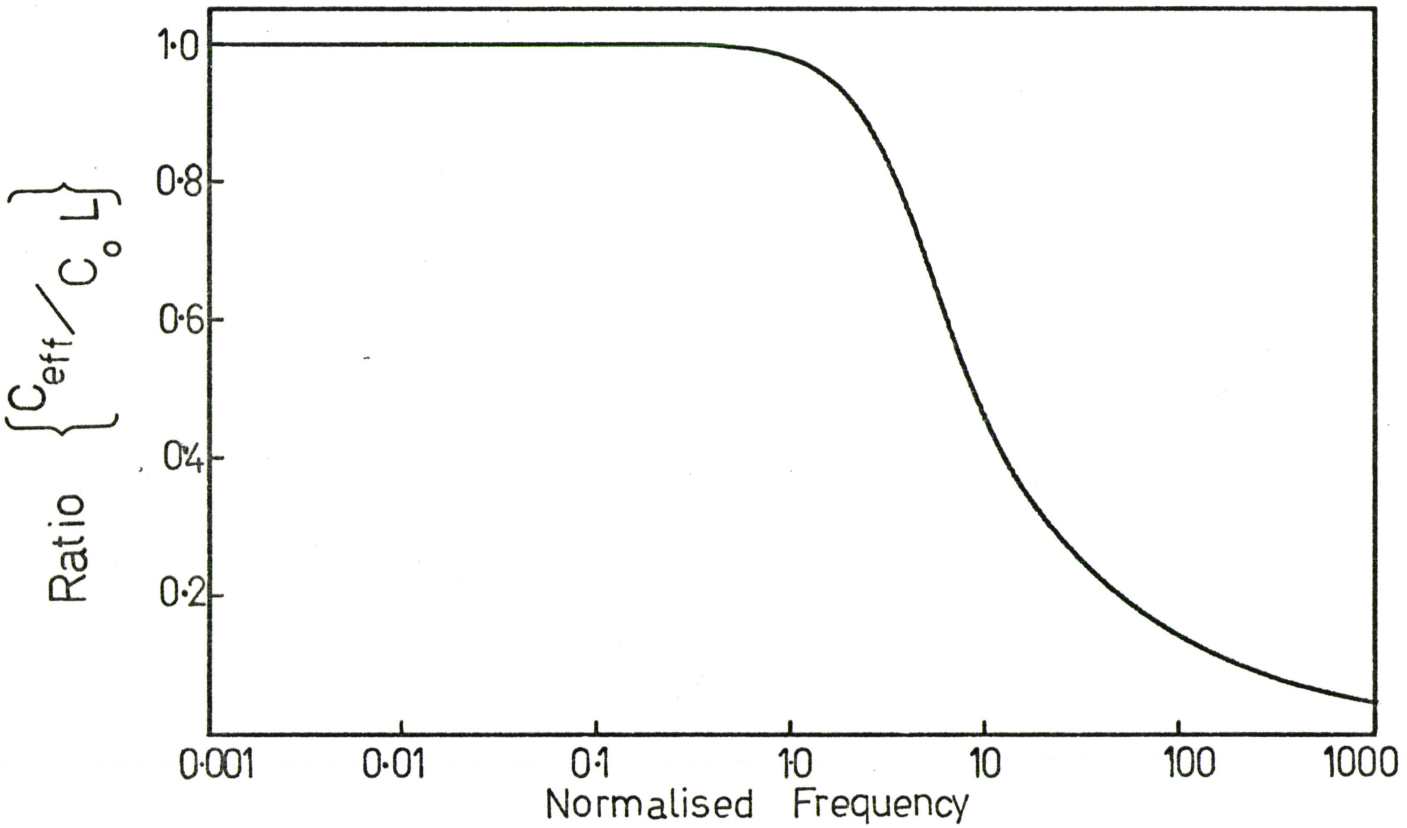

Figure 24 Ratio of URC Effective Input Capacitance C_{eff} to Total Distributed Capacitance $C_o L$ Evaluated Theoretically as a Function of Frequency

$$I_m[z_{11}] = -\frac{1}{2\pi f C_{eff}} \tag{5.4}$$

Combining equation (5.0) with equation (3.20) yields an expression for effective capacitance as a function of frequency, equation (5.5)

$$C_{eff} = -\frac{1}{2\pi f \, I_m\{Z_o \coth \gamma L\}} \tag{5.5}$$

The ratio of C_{eff}/C_oL was then evaluated as a function of normalized frequency (Figure 24). The ratio does not depend on the relative size of the distributed resistance and capacitance, only on the normalized frequency. At normalized frequencies much less than 1, the ratio becomes 1, so that the effective capacitance is equal to the total distributed capacitance. At low frequencies the distributed resistance is insignificant in comparison to the capacitive reactance of the structure.

The distributed capacitance was measured by measuring the effective capacitance C_{eff} of the input impedance at a frequency of 100 Hz. To correct for the change of capacitance with frequency a capacitor was constructed with similar geometry to the URC, but with the Teledeltos paper replaced by a sheet of brass foil. A capacitance bridge, General Radio Type GR 1615A, was used to obtain the capacitance and dissipation measurements as a function of frequency. From Figure 25 it can be seen that there was a 5% decrease in capacitance over the frequency range 100Hz to 1.0MHz.

5.2.2 Dielectric Losses

A nonideal capacitor may be represented by the equivalent circuit shown in Figure 27, where G represents the total leakage conductance

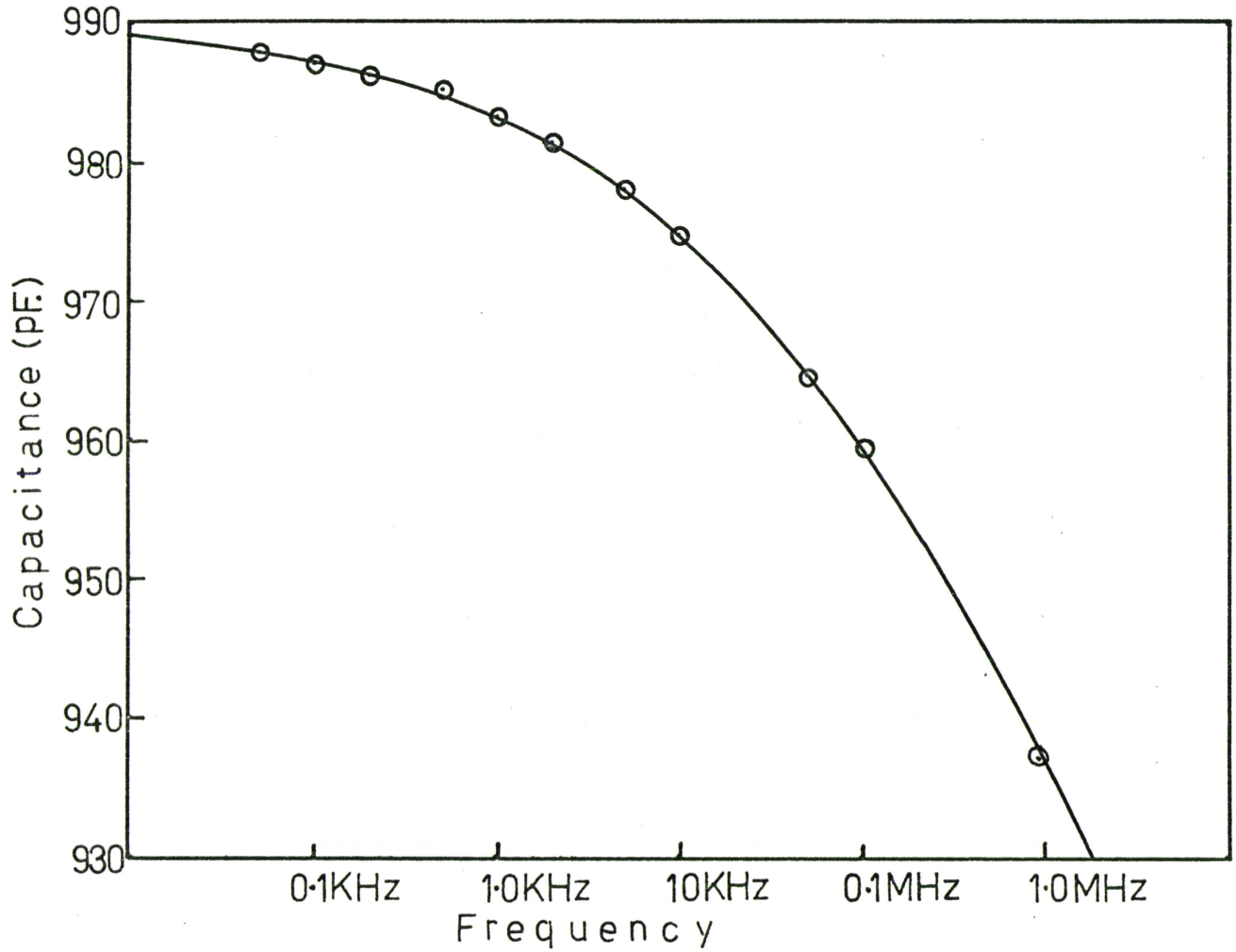

Figure 25 Graph of Capacitance vs. Frequency For a capacitor using Mylar film

and R_s the effective dielectric loss parameter. The dissipation factor D for the capacitor is defined by

$$D = \omega R_s C \tag{5.6}$$

and is frequency dependent. Carson[18] has investigated the influence of dielectric loss on the response of the network, as a function of the parameter B defined by

$$B = \frac{R_s}{r_o L} \tag{5.7}$$

The value of R_s was calculated from the dissipation factor (see equation (5.6)) and plotted as a function of frequency (Figure 26). At 1 MHz, R_s was 1.10^{-2} ohms and B less than 5.10^{-6} so from Table 1 it can be seen that the dielectric losses had negligible influence on the network response.

B	ω_n/ω_o	α_n
0	11.190	17.786
10^{-4}	11.200	17.865
10^{-3}	11.365	18.525
10^{-2}	13.791	29.960
1.5×10^{-2}	16.800	48.700

TABLE 1: Influence of B on Notch Filter Characteristic (After Carson[18])

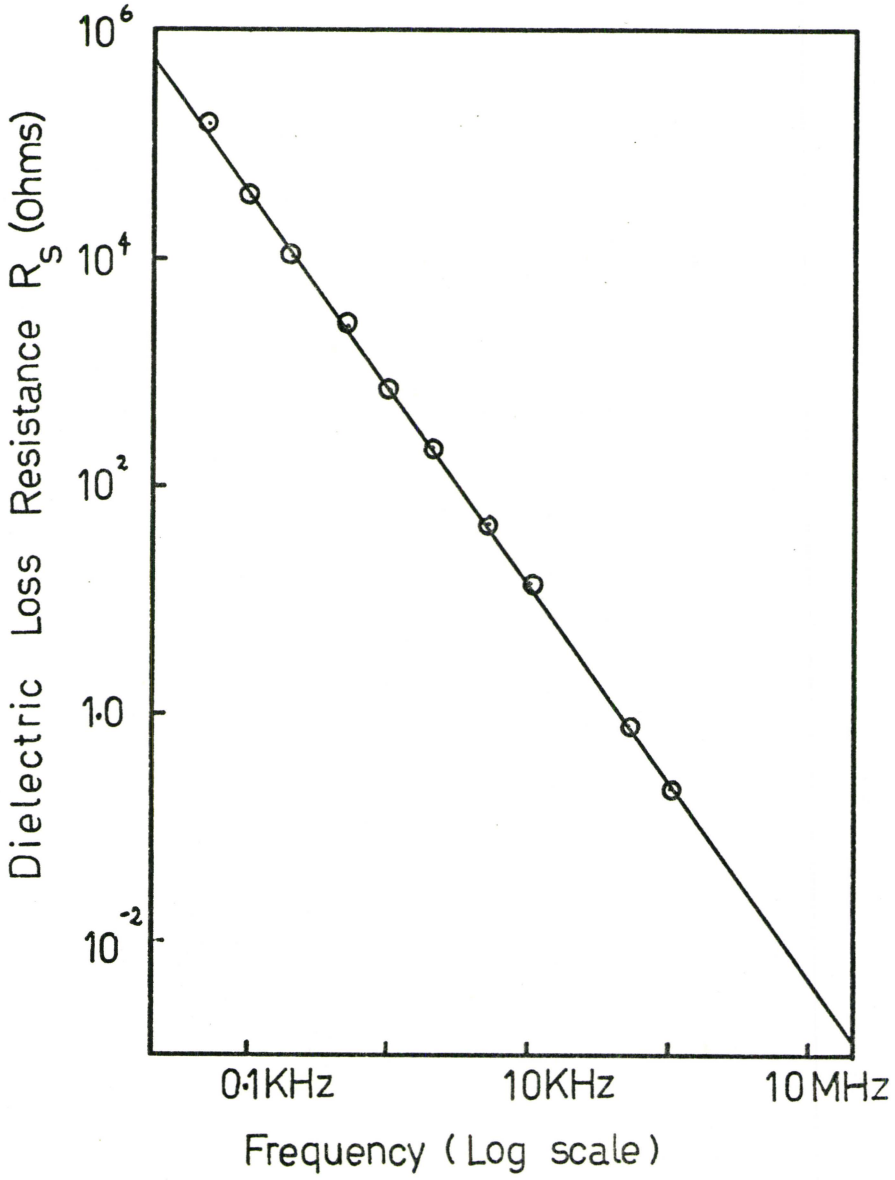

Figure 26 Effective Dielectric Loss Resistance R_S for Mylar Capacitor Measured for Different Frequencies

5.2.3 D.C. Leakage Conductance:

The influence of D.C. leakage conduction on the notch filter response has also been studied by Carson[18], who defines a parameter A such that

$$A = Gr_oL \qquad (5.8)$$

where G is the total leakage conduction. He has shown that for $A < 0.1$ the leakage effects are negligible.

A digital multifunction meter, Hewlett Packard type H.P. 3450A, was used to measure this leakage. The value of $G = 5.10^{-9}$ MHOS was obtained and this resulted in a value of 1×10^{-5} for A; hence leakage effects could be neglected as being insignificant.

5.3 Open Circuit Voltage Transfer Function Measurements

5.3.1 Introduction:

An automatic network analyser system was used to obtain the filter characteristics experimentally. Sweep frequency techniques were particularly useful in locating the optimum notch condition.

The block schematic diagram for the system is shown in Figure 28. It consists of a sweeping signal generator, Hewlett Packard HP 675A, a phase/amplitude tracking detector, HP 676A, and two high impedance voltage probes HP 1123A. In addition, a log-converter, Hewlett Packard 7562A was used to obtain a logarithmic frequency display on the 'scope. This was necessary for the Bode presentation of the filter characteristics. A photograph of the measurement system is shown in Figure 29.

It was found necessary to use slow sweep rates in order to obtain accurate measurements in the region of the null.

Equivalent Circuit for Lossy Capacitor

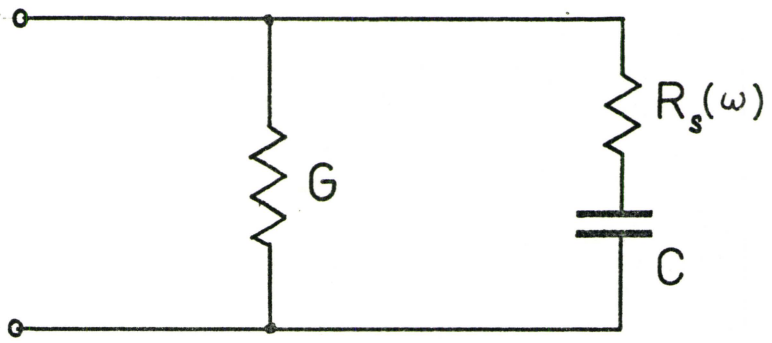

Where G represents Leakage Conductance
C " Capacitance
R_s " Dielectric Losses (which are frequency dependent)

Figure 27

Using the logarithmic frequency display it was difficult to obtain good photographs of the oscilloscope traces because of the non-uniform progression of the 'spot' across the screen.

5.3.2 URC Low-Pass Filter:

The low-pass characteristic of the $\overline{URC}$ structure is shown in Figure 30. The presence of a spurious notch was detected at 16 MHz. This was due to the small but finite contact resistance to the bottom plate of the $\overline{URC}$[18]. This non ideal behaviour will have had some influence on the performance of the URC phase shift oscillator; the filtering action will be adversely effected. However, because this notch occurred at a very much higher frequency than the frequency of oscillation and because the attenuation was still better than 40 dB these effects should be negligible.

5.3.3 URC Notch Filter:

The notch filter characteristics for three different values of notch resistor are shown in Figures 31, 32, and 33. Figure 33 represents the deepest notch and is the nearest to the optimum notch condition. In the region of the notch the phase characteristic rises sharply indicating that the actual value of R_n was very slightly greater than the optimum value. The notch resistance R_n was 93Ω. Using the measured values for the distributed resistance and capacitance, the theoretical notch frequency was calculated. The notch frequency was measured using an electronic counter, Hewlett Packard Model 5216A.

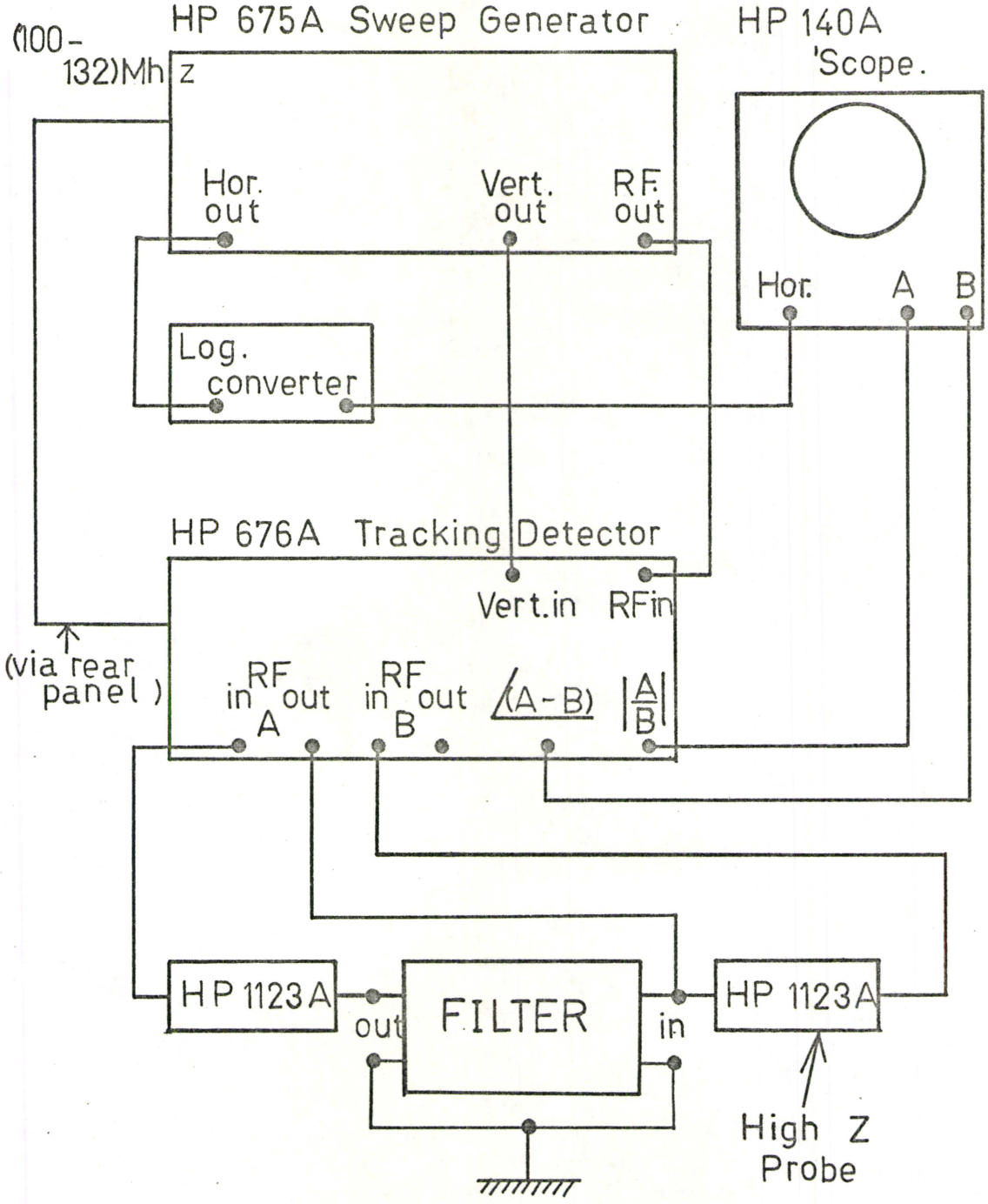

Figure 28 Open-Circuit Voltage Transfer Function Measurement

Figure 29 Photograph of the Automatic Network Analyser used to obtain open-circuit voltage transfer function measurements.

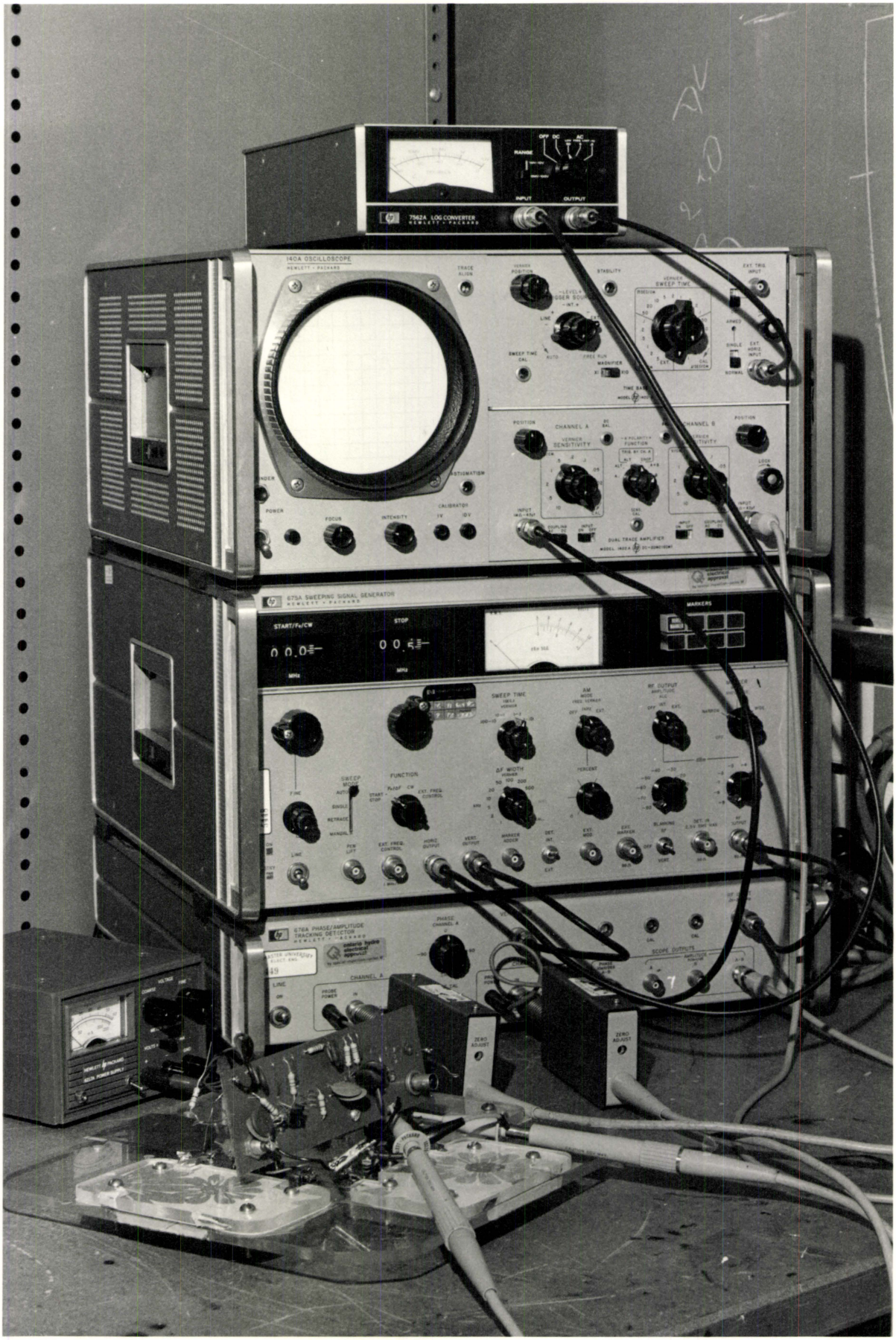
7562A LOG CONVERTER
HEWLETT-PACKARD
INPUT
OUTPUT
140A OSCILLOSCOPE
HEWLETT-PACKARD
675A SWEEPING SIGNAL GENERATOR
HEWLETT-PACKARD
START/Fo/CW
STOP
MARKERS
SWEEP TIME
FUNCTION
RF OUTPUT
CHANNEL A
CHANNEL B
DUAL TRACE AMPLIFIER
676A PHASE/AMPLITUDE
TRACKING DETECTOR
HEWLETT-PACKARD
CHANNEL A
ZERO ADJUST
SCOPE OUTPUTS

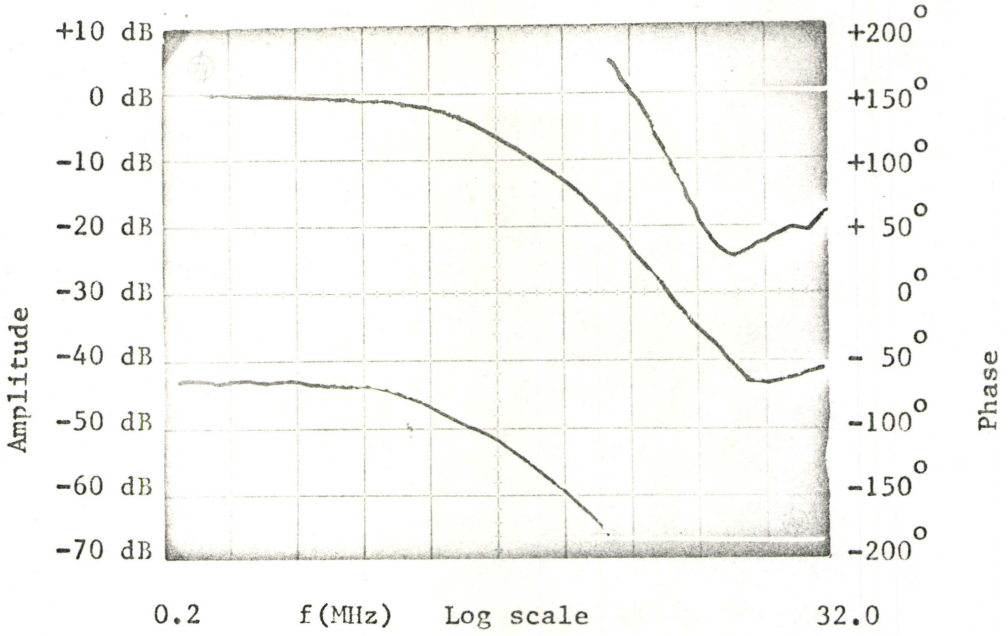

Figure 30

URC Low pass filter
Distributed C=850 pF
Distributed R=1676 ohms

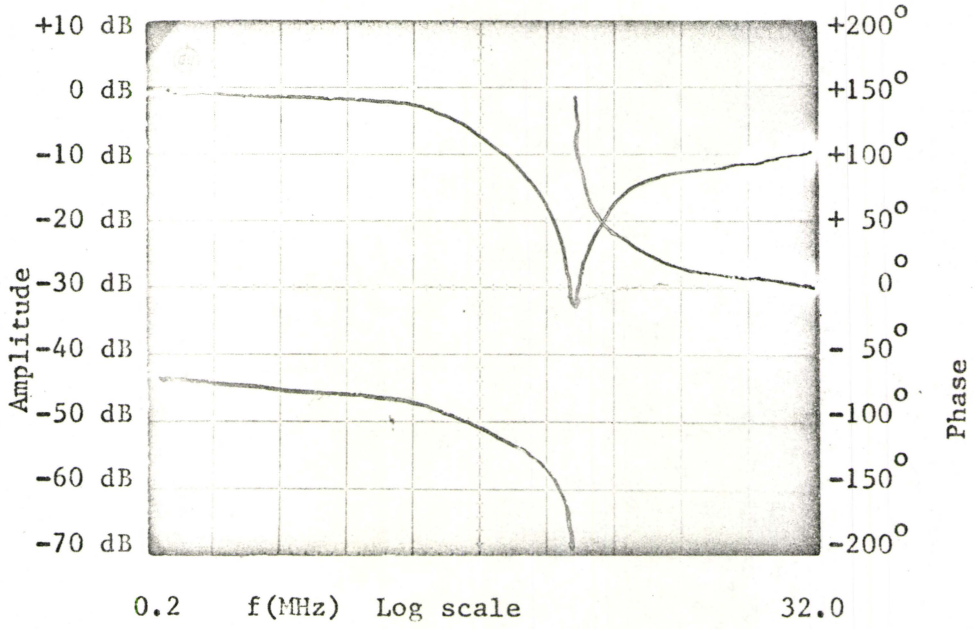

Figure 31

URC Notch filter Rn= 68 ohms
Distributed C=850 pF
Distributed R=1676 ohms.

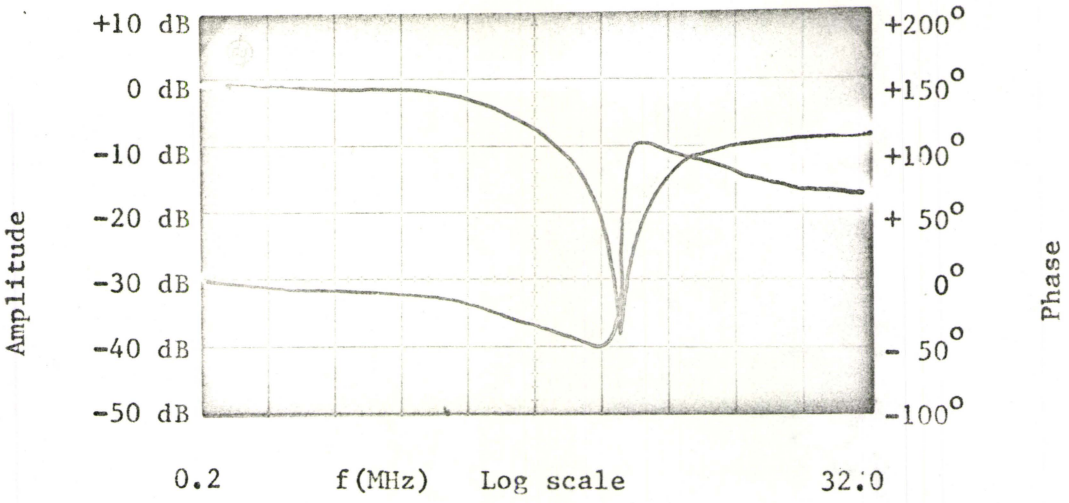

Figure 32

URC Notch filter Rn = 97 ohms
Distributed R = 1676 ohms
Distributed C = 850 pF.

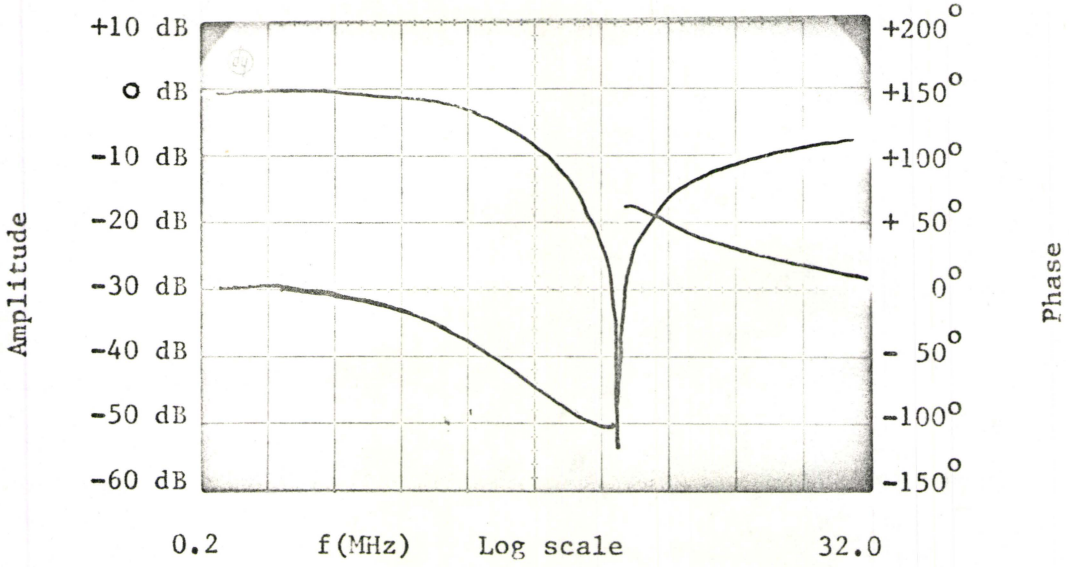

Figure 33

URC Notch filter Rn = 93 Ohms
Distributed R = 1676 Ohms.
Distributed C = 850 pF.

Notch Filter Parameters (Measured)

Total distributed resistance r_oL	1.676 KΩ
Total distributed capacitance c_oL	850 pf
Notch resistance R_n	93Ω
Bandwidth	19.5 KHz
Q Factor	63

	Theoretical	Measured
Notch Frequency	1.250 MHz	1.236 MHz
Notch Parameter	17.786	18.020

TABLE 2: Comparison of Measured and Theoretical Notch Characteristics

The experimental results obtained show close agreement with theory and emphasise the suitability of Mylar Teledeltos models.

The phase response of the filter (Figure 33) would indicate that the notch parameter α was slightly less than 17.78, the measured value of 18.02 can be explained by the error introduced into the measurement of the distributed resistance due to the presence of a finite contact resistance, the actual value of distributed resistance being slightly less than 1.676 KΩ. (This also implies that the theoretical notch frequency should be higher.)

The presence of some parasitic inductance in the notch impedance can explain the discrepancy between the measured and predicted notch frequencies[19].

CHAPTER VI

CONSTRUCTION AND EVALUATION OF ACTIVE CIRCUITS

6.0 Introduction

This chapter is devoted to the practical aspects of the construction and evaluation of the distributed parameter feedback circuits. The method of experimentally determining the open loop response is described. The high frequency compensation necessary in order to obtain a stable band-pass characteristic, and the influence of the notch and amplifier parameters on the band-pass characteristic are considered.

6.1 Open Loop Measurements

6.1.1 Introduction:

In order to determine the open loop response the output of the feedback network should be terminated with the impedance that it would 'see' when the loop is closed. For the oscillator circuits the open loop should be terminated with the amplifier input impedance, while for the band-pass circuit the loop should be terminated with the parallel combination of the amplifier input, and the signal generator impedance with the resistance R_{iso}. It was therefore necessary to know the amplifier input impedance. Having correctly terminated the network the open loop response was obtained using the system shown in Figures 28 and 29.

6.1.2 Amplifier Input Impedance:

A simple parallel combination of resistance r_{in} and capacitance c_{in} was used to model the amplifier input impedance. In principal the

values of R_{in} and C_{in} could be found by comparing the voltage developed across a known resistance (connected in series with the amplifier) with that across the input terminals of the amplifier (see Figure 34). In order to minimize the effects of loading, high impedance probes were required. However, as only one probe was available it was necessary to modify the technique because the phase information could not be obtained. Instead, the values of R_{in} and C_{in} were found by comparing the magnitudes of the voltage across the known resistance and the amplifier input at two different frequencies.

Even though a high impedance probe (Tektronix P6045) was used, it still loaded the network at frequencies greater than 5 MHz. (This was detected by monitoring the output level of the amplifier and observing the reduction in signal level when the probe was shunted across the input.)

This loading was attributed to the shunt capacitance of the probe which was of the same order of magnitude as the capacitance across the amplifier input. The probe conductance was very much smaller than that of the amplifier and so had negligible effect.

The experimental system used to measure the input impedance is shown in Figure 35. C_p was the small 5 pf capacitor which was used to simulate the loading effects of the probe. To measure V_1 the switch S_1 is connected to position 1 and the capacitor C_p is connected to the amplifier input terminals. To measure V_2 the switch S_1 is connected to position 2 and the capacitor C_p is disconnected from the amplifier input.

The equivalent circuit for the system used to measure the amplifier input impedance is shown in Figure 34. By inspection, the ratio of V_2 to V_1 is defined by

Measurement of Amplifier Input Impedance

Principle

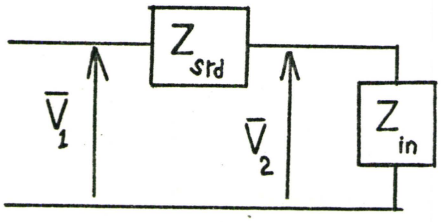

where :—

Z_{std} Know Impedance

Z_{in} Amplifier Input Impedance

Thus $$Z_{in} = \frac{\bar{V}_1 - \bar{V}_2}{\bar{V}_2}$$ Phase information is required

Equivalent Circuit for Actual Measurement System

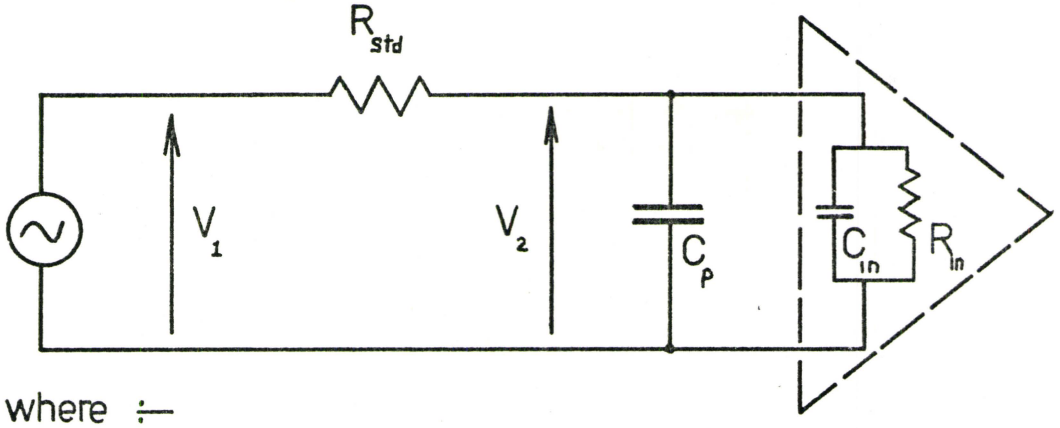

where :—

R_{std} Known Resistance

C_p Probe Capacitance

(C_{in} , R_{in}) Unknowns used to model input impedance

Figure 34

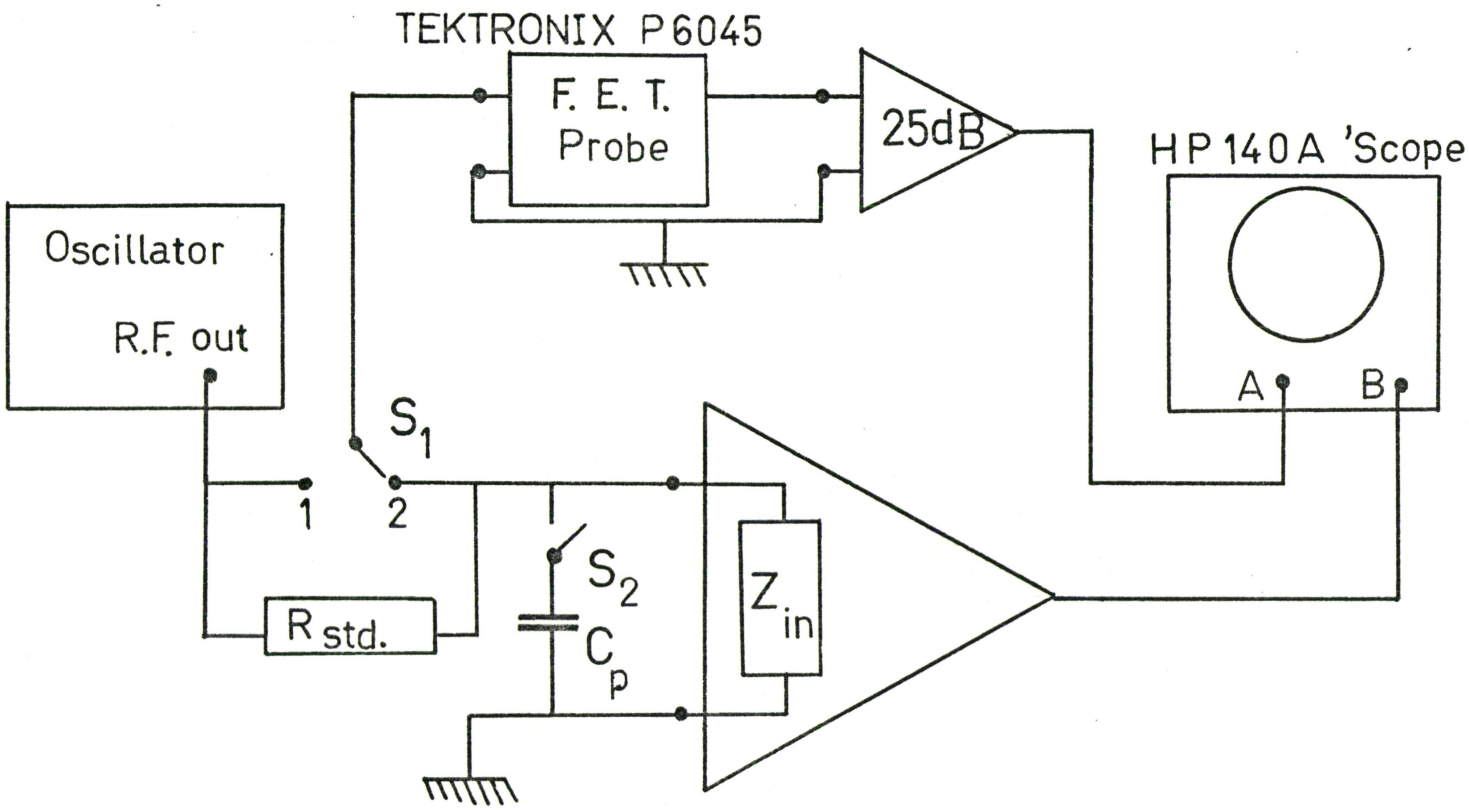

Figure 35 Amplifier Input Impedance Measurement.

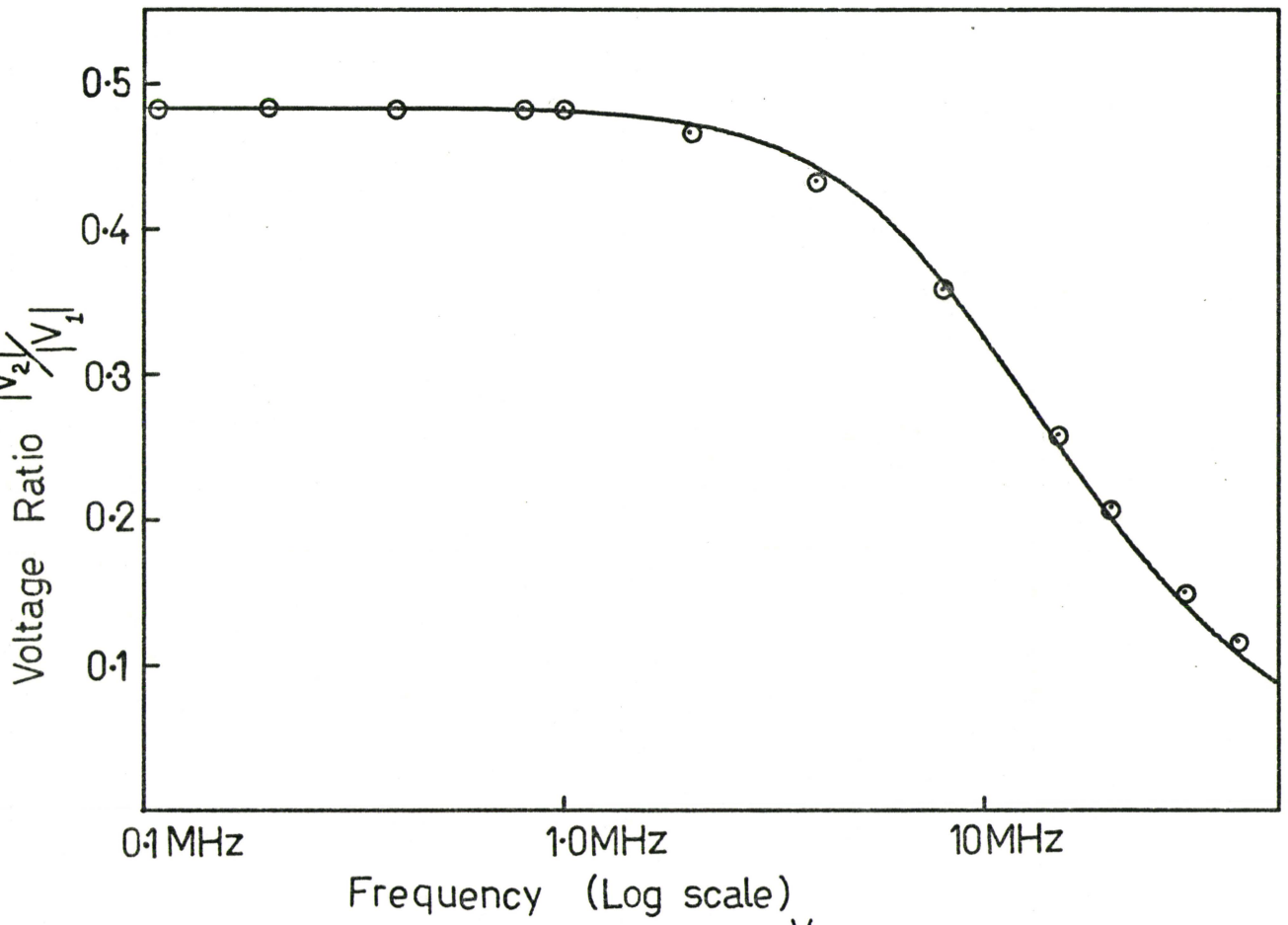

Figure 36 Measured & Calculated Values of V_2/V_1 vs Frequency

Where C_{in}=10pF C_p=5pF R_{in}=2·25K $R_{std.}$=2·41K (see Figure 34)

$$\frac{|V_2|}{|V_1|} = \frac{\left| \frac{R_{in}}{1 + j\omega R_{in}(C_p + C_{in})} \right|}{\left| R_{std} + \frac{R_{in}}{1 + j\omega R_{in}(C_p + C_{in})} \right|} \qquad (6.0)$$

At low frequencies this reduces to

$$\frac{|V_2|}{|V_1|} = \frac{R_{in}}{R_{std} + R_{in}} \qquad (6.1)$$

Hence R_{in} may be found. Knowing R_{in}, C_{in} can be obtained by solving equation (6.0) knowing the ratio of the voltages measured at a higher frequency.

R_{std} was measured using a multifunction meter, Hewlett Packard HP 3450A. The values for the input impedance were found to be

$$R_{in} = 2.25\ K\Omega$$

$$C_{in} = 10\ pf$$

The theoretical response associated with these values was evaluated as a function of frequency and compared with experimental values, (Figure 36) and the close agreement confirms the validity of this simple equivalent circuit.

6.1.3 Control of Loop Gain:

To control the overall level of gain in the loop a resistive potential dividernetwork was incorporated in the amplifier input. (In adjusting the overall loop gain the potentiometer setting affected the

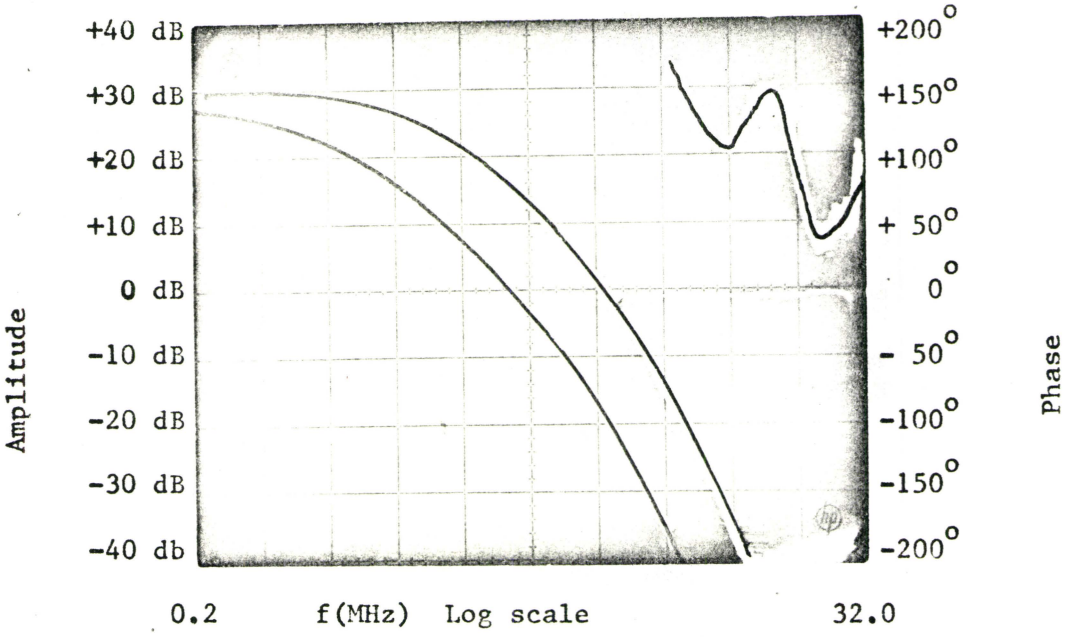

Figure 37 URC Phase shift oscillator open loop response Gain Margin -15dB
Rdist. 1676 ohms Cdist. 850 pF

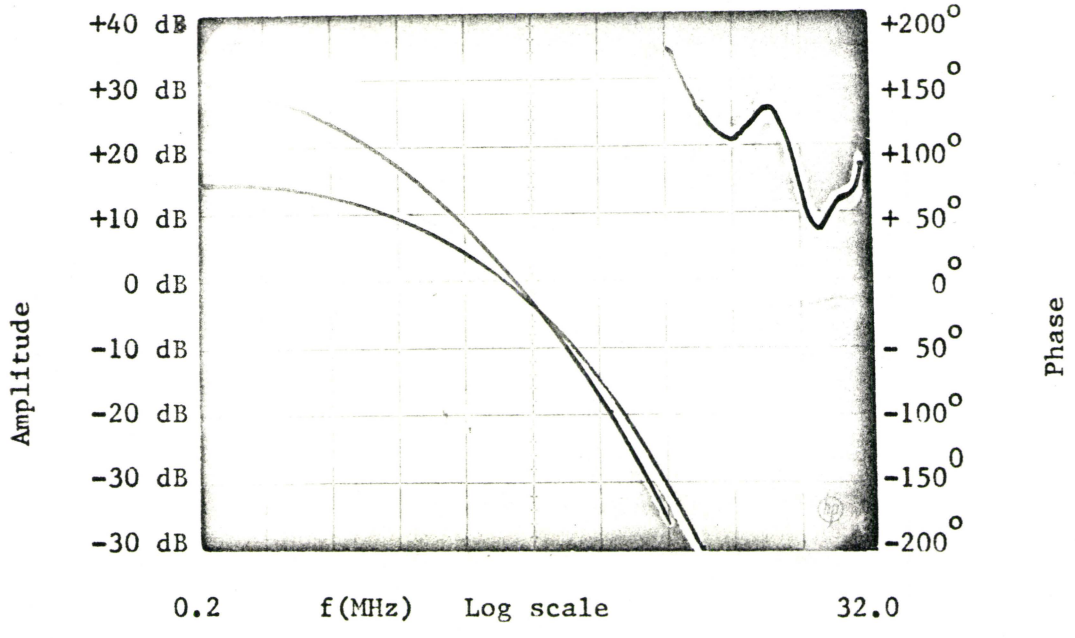

Figure 38 URC Phase shift oscillator open loop response limiting case Gain Margin 0dB
Rdist. 1676 ohms Cdist. 850 pF

	URC Phase Shift Oscillator.	URC Notch Oscillator.
Signal at Amplifier Out-put. Scale 0.5 V / div.	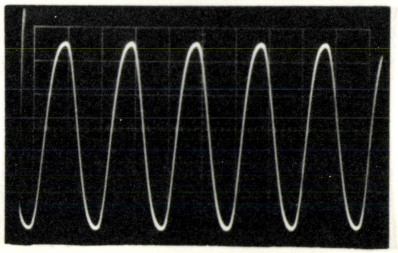	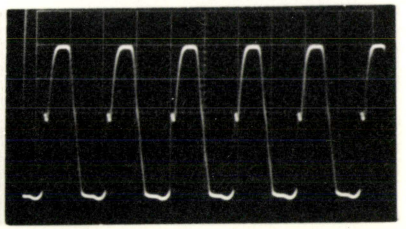
Signal at Amplifier In-put. Scale 0.1 V / div.	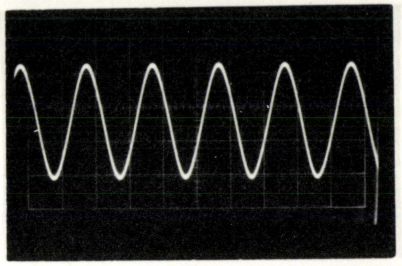	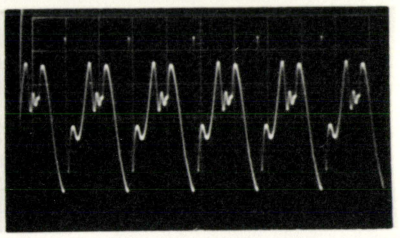
	frequency 1.001 MHz.	frequency 1.080 MHz.

Figure 39

amplifier input impedance and so the open loop terminations had to be adjusted accordingly.)

6.2 Oscillators

6.2.1 URC Phase Shift Oscillator:

The URC oscillator was set up with the loop gain adjusted to a large value to ensure oscillation. This use of excessive gain caused the amplifier to overload and so the oscillator output was of poor quality. The open loop response was measured and it was seen that the loop gain was 15 dB in excess of the value required to sustain oscillation (Figure 37).

In order to check the validity and accuracy of the Bode stability analysis the circuit was connected in closed loop and the amplifier gain was progressively reduced until there was just sufficient gain to sustain oscillation. The open loop response associated with this condition may be seen in Figure 38. Note that at the frequency at which the loop phase shift is zero the loop gain has fallen to 0 dB just as expected.

This was the limiting case so that the gain was increased by several dB before the loop was closed and the oscillator was subjected to further tests.

The oscillator wave forms derived at the amplifier output and after filtering by the phase-shift network may be seen in Figure 39. Note the presence of distortion due to amplifier non linearity which was effectively removed by the filtering action of the URC. The frequency of oscillation was measured using an electronic counter (Hewlett Packard 5216A) and found to be 1.008 MHz. This is in contrast to the value of

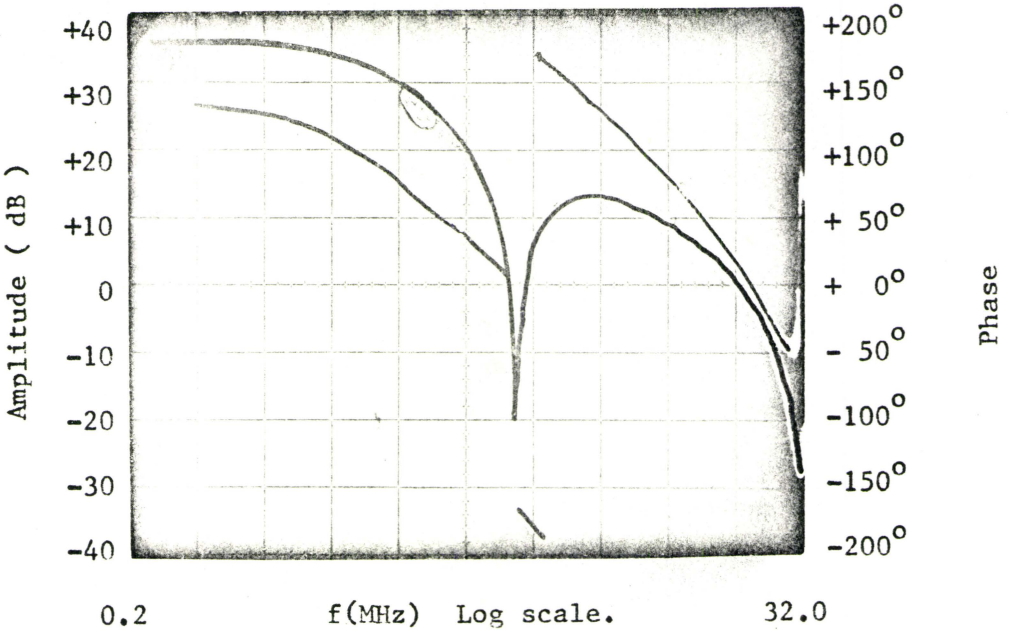

Figure 40. URC Notch Oscillator limiting case gain margin 0dB R_n=88ohms R_{dist}=1676ohms C_{dist}=850 pF.

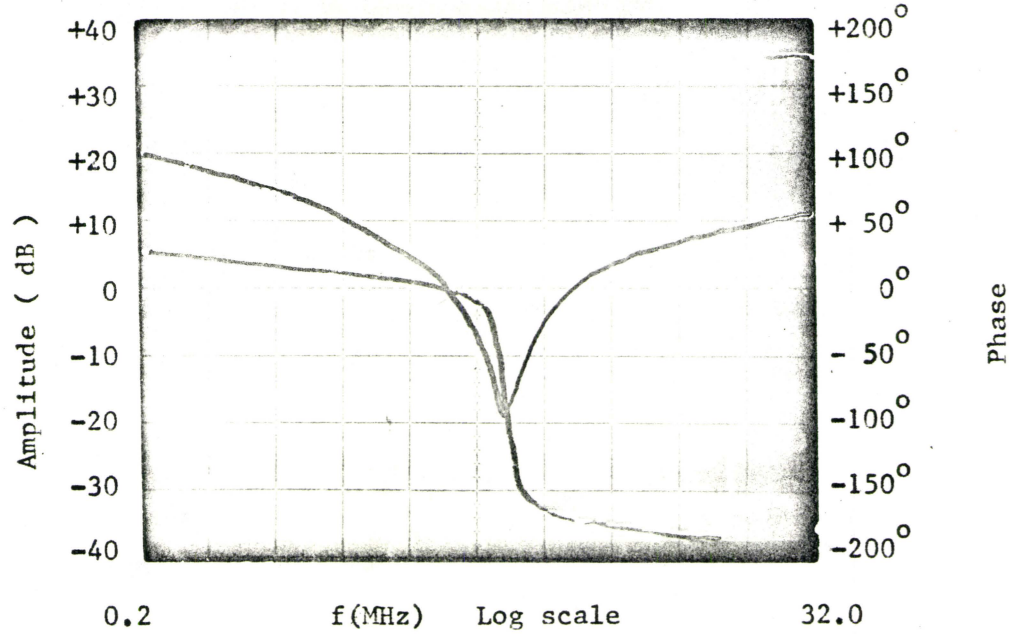

Figure 41. URC Notch Oscillator open loop response frequency scale expanded in the region of the null.

2.2 MHz predicted by equation (4.3). The large discrepancy is primarily due to the amplifier phase shift which at 1 MHz had fallen to 115°.

From Figure 7 it can be seen that the URC has a phase shift of -115° at a normalized frequency of $\omega/\omega_o = 9.9$. This value would predict an oscillation at 1.1 MHz. The small difference between this and the experimental value is due to excessive amplifier gain which will create a reduction in the frequency of oscillation.

The spectrum analysis system shown in Figure 43 was used to obtain an indication of the short term oscillator frequency stability. The spectrum analyser required an external V.F.O. signal and this was obtained from the Hewlett Packard HP 8601A signal generator. An indication of the residual F.M. of the oscillator output was obtained by using a relatively long exposure (30 seconds) when photographing the display from the spectrum analyser. The presence of any residual F.M. on the V.F.O. signal would contribute to the apparent residual F.M. of the oscillator under test so the V.F.O. should have good frequency stability. The V.F.O. signal was specified to have less than 50 Hz residual F.M. and the spectrum analyser output associated with this signal has been included for comparison purposes.

6.2.2 URC Notch Oscillator:

The URC notch filter was adjusted for maximum notch depth and with $\alpha \geq 17.786$ so that the phase response fell from 0° through -180° to -360°. The feedback path was then closed and the amplifier gain increased until oscillation was sustained. The open loop response of the system is shown in Figure 40. In Figure 41 an expanded frequency scale has been used to

URC Phase Shift Oscillator

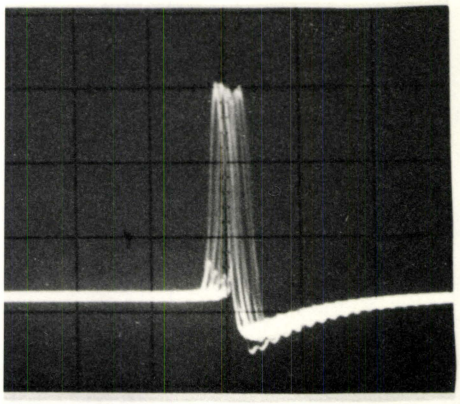

URC Notch Oscillator

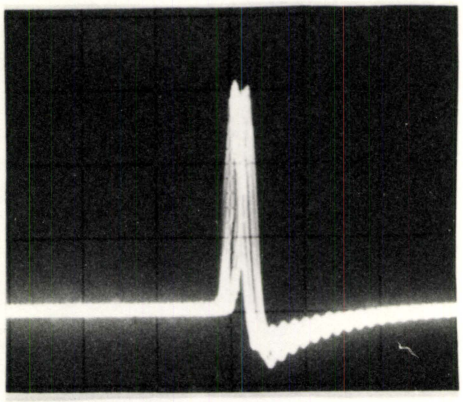

V.F.O. Signal (0.546 MHz.)

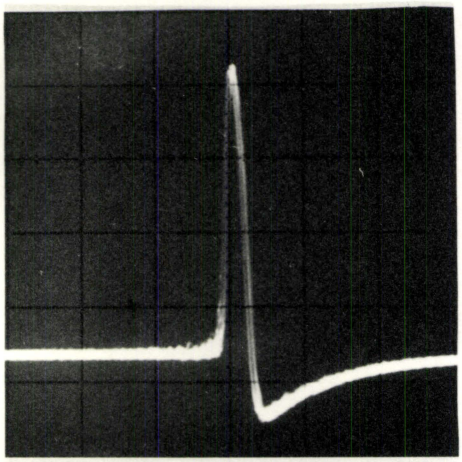

Scales: Horizontal 1KHz./cm. Vertical 10dB./cm.

Figure 42 Spectrum analysis of oscillator fundamental frequency. 30 second exposure used to indicate the amount of residual F.M. The V.F.O. signal is shown for comparison. Residual F.M. < 50 Hz

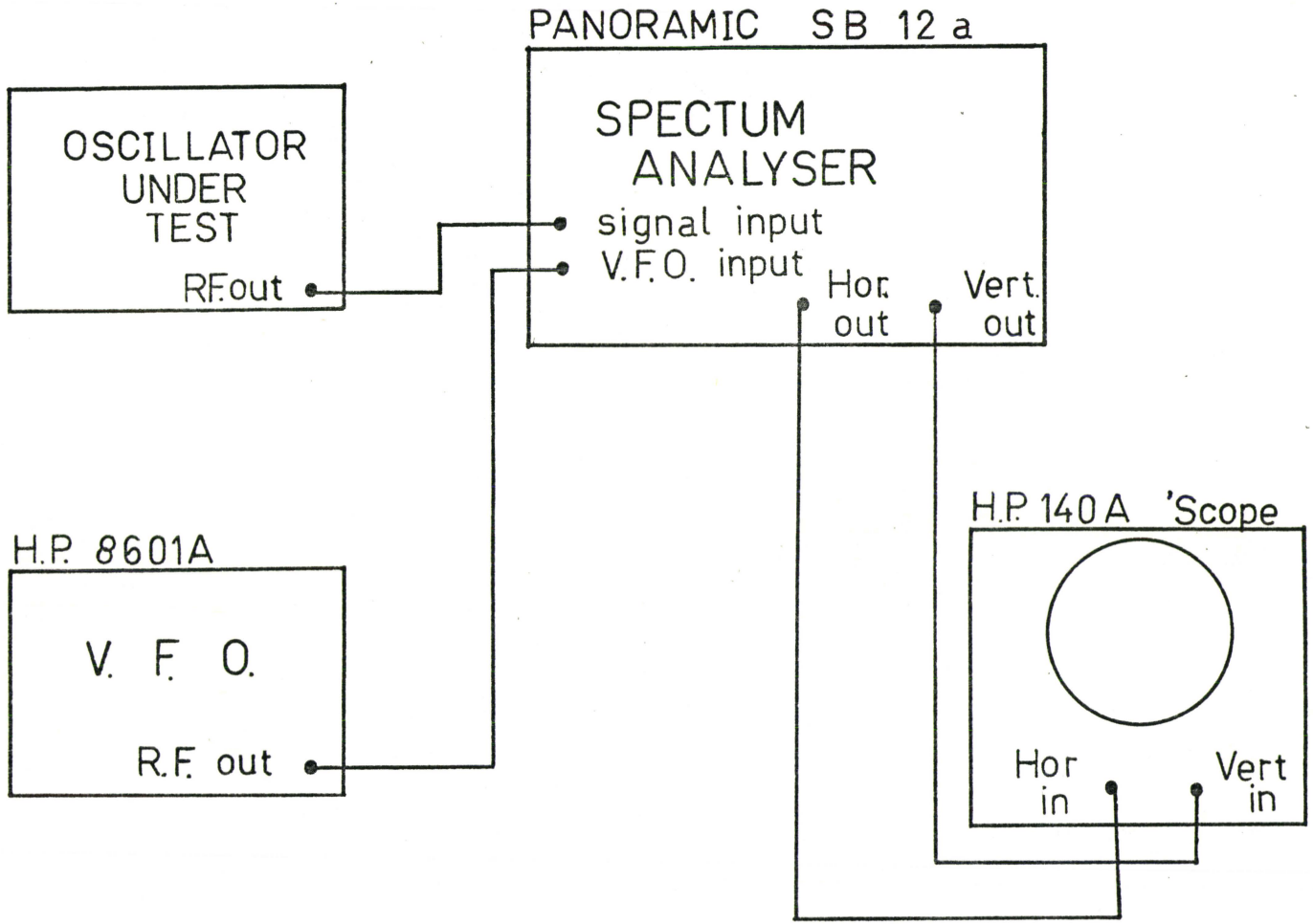

Figure 43 Spectrum Analysis Measurement

display the response in the region of the notch. It can be seen that the frequency of oscillation is not located in the region where the open loop phase response has the maximum steepness, but due to loss of amplifier phase shift the oscillation occurred at a lower frequency. Even so, Figure 42 shows that the residual F.M. associated with this design is an improvement over that of the $\overline{\text{URC}}$ phase shift oscillator. If frequency stability were a crutial design consideration amplifier phase compensation could be employed to counteract the loss of amplifier phase shift and insure operation in the region's steepest phase.

The oscillator waveform is shown in Figure 39. It is highly distorted by the presence of high frequency components (due to the non-ideal phase shift of the amplifier). Considerable improvement in spectral purity could have been achieved by using a low-pass filter to couple the oscillator to the load. This idea was not developed as the main object of the research was to design a stable band-pass amplifier. A study of the notch oscillator was only important in that it provided insight and understanding of the operation of the band-pass active filter, which also employed notch filter feedback.

6.3 Active Band-Pass Filter

6.3.1 Amplifier Compensation:

Initial attempts to set up the circuit in Figure 18 to obtain a band-pass filter characteristic were unsuccessful. The circuit was unstable and oscillated at high frequencies.

High frequency compensation was required to pull the system loop gain to 0 dB before the loop phase shift had fallen to 0 degrees. The

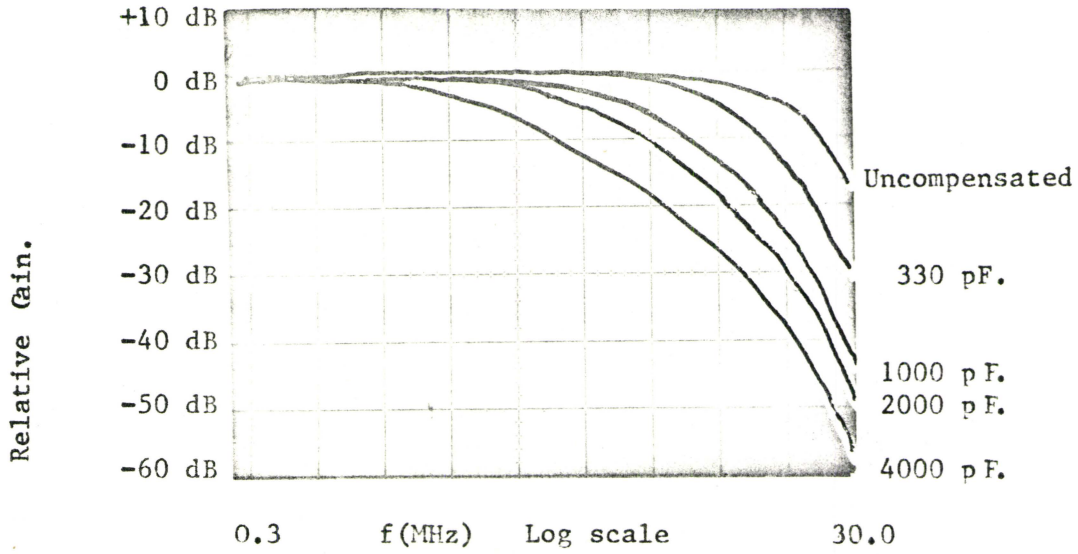

Figure 44

Amplifier response for various degrees of high frequency compensation. For convenience low frequency gain is is assigned value of 0 dB.

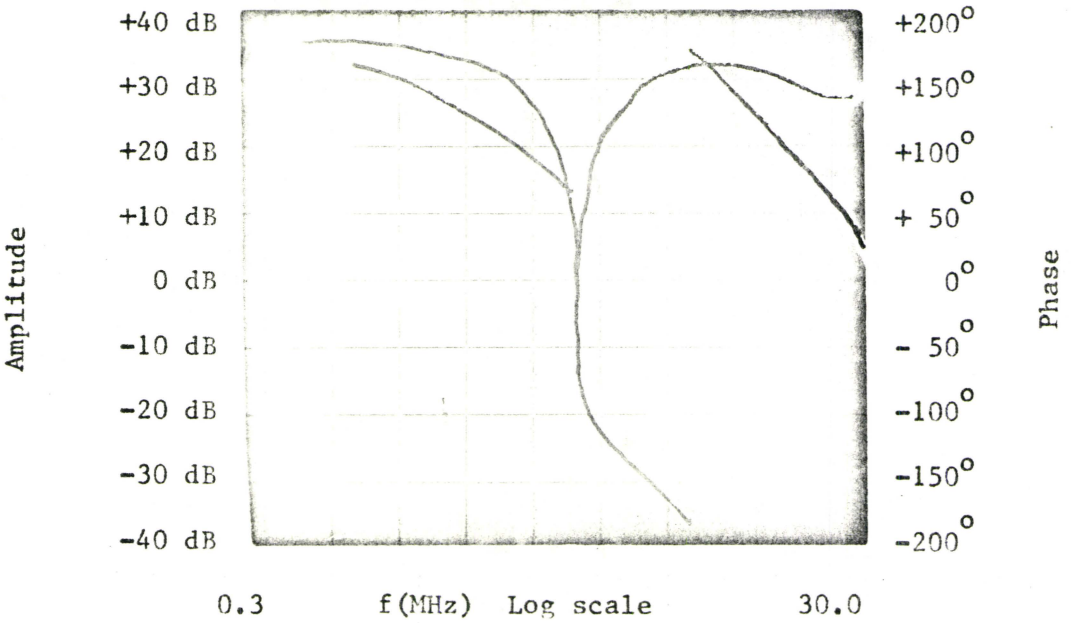

Figure 45

Bode plot of the open loop transfer fn. No amplifier compensation. Unstable.

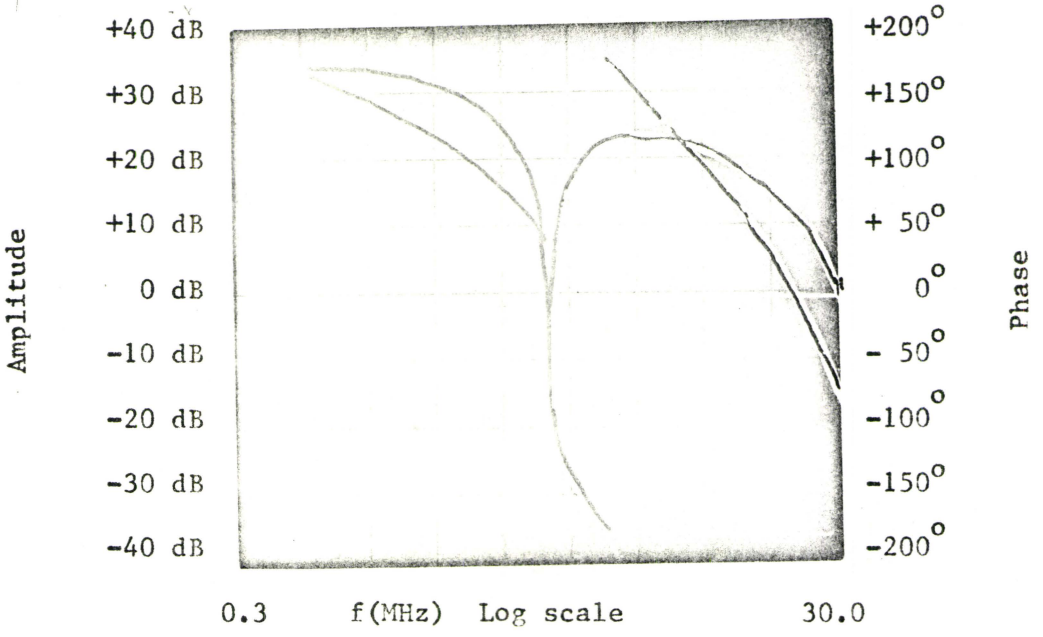

Figure 46 Bode plot of the open loop transfer fn. 1000 pF amplifier compensation. Unstable

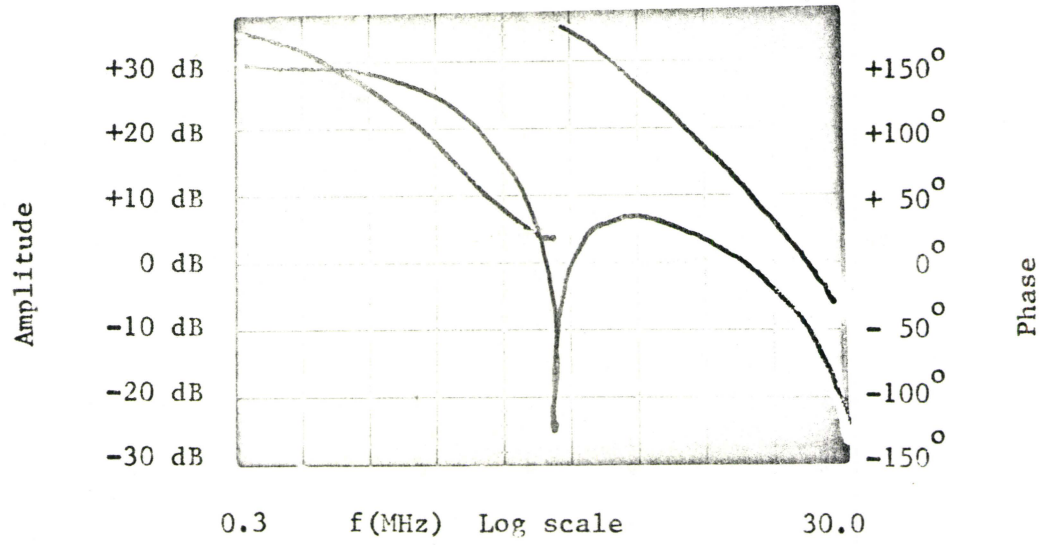

Figure 47 Bode plot of the open loop transfer fn. 5900 pF amplifier compensation. Stable Gain margin = 10dB Phase margin = 60°

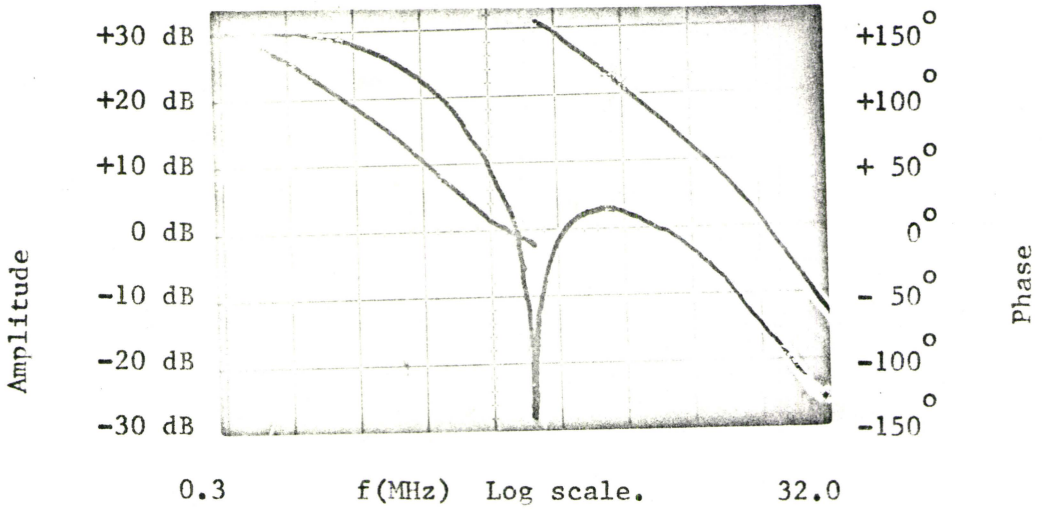

Figure 48

Bode plot of the open looptransfer fn.
Amplifier overcompensated (10,000 pF)
The system is verging on oscillation
at a frequency near the notch

wide band amplifier that was used for these experiments had been designed and tested by Mr. John Wragg[9] and it was he who implemented the necessary h.f. compensation.

The compensation was designed to reduce the amplifier gain at high frequencies. Figure 44 shows the relative gain of the amplifier under various degrees of compensation. The influence of this compensation on the system open loop response may be seen in Figures 45, 46, and 47. Only the system characterised by the response (shown in Figure 47) is stable.

It was possible by using excessive compensation to induce oscillation in the region of the notch frequency. This is difficult to understand if only the amplitude response is considered. However, compensation also modifies the system phase response; it causes a reduction in the loop phase shift, and when large amounts of compensation were employed the system phase shift fell to zero at the notch frequency and oscillation occurred. The circuit oscillated even though $\alpha < 17.78$ because the actual amplifier phase shift instead of being 180° had fallen to about 100 degrees at the notch frequency, resulting in zero phase shift round the loop (Figure 48).

6.3.2 Notch Parameter α:

The nature of the closed loop response is critically dependent on the value of the notch parameter because of its influence of the loop phase response. It has earlier been shown that the choice of notch parameter $\alpha \geq 17.786$ produces positive feedback at the notch frequency and this feature was exploited in the design of the URC notch oscillator: By limiting the loop gain so that oscillation is not sustained, a form of

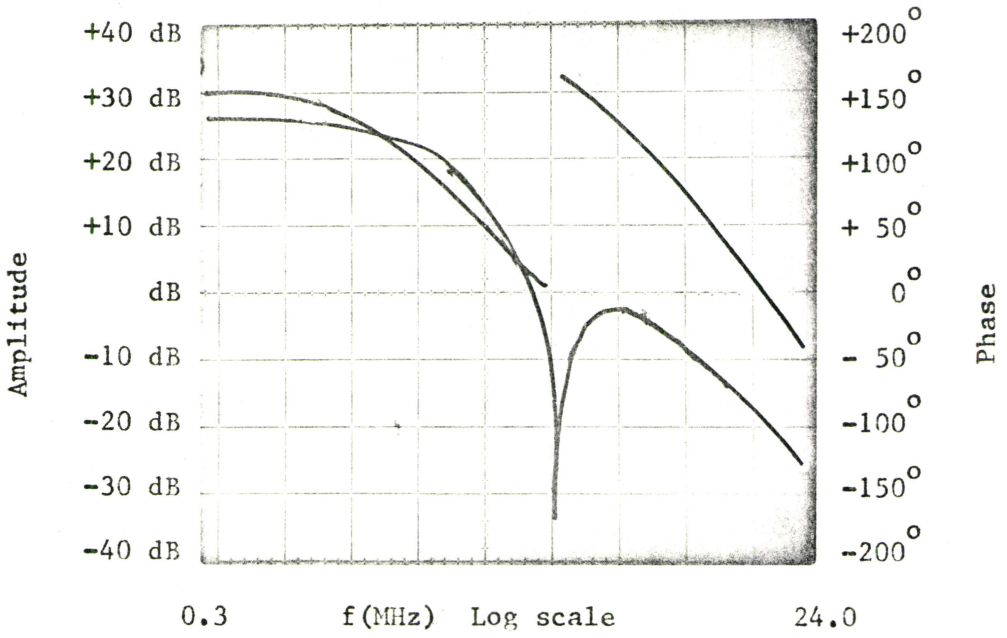

Open loop transfer function .

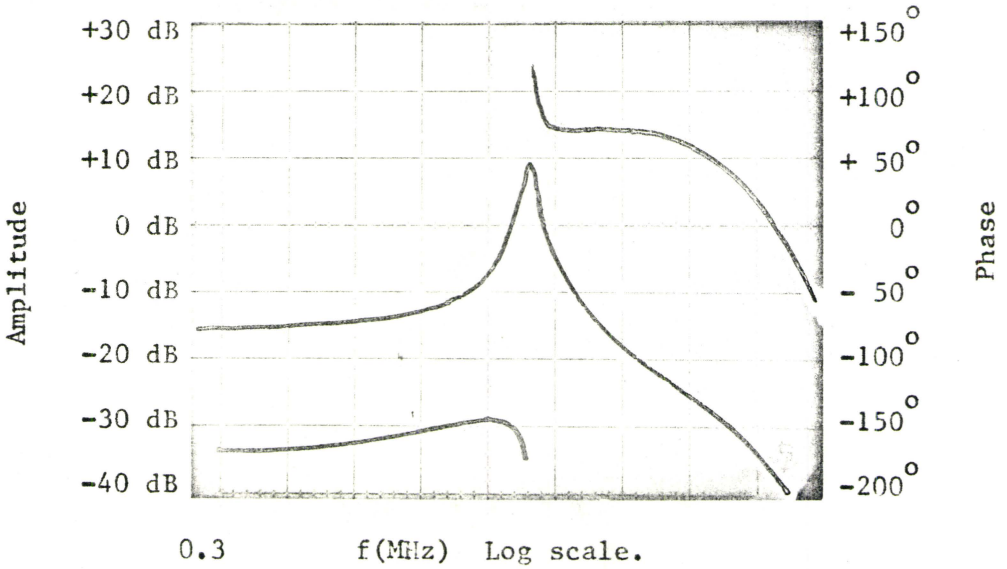

Closed loop response amplifier low freq. gain 25dB
Centre freqency 0.9123 Mhz. Q-factor 12.

Figure 49

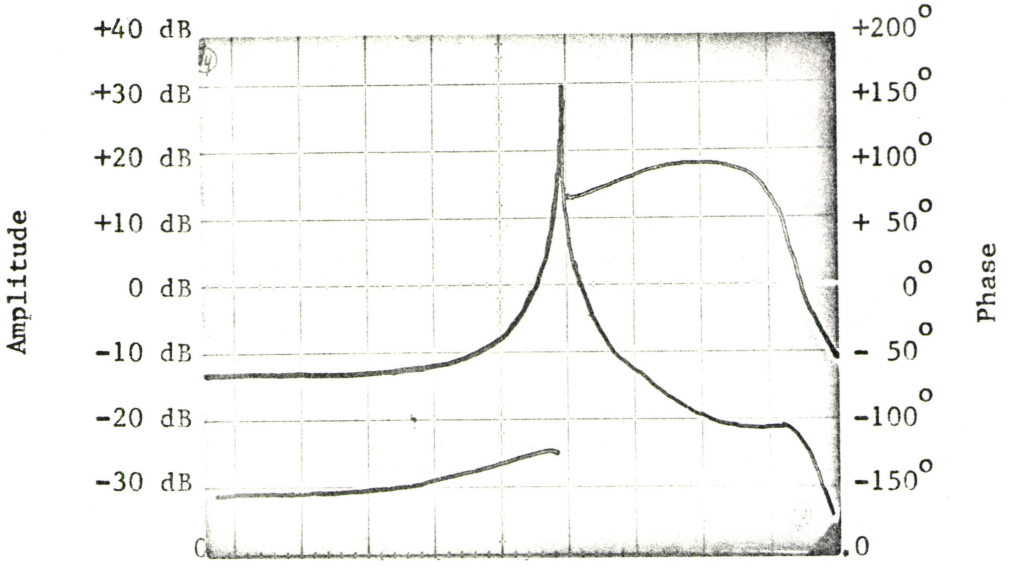

Open loop transfer function.

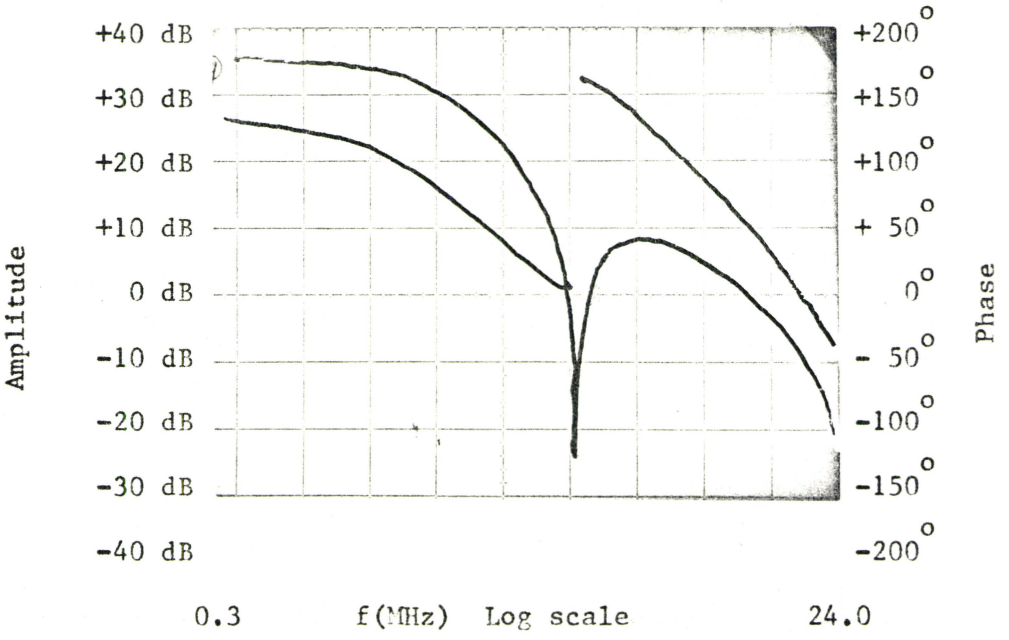

Figure 50 Closed loop response amplifier low freq. gain 35dB
Centre frequency 1.079 MHz Q - factor 50 .

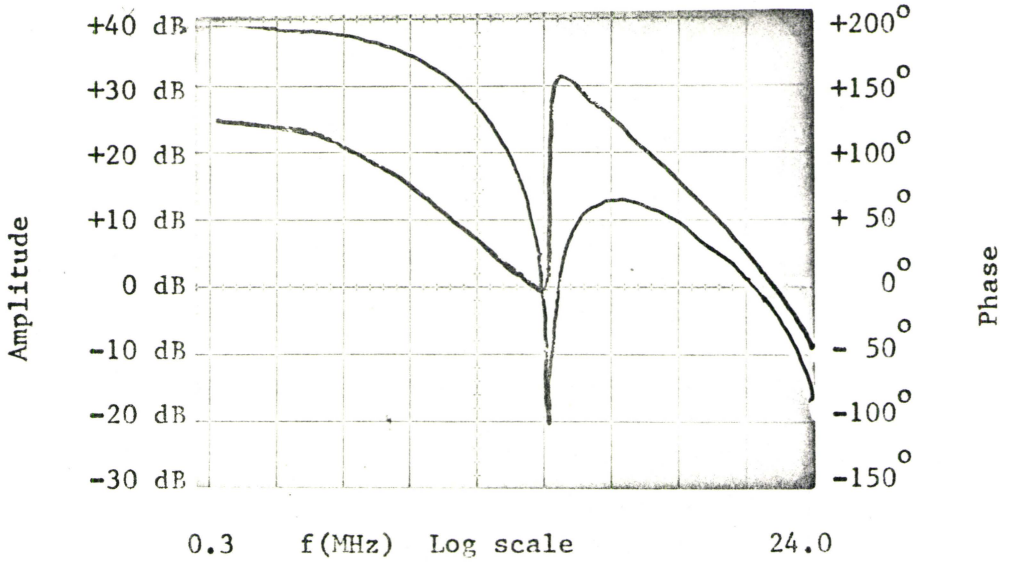

Open loop transfer function.

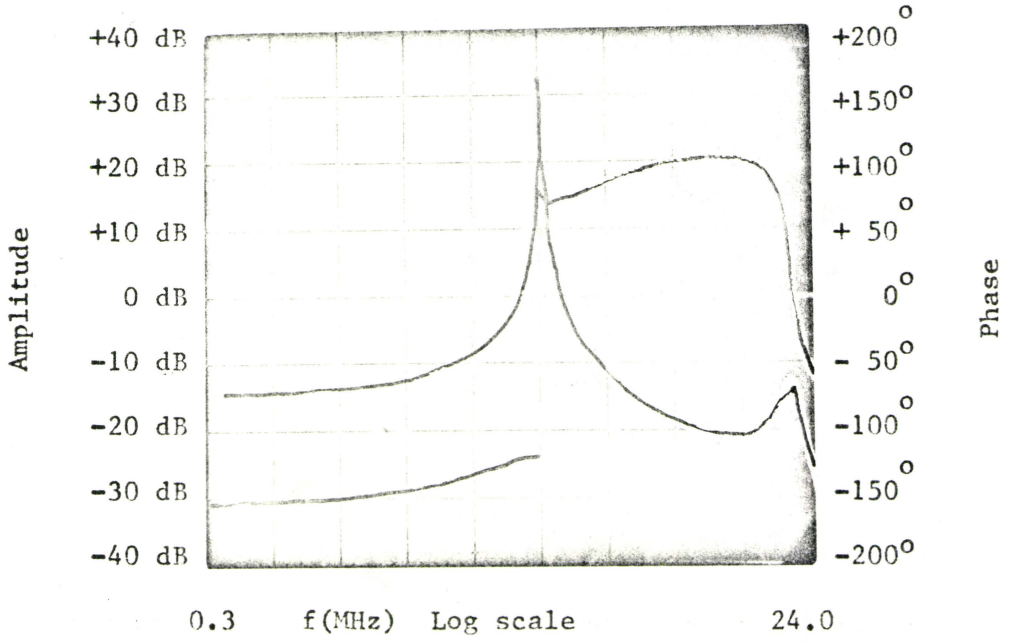

Figure 51 Closed loop response amplifier low freq. gain 40dB
Centre frequency 1.1764 MHz. Q factor 102.

band-pass characteristic is obtained. However, this design represents poor engineering practise as positive feedback is associated with problems of noise and parameter sensitivity.

Positive feedback can be avoided by restricting $\alpha < 17.786$ which constrains the notch filter phase shift to lie between approximately $\pm 90°$. In this discussion the phase shift of the amplifier has been assumed to be ideal (i.e., $\phi = 180°$), but any loss of amplifier phase will tend to create positive feedback even though $\alpha < 17.786$. The influence of the amplifier phase shift on the closed loop characteristic will be discussed later.

6.3.3 Isolating Resistance R_{ISO}:

This resistance serves two functions. It is necessary for the application of feedback, and it prevents the low impedance of the signal generator from loading the output of the URC notch filter by shunting the amplifier input impedance. R_{ISO} was chosen to be 10 KΩ, but the actual value used was not critical.

6.3.4 Non-Ideal Amplifier:

The frequency response of the active band-pass filter is influenced by the characteristics of the amplifier.

The influence of the amplifier input impedance and output impedance was not critical. The input impedance of the amplifier loads the URC notch filter, and since reasonable transfer characteristics were obtained when the notch filter was terminated in 50Ω, the actual impedance of 2.25 KΩ shunted with 10 pf introduced negligible loading at the frequencies associated with the notch.

Ideally, the amplifier output impedance should be as small as possible. An amplifier with high output impedance used to drive a low impedance load would result in a loss of effective gain. The amplifier output impedance was measured to be 12 Ω and as the input impedance of the notch filter even at high frequencies was greater than that of the notch resistance ($R_n \approx 90\ \Omega$), this introduced negligible amplifier loading.

The closed loop response was profoundly effected by the amplifier gain and phase shift. The influence of gain on the band-pass characteristic was investigated experimentally (see Figures 49, 50, and 51) and the salient features are summarized below (Table 3).

Amplifier Gain (at notch freq.) dB	Centre Frequency MHz	Mid Band Gain dB	Q
25 dB	0.912 MHz	10 dB	10
35 dB	1.079 MHz	29 dB	50
40 dB	1.176 MHz	32 dB	102
Notch Filters	1.236	-	63

TABLE 3: Influence of Amplifier Gain on Filter Response (Experimental)

Using an amplifier with 40 dB in the region of the notch it was possible to obtain a Q-factor of 102. This is much higher than the value of 63 associated with the notch filter itself, and this indicates the presence of positive feedback. When the amplifier gain was reduced to 35 dB positive feedback was still present even though the filter Q was

less than the measured Q for the notch. The positive feedback was due to loss of amplifier phase shift which at the frequencies of interest has fallen to 103°. The theoretical response of the filter was computed using the measured values for the notch filter and amplifier parameters, and the frequency response is shown (Figure 52), and should be compared with Figure 50, which is the oscillograph of the actual system response. The close agreement between theoretical and experimental results may be seen in Table 4.

	Predicted	Measured
Midband Frequency MHz	1.168	1.079
Midband Gain dB	29	30

TABLE 4: Comparison of Measured and Predicted Band-Pass Response

Had the amplifier phase shift been 180° the amplifier gain of 65 dB would have been required to produce a midband gain of 30 dB, confirming presence of positive feedback. The detailed specifications of the active filter are shown below.

Band-Pass Amplifier Specifications

Band-pass gain	+30 dB	(output open circuit)
	+25 dB	(50Ω load)
Centre Frequency	1.08 MHz	
Bandwidth	22 KHz	
Input Impedance (at 1.08 MHz)	10K	
Maximum input signal for linear operation	20mV (3 dB compensation)	

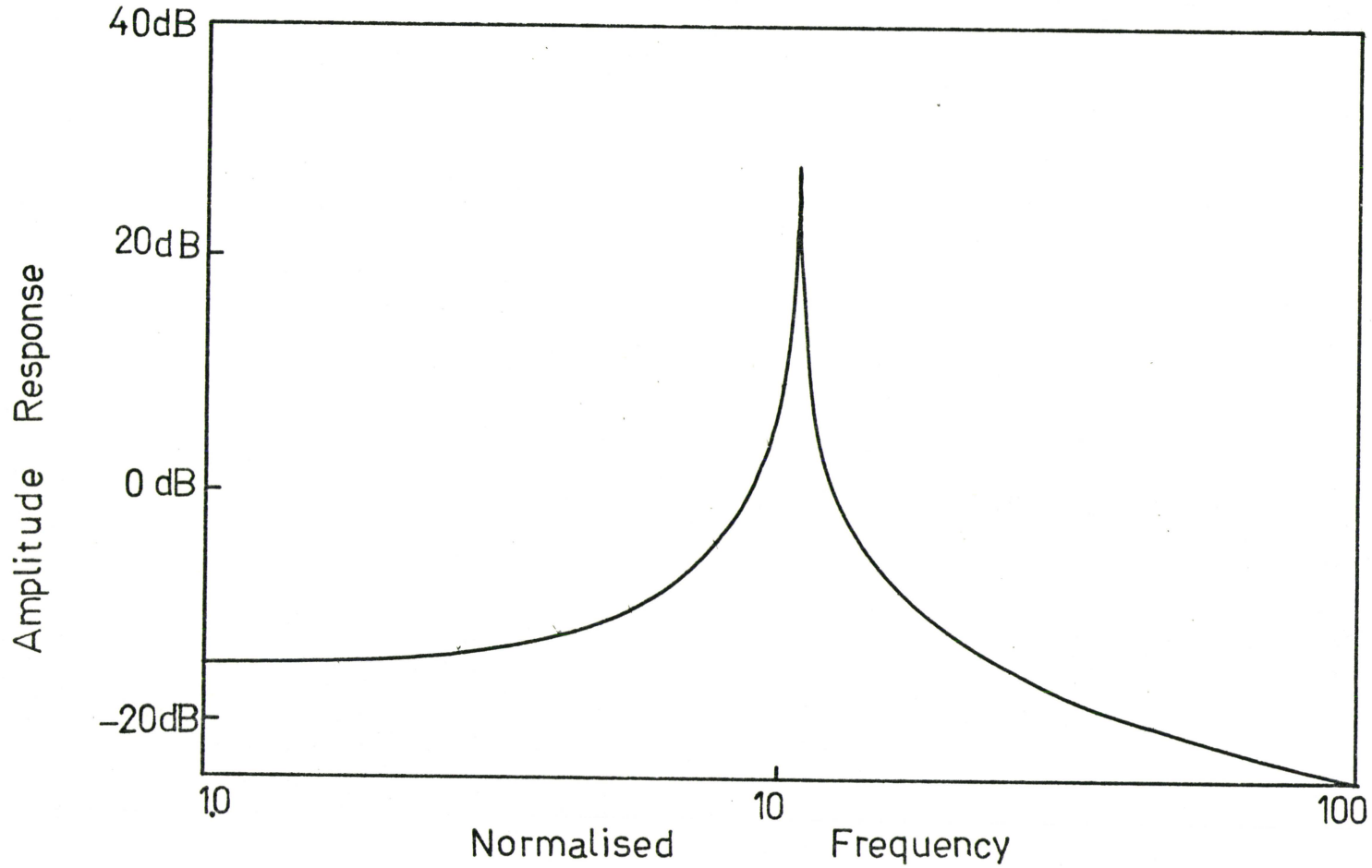

Figure 52 Theoretical Amplitude Response for Bandpass Filter using values for system parameters obtained by experiment.

6.3.5 Cascaded Notch Feedback Elements:

The bandwidth of the active filter could be increased by deliberately choosing the amplifier to have low gain, or by adjusting the value of notch resistance away from the optimum (deepest notch) condition. Unfortunately, both these approaches result in poor out-of-band rejection characteristics.

The use of two notch filters with staggered frequencies and connected in series, was investigated experimentally in an attempt to obtain increased bandwidth and still retain good out-of-band rejection[24]. This approach was unsuccessful. It was impossible to obtain a stable closed loop response.

The Q of each notch filter was high so that the frequency separation of the notch filters was small. As a good approximation, the frequency separation can be neglected and the phase shift of the feedback network is simply twice that due to a single notch filter (loading effects are neglected). Consequently, a low frequency oscillation ensues as the phase falls from 0° to -200° when the frequency is increased from zero the notch frequency. Note that it is possible to obtain a stable response using cascaded notch filters in the feedback path if the separation of the notch frequencies is sufficiently large[24].

CHAPTER VII

CONCLUSIONS AND RECOMMENDATIONS

The frequency selective feedback provided by a distributed notch filter has been used to develop an active 1 MHz band-pass filter. The design is attractive for its engineering simplicity (the notch circuit consists of only two elements -- one lumped and one distributed), and because high Q's ($Q > 50$) can be achieved without the need for inductance.

The filter characteristic is dependent on the value of the notch parameter α and should be restricted to values of $\alpha < 17.786$ in order to avoid positive feedback being applied in the region of the notch frequency. Positive feedback aggravates problems of noise, makes the filter response more sensitive to parameter variations and may cause instability.

The influence of the amplifier parameters on the filter response has been investigated. Research has shown that the choice of amplifier input and output impedances is not very critical but the amplifier gain and phase response requires careful consideration. The gain should be large to reduce parameter sensitivity and to achieve high Q, but should be considered in conjunction with the phase response in order to avoid instability problems associated with the loss of amplifier phase shift at high frequencies.

For convenience the distributed RC structures were constructed from Mylar film and Teledeltos paper, and the close agreement between predicted and measured filter characteristics emphasises the validity of using these models to simulate the performance of evaporated thin

film structures.

The maximum usable Q is limited by the frequency stability of the filter. Frequency drift induced by system parameter fluctuations (particularly amplifier gain) results in large signal variations if the filter response has high selectivity (Q). The use of a voltage tunable notch filter in conjunction with corrective feedback should be investigated as a possible solution to the problem of drift. The notch frequency is a function of distributed capacitance so voltage tuning can be achieved by exploiting the C-V characteristic of a reversed biased p-n junction.

REFERENCES

1. Googe, J. M., and Su, K. L., Trans. IEEE, CT-11, pp. 372-377, 1964.
2. Fu, Y. Fu, J. S., "n-port Rectangular RC Networks", Trans. IEEE, CT-13, pp. 223 - 225, 1966.
3. Ghausi, M. S., and Kelly, J. J., "Introduction to Distributed Parameter Networks", Holt, Rinehart and Winston, New York, 1968.
4. Castro, P. S., and Happ, W. W., "Distributed Parameter Circuit Design Techniques", Proc. NEC, pp. 45 - 69, 1961.
5. Heizer, K. W., "Distributed RC Networks with Rational Transfer Functions", IRE Trans. on Circuit Theory, CT-9, pp. 356 - 362, 1963.
6. Wyndrum, R. W., "The Exact Synthesis of Distributed RC Networks", Technical Report 400-76, New York University, College of Engineering, 1963.
7. O'Shea, R. P., "Synthesis using Distributed RC Networks", IEEE International Convention Record, Vol. 13, Part 7, pp. 18 - 29, 1965. Also,
   Trans. IEEE, CT-12, pp. 546 - 554, 1965.
8. Chinn, H. R., "The Synthesis of Exponentially Tapered Distributed RC Networks Realizing Driving Point Immittance Functions", Ph.D. Thesis, University of British Columbia, 1966.
9. Wragg, E. J., Practical Filters Using Distributed RC Structures", M.Eng. Thesis, McMaster University, 1972.

10. Kaufman, W. M., "Theory of a Monolithic Null Device and Some Norel Circuits", Proc. IRE, 48, pp. 1540 - 1545, 1960.

11. Yani, T., et al., "Microelectronic Circuits and Applications", Ed Carrol, J.M., McGraw-Hill, New York, p. 125, 1965.
Also,
Holm, C., "Distributed Parameter Networks", Electrical Manufacturing, pp. 92 - 96, April 1960.
Also,
Hager, C. K., "Network Design of Microcircuits", Electronics, pp. 44 - 49, September 4, 1959.

12. Swart, P. L., "Evaporated Thin Film Tunable Distributed RC Filters", Ph.D. Thesis, McMaster University, March 1971.

13. Chipman, R. A., "Transmission Lines", McGraw-Hill, Schaum's Series, New York, 1968.

14. Friedland, B., and Schwartz, R. J., "Linear Systems", McGraw-Hill, Electrical and Electronic Engineering Series, New York, 1965.

15. Fuller, W. D., and Castro, P. S., "A Microsystems Band-pass Amplifier", Proc. NEC, Vol. 16, pp. 139 - 151, 1960.

16. Stein, J., "A New Look at Distributed RC Notch Filters", Proc. IEEE, 58, p. 596, 1970.

17. Campbell, C. K., "Transmission-line Graphical Analysis of a Distributed RC Notch Filter", Proc. IEEE, 59, pp. 1362 - 1363, 1971.

18. Carson, J. A., "Evaporated Thin Film Distributed RC Networks", M.Eng. Thesis, McMaster University, 1969.

19. Swart, P. L., and Campbell, C. K., "Effect of Inductance on Characteristics of a Distributed RC Notch Filter", Proc. IEEE, 59,

pp. 1371 - 1373, 1971.

20. Haykin, S. S., "Active Network Theory", Addison Wesley, London, 1970.

21. Bandler, J. W., "Optimization Methods for Computer-aided Design", Trans. IEEE, MTT-17, pp. 533 - 552, 1969.

    Also,

    Bandler, J. W., and Seviora, R. E., "Current Trends in Network Optimization", Trans. IEEE, MTT-18, 1970.

22. Su, K. L., "RC Filters with Staggered Notch Frequency", Proc. IEEE, 54, p. 1199, 1966.

23. Holland, L., "Vacuum Deposition of Thin Films", Wiley, New York, 1961.

24. Ramakrishna, K., "Generalized Feedback Analysis of Cascaded Null Networks", Trans. IEEE, CT-19, pp. 130 - 136, 1972.

25. Truxal, J. G., "Automatic Feedback Control System Synthesis", McGraw-Hill, New York, 1955.

26. Bode, H. W., "Network Analysis and Feedback Amplifier Design", Van Nostrand, 1945.

27. Shinners, S. M., "Control System Design", Wiley, New York, 1964.

28. Cheng, D. K., "Analysis of Linear Systems", Addison Wesley, 1959.